FINAL CONTRACT REPORT

CREEP OF HIGH-STRENGTH NORMAL AND LIGHTWEIGHT CONCRETE

Edward C. Vincent
Graduate Research Assistant

Bradley D. Townsend
Graduate Research Assistant

Richard E. Weyers, P.E., Ph.D.
Charles E. Via, Jr. Professor

Charles E. Via, Jr. Department of Civil and Environmental Engineering
Virginia Polytechnic Institute & State University

Project Manager
Michael M. Sprinkel, P.E., Associate Director, Virginia Transportation Research Council

Contract Research Sponsored by the
Virginia Transportation Research Council

Virginia Transportation Research Council
(A Cooperative Organization Sponsored Jointly
by the Virginia Department of Transportation
and the University of Virginia)

Charlottesville, Virginia

May 2004
VTRC 04-CR8

NOTICE

The project that is the subject of this report was done under contract for the Virginia Department of Transportation, Virginia Transportation Research Council. The contents of this report reflect the views of the authors, who are responsible for the facts and the accuracy of the data presented herein. The contents do not necessarily reflect the official views or policies of the Virginia Department of Transportation, the Commonwealth Transportation Board, or the Federal Highway Administration. This report does not constitute a standard, specification, or regulation.

Each contract report is peer reviewed and accepted for publication by Research Council staff with expertise in related technical areas. Final editing and proofreading of the report are performed by the contractor.

ABSTRACT

In addition to immediate elastic deformations, concrete undergoes time-dependent deformations that must be considered in design. *Creep* is defined as the time-dependent deformation resulting from a sustained stress. Shrinkage deformation is the time-dependent strain that occurs in the absence of an applied load. The total strain of a concrete member is the sum of elastic, creep, and shrinkage strains.

Test beams for the Pinner's Point Bridge were produced by Bayshore Concrete Products Corp. using a high-strength normal weight concrete (HSC) mixture and the Chickahominy River Bridge beams using a high-strength lightweight concrete (LTHSC) mixture. The test beams and the Chickahominy River Bridge beams were fabricated with thermocouples to track interior concrete temperatures, and vibrating wire gages (VWGs) were placed at the center of prestressing to record changes in strain.

Laboratory creep and shrinkage testing was conducted on specimens prepared with identical materials and similar mixture proportions in the casting of the bridge beams. The temperature profile from the beams during steam curing was used to produce match-cured specimens for laboratory testing. Two match-cured batches were produced, along with two standard cured batches. The creep room had a temperature of 23.0 ± 1.7°C (73.4 ± 3ºF) and a relative humidity of 50 ± 4%. Companion shrinkage specimens were also placed in the creep room. Measurements were taken on the creep and shrinkage specimens using a Whittemore gage. Four HSC cylinders were also equipped with embedded VWGs so that the interior and exterior strains could be compared. The Whittemore and VWG elastic and creep strains were similar, while the VWGs recorded significantly less shrinkage.

The measured creep and shrinkage strains were compared to different prediction models to determine which model was the most accurate. The models considered were ACI 209, ACI 209 modified by Huo, CEB Model Code 90, AASHTO-LRFD, Gardner GL2000, Tadros, and Bazant B3. The ACI 209 modified by Huo was the most accurate in predicting time-dependent strains for the HSC mixture. The best overall predictor for the LTHSC time-dependent deformations was the Gardner GL 2000 model for the standard cure LTHSC specimens, whereas the ACI 209 model was the best predictor of the total stains and individual time-dependent deformations for the match-cured LTHSC mixture.

INTRODUCTION

Concrete undergoes volumetric changes throughout its service life. These changes are a result of applied loads and shrinkage. Applied loads result in an instantaneous recoverable elastic deformation and a slow, time-dependent, inelastic deformation called *creep*. Creep without moisture loss is referred to as basic creep and with moisture loss is referred to as drying creep.

Shrinkage is a combination of autogeneous, drying, and carbonation shrinkage of the hardened concrete. Plastic shrinkage is not included since it occurs due to moisture loss before the concrete has set. Autogeneous shrinkage is a result of the hydration process. The hydrated cement paste has a smaller volume than the cement and water reactants. Drying shrinkage occurs as surface water evaporates and internal water moves outward in an attempt for hygral equilibrium. The opposite reaction is called *swelling*. Carbonation shrinkage occurs with the carbonation of the hydrated cement products with carbon dioxide in the atmosphere.

Creep testing is conducted on sealed or unsealed specimens. Sealed specimens with an applied stress have volumetric changes due to elastic deformation, basic creep, and autogeneous shrinkage. Sealed specimens without an applied stress deform due to autogeneous shrinkage. Basic creep is the total deformation of a loaded, sealed specimen minus the elastic deformation and autogeneous shrinkage.

Unsealed specimens are the most commonly used test method. Unsealed specimens without an applied stress have volumetric changes due to autogeneous and drying shrinkage. The total deformation of unsealed specimens is the result of an applied stress producing an elastic deformation, creep, and shrinkage. Creep includes both basic and drying creep. Shrinkage includes autogeneous and drying shrinkage. Drying creep of a loaded specimen is the total deformation minus the elastic deformation, basic creep, and shrinkage and requires the testing of both sealed and unsealed specimens. Therefore, creep is typically examined as the total of basic and drying creep.

PURPOSE AND SCOPE

The objectives of this study were twofold: first to determine the laboratory time-dependent deformation of the high strength concrete mixtures used in the prestressed beams in the Pinner's Point and Chickahominy River bridges, and second, to compare standard laboratory test results with fabricated bridge beam time-dependent deformations. Each set of specimens was tested under laboratory exposure conditions after undergoing the standard cure or an accelerated cure with the time-temperature match cure system. The creep results of the HSC mixture were compared with the seven most current prediction models and the LTHSC mixture with four prediction models. The results of this study may be used to determine the best existing model of the models evaluated to predict prestress losses for HSC and LTHSC mixtures. The results may also be compared with the results of the field assessment task of a concurrent project.

The HSC and LTHSC mixture ingredients and proportions from Bayshore Concrete Products Corporation and used in the fabrication of the prestressed beams were used in this study. At loading, the maturity of the accelerated cured specimens was consistent with that of the prestressed beams at the centroid of the prestressing strand. The curing methods, accelerated and standard cures, are a variable. The ambient laboratory exposure conditions were held constant.

METHODS AND MATERIALS

The study was performed using two uniquely different HSC mixtures, a normal and a lightweight mixture. Thus, in this and the remaining sections, the discussion of the two mixtures are presented under separate headings.

HSC

Test Specimens

Table 1 presents the HSC creep and shrinkage test matrix. Batching and mixing were conducted in accordance with ASTM C192-98. Mixture proportions were based on the 55.2 MPa (8000 psi) mixture used in the test beams at Bayshore and are presented in Table 2. Tables 3 and 4 present the laboratory fresh concrete properties for the accelerated cure and standard cure batches, respectively. Table 3 also includes the prestressed beam fresh concrete properties and specifications of the Virginia Department of Transportation (VDOT).

The coarse aggregate was a #67 crushed diabase, and the fine aggregate a natural sand. Cementitious materials were Type I/II portland cement and a Grade 120 slag. Admixtures were an air-entraining agent, a water reducer, a high-range water reducer, and a corrosion inhibitor.

Table 1 HSC Test Matrix

Curing Method	Batches	Age at Loading	Specimens/Batch
Standard	HSC8-1A HSC8-2A	7 days	8 Compressive Strength 4 Tensile Strength 1 Modulus 3 Shrinkage cylinders 3 Creep 3 Shrinkage Prisms
Accelerated	HSC8-3A HSC8-4A	1 day	5 Compressive Strength 2 Tensile Strength 1 Modulus 4 Shrinkage Cylinders 4 Creep Cylinders

Table 2 Bayshore Mixture Proportions

Materials	SSD weights, kg/m^3 (lb/yd^3)
Portland Cement	303 (510)
Slag Cement	202 (340)
Coarse Aggregate	1157 (1950)
Fine Aggregate	586 (988)
Water	149 (252)
AEA (Daravair)	580 ml/m^3 (15 oz/yd^3)
WR (Hycol)	1044 ml/m^3 (27 oz/yd^3)
HRWR (Adva)	6764 ml/m^3 (175 oz/yd^3)
Cl or Accel (DCI)	19.8 L/m^3 (4.0 gal/yd^3)

Table 3 Accelerated Cure Laboratory and Beam Fresh Concrete Properties

Properties	HSC8-1A	HSC8-2A	Bayshore	VDOT Specs.
Slump, mm (in.)	152 (6)	152 (6)	203 (8)	0-178 (0-7)
Air Content, %	5.6	4.4	6.2	3-6
Temperature, °C (°F)	24.4 (76)	25.6 (78)	25.0 (77)	4.4-32.2 (40-90)
Unit Weight, kg/m^3 (pcf)	2468 (154)	2484 (155)	----	----
Yield	1.02	1.03	----	----
w/cm ratio	0.30	0.30	~ 0.33	< 0.4
Curing Method	Match Cure	Match Cure	Steam	N/A

Table 4 Standard Cure Laboratory Fresh Concrete Properties

Properties	HSC8-3A	HSC8-4A
Slump, mm (in.)	216 (8.5)	114 (4.5)
Air Content, %	3.5	3.5
Temperature, °C (°F)	25.6 (78)	23.9 (75)
Unit Weight, kg/m^3 (pcf)	2549 (159)	2549 (159)
Yield	1.05	1.05
w/cm ratio	0.30	0.30

Creep and Shrinkage Testing

Creep testing was performed in accordance with ASTM C512-87. Because of equipment constraints, there were differences in test procedure between the standard cure and accelerated cure batches.

From each accelerated cure batch, four cylindrical creep and shrinkage specimens were cast. Because the accelerated cure specimens are smaller, four specimens could be stacked in a loading frame, whereas only three standard cure specimens were placed in a frame. The cast-in-place inserts for attaching gage points could not be used with the accelerated cure Sure Cure cylinder molds. Instead, holes were drilled in the cylinders and the gage points were attached using a 5-minute epoxy. The gage points were spaced 150 mm (6 in.) apart for the accelerated cure specimens.

From each standard cure batch, three cylindrical creep and shrinkage specimens were cast, along with the strength and elastic modulus specimens. Brass inserts were cast into each creep and shrinkage cylinder, and gage points attached after curing. Each cylinder had four gage points, with two on each diametrically opposite side; the separation distance was 200 mm (8 in.).

Test specimens were sulfur-capped immediately after curing in accordance with ASTM C617-98. Compressive strength was determined immediately after curing, and the creep, shrinkage, elastic modulus, and remaining strength specimens were placed in the controlled environment of 23.0 ± 1.7 °C (73.4 ± 3 °F) and 50 ± 4% relative humidity. The creep specimens were stacked in the loading frames and loaded to 30% of their after cure compressive strength, 7 days for the standard cure and 1 day for the accelerated cure specimens. The applied load was kept constant throughout the test. Within-batch deviations in stress were eliminated since all loaded specimens from a batch were placed in the same loading frame.

Creep and shrinkage measurements were taken on the schedule set forth in ASTM C512-98 using a Whittemore gage to measure changes in length between the gage points over time. The Whittemore gage reads lengths in increments of 0.0025 mm (0.0001 in.), which equals 17 and 13 microstrain for the accelerated and standard cure specimens, respectively. Measurements were repeated 4 times on each side of the cylinder, so that each reading was an average of eight measurements.

For the two accelerated cure batches, cylindrical specimens were cast in 100 mm x 200 mm (4 in. x 8 in.) molds whose surface temperatures were controlled by the Sure Cure system. A 22-hour heated curing regimen was used to simulate steam curing of the test girders at Bayshore. The temperature profile of the test girders during steam curing was recorded using embedded thermocouples. This profile was entered into the Sure Cure system, so that the test specimens would experience the same curing temperatures as the test girders. In order to maintain a moist environment, wet burlap and plastic sheeting were placed over the molds during curing.

The cylindrical standard cure creep and shrinkage specimens were cast in 150 mm x 300 mm (6 in. x 12 in.) steel molds, while the cylindrical strength and modulus specimens were cast

in 100 mm x 200 mm (4 in. x 8 in.) plastic molds. Shrinkage prisms were cast in 75 mm x 75 mm x 280 mm (3 in. x 3 in. x 11.25 in.) steel rectangular molds. The test specimens were stored in a moist room for 7 days after casting, in accordance with ASTM C192-98.

Strains were calculated by dividing the change in length by the original gage length. In order to calculate creep strain, loaded cylinders were paired with unloaded cylinders by relative magnitudes of deformation within each batch. For example, the creep cylinder having the largest total strain within a batch was paired with the shrinkage cylinder having the largest shrinkage strain within the same batch, and so on. Creep strains for each pair were then calculated by subtracting initial elastic strain and companion shrinkage cylinder strain from the total strain.

Vibrating wire gages (VWG) identical with the ones used in the test beams were embedded in the center of two cylindrical creep and shrinkage specimens of accelerated batch 2A. The VWGs are Geokon Model VCE-4200 and have a gage length of 6 in. Readings were taken at the same time increments as were the Whittemore measurements, and the two were compared in order to observe differences in creep and shrinkage behavior between the center of a concrete specimen and the outer surface

In addition to the cylinders for measuring shrinkage, three shrinkage prisms were cast from each standard cure batch and tested in accordance with ASTM C157-99. Gage points were cast in the ends of each prism. The prisms were kept in the same environment as the creep and shrinkage cylinders and measured at the same time increments using a comparator.

Strength and Modulus Testing

Compressive and tensile strength tests were performed for each batch. Compressive tests followed ASTM C39-99, using 100 mm x 200 mm (4 in. x 8 in.) cylinders that were sulfur-capped and stored in the creep room after curing. For the standard cure batches, compressive tests on two specimens were performed at 7, 28, 56, and 90 days after casting. The Sure Cure system limited the number of accelerated cure specimens that could be made, so compressive tests were performed at 1, 7, and 28 days after casting.

Tensile strength for each batch was evaluated using the splitting tensile test of ASTM C496-96. Two specimens were tested at 7 and 28 days after casting for the standard cure batches and one or two specimens at 28 days after casting for the accelerated cure batches.

Tests were performed on one 100 mm x 200 mm (4 in. x 8 in.) cylinder from each batch to determine the modulus of elasticity, following the procedure of ASTM C469-94. The modulus of elasticity measurements were taken at 7, 28, 56, and 90 days for the standard cure batches and 1, 28, and 90 days for the accelerated cure batches.

Thermal Coefficient

The thermal coefficient was measured using two of the accelerated batch 2A shrinkage specimens after the end of creep testing. The specimens were subjected to two air temperatures, 33°F and 120°F (0°C to 49°C), for 3 days at each temperature. Strain measurements were taken using both the embedded VWGs and the Whittemore gage. Measurements were taken at ambient conditions before and after thermal testing to ensure that strains were due to temperature differences and not moisture loss or gain.

LTHSC

Test Specimens

Table 5 presents the LTHSC test matrix. The mixture proportions and materials were the same as with the Chickahominy River Bridge beams; see Table 6.

Table 7 presents the fresh concrete properties for the two standard cure batches. Table 8 presents the fresh concrete properties for the two accelerated cure batches and two of the Bayshore beams.

Table 5 LTHSC Test Matrix

Curing Method	Mix	Age at Loading	Shrinkage Prisms
Standard Cure	2 batches	7 and 28 days	Yes
Match Cure	2 batches	1, 7, and 28 days	No

Table 6 Bayshore Mixture Proportions

Materials	SSD weights, kg/m^3 (lb/yd^3)
Portland Cement (Type II)	268 (451)
Slag Cement (Grade 120)	179 (301)
Coarse Aggregate (lightweight)	413 (696)
Coarse Aggregate (normal weight)	359 (605)
Fine Aggregate (lightweight)	231 (390)
Fine Aggregate (normal weight)	321 (541)
Water	151 (255)
AEA (Daravair)	355 mL/m^3 (12 oz/yd^3)
WR (Hycol)	651 mL/m^3 (22 oz/yd^3)
HRWR (Adva)	1656 mL/m^3 (56 oz/yd^3)
CI or Accel (DCI)	11.4 L/m^3 (3 gal/yd^3)

Table 7 Fresh Concrete Properties for Standard Cure Batches

Properties	LTHSC 2B	LTHSC 3B
Slump, mm (in.)	165 (6.5)	140 (5.5)
Air Content (%)	6.5	5.5
Temperature, ^{o}C (^{o}F)	26 (78)	26 (78)
Unit Weight, kg/m^3 (pcf)	1880 (117.3)	1910 (119.1)
Yield	1.02	1.01
w/cm ratio	0.369	0.369
Curing Method	Standard	Standard

Table 8 Fresh Concrete Properties for Accelerated Cure Batches

Properties	LTHSC 4B	LTHSC 5B	Bayshore BB1	Bayshore BB2	VDOT Specs.
Slump, mm (in.)	100 (4.0)	150 (6.0)	180 (7)	215 (8.5)	0-100 (0-4)
Air Content (%)	6.0	7.1	5.5	6.0	3 – 6
Temperature, ^{o}C (^{o}F)	24 (75)	24 (76)	21(70)	20 (68)	----
Unit Weight, kg/m^3 (pcf)	1930 (120.3)	1875 (117.1)	1950 (122.0)	1900 (118.8)	----
Yield	1.00	1.02	0.98	1.01	----
w/cm ratio	0.369	0.369	0.369	0.369	<0.4
Curing Method	Sure Cure	Sure Cure	Steam	Steam	N/A

The LTHSC mixture had two fine and two coarse aggregates, a normal and a lightweight aggregate. The lightweight aggregate was both a fine and #67 expanded slate from the Carolina Stalite Company. The normal weight aggregates were natural sand and #67 crushed diabase.

The cementitious materials were a Type I/II portland cement and a Grade 120 slag. The LTHSC admixtures were the same as the HSC mixture. The methods used in the LTHSC study were the same as those presented in the HSC methods section.

RESULTS

HSC

The following sections present the results of the HSC creep and shrinkage study: Batches 1A and 2A were subjected to heated accelerated curing, and batches 3A and 4A were the standard moist curing regimen. Whenever possible, experimental results are compared with field measurements obtained from Bayshore Concrete Products. Field compressive strength measurements were performed at Bayshore, and the field modulus of elasticity measurements were performed at Virginia Tech on cylinders obtained from Bayshore. Compressive strength, modulus of elasticity, and tensile strength results were compared to specified values or ACI and AASHTO design values.

Compressive Strength

Accelerated Cure

Figure 1 presents the HSC laboratory compressive strength results for accelerated batches 1A and 2A and field results from Bayshore. Each 1-day laboratory result represents an average of two measurements, and the others represent single measurements. Each result from Bayshore is an average of three measurements. The specified 28-day compressive strength (f'_c) of 55 MPa (8000 psi) and release strength (f'_{ci}) of 44 MPa (6400 psi) are presented for comparison.

The 1-day compressive strengths for batches 1A and 2A were 68.3 MPa and 68.1 MPa (9910 and 9870 psi), respectively. The 7-day compressive strengths for batches 1A and 2A were 71.0 MPa and 74.1 MPa (10300 and 10740 psi), respectively. The 28-day compressive strengths for batches 1A and 2A were 86.9 MPa and 85.5 MPa (12600 and 12400 psi), respectively. The 90-day compressive strengths for batches 1A and 2A were 82.1 MPa and 83.4 MPa (11900 and 12100 psi), respectively. The Bayshore 1-day, 7-day, and 28-day compressive strengths were 45.3 MPa, 50.0 MPa, and 59.0 MPa (6570, 7250, and 8560 psi), respectively

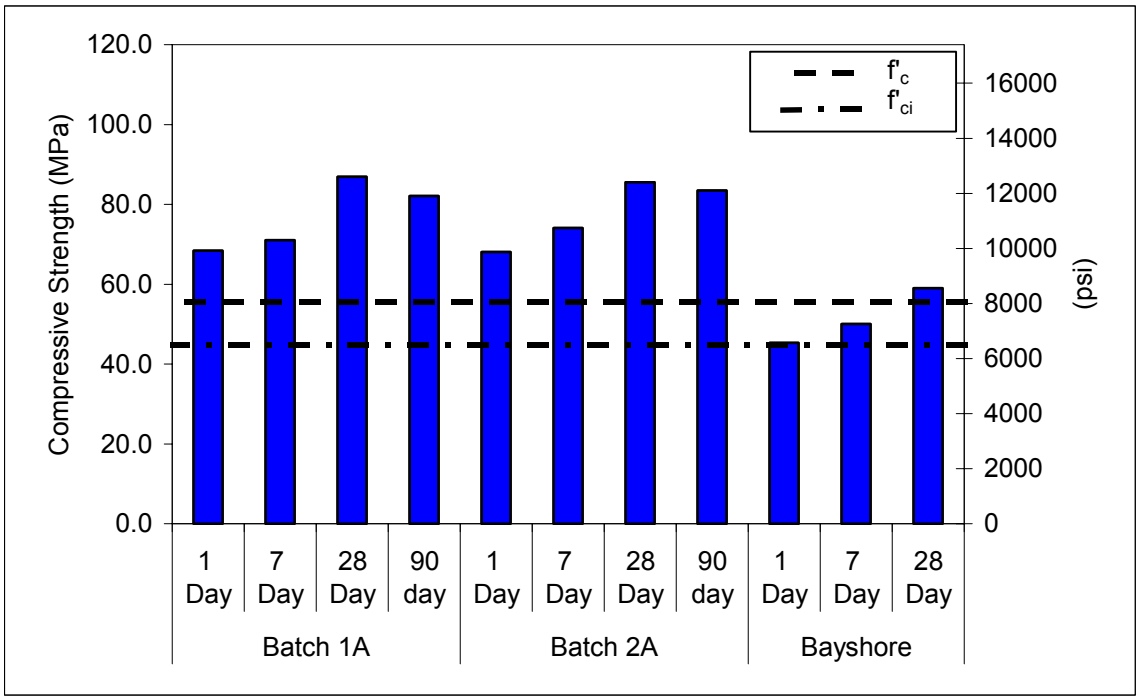

Figure 1 Accelerated Cure Compressive Strengths, HSC

Standard Cure

Figure 2 presents the HSC laboratory compressive strength results for standard cure batches 3A and 4A. Each result represents an average of two compressive strength measurements. The specified 28-day compressive strength (f'_c) of 55 MPa (8000 psi) and release strength (f'_{ci}) of 44 MPa (6400 psi) are presented for comparison.

The 7-day compressive strengths for batches 3A and 4A were 69.0 MPa and 73.1 MPa (10000 and 10600 psi), respectively. The 28-day compressive strengths for batches 3A and 4A were 90.3 MPa and 91.7 MPa (13100 and 13300 psi), respectively. The 56-day compressive strengths for batches 3A and 4A were 95.9 MPa and 97.2 MPa (13900 and 14100 psi), respectively. The 90-day compressive strengths for batches 3A and 4A were 87.6 MPa and 90.5 MPa (12700 and 13100 psi), respectively.

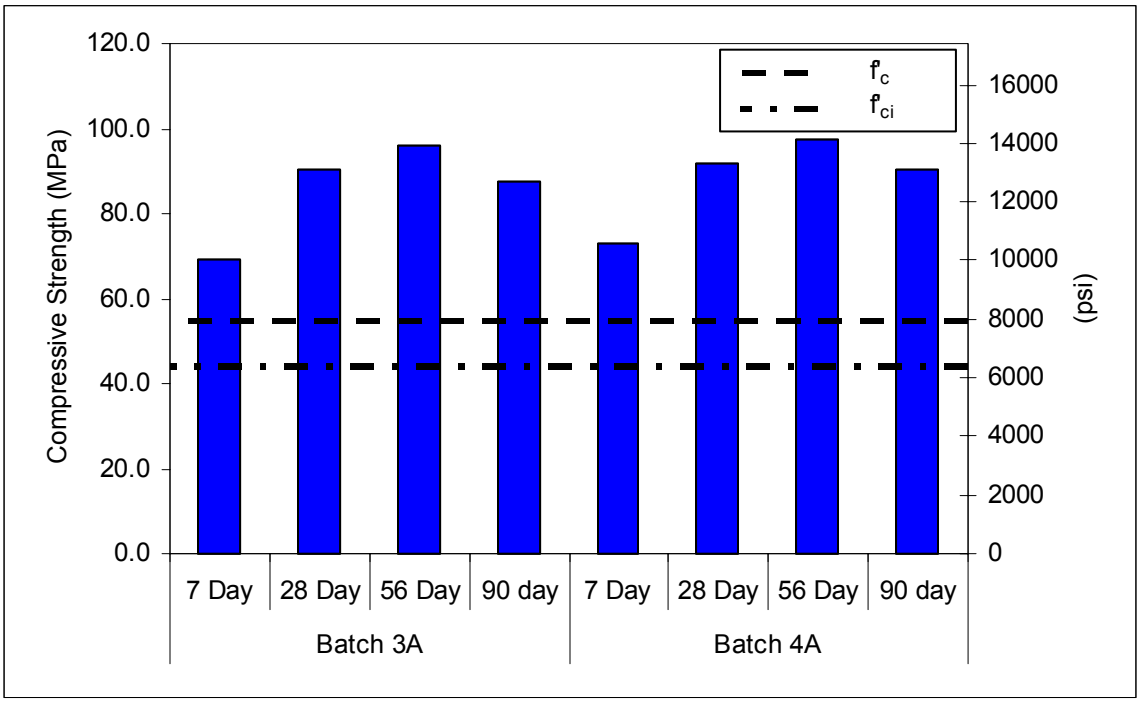

Figure 2 Standard Cure Compressive Strengths, HSC

Tensile Strength

The 1-day tensile strengths for batches 1A and 2A were 6.5 MPa and 6.3 MPa (940 and 910 psi), respectively. The 7-day tensile strengths for batches 3A and 4A were 7.3 MPa and 7.2 MPa (1060 and 1040 psi), respectively. The 28-day tensile strengths for batches 1A, 2A, 3A, and 4A were 6.9 MPa, 7.4 MPa, 8.0 MPa, and 7.8 MPa (1000, 1070, 1160, and 1135 psi), respectively. The results for batches 1A and 2A are single measurements. The results for batches 3A and 4A represent averages of two measurements.

Modulus of Elasticity

Accelerated Cure

Figure 3 presents the HSC modulus of elasticity results for accelerated batches 1A and 2A, along with the results from Bayshore. For the laboratory mixtures, measurements were taken on one specimen per batch at ages of 1, 28, and 90 days. Three Bayshore specimens were tested at 28 days, and the average measurement is presented. The AASHTO design modulus of elasticity of 39.1 GPa (5650 ksi) is shown for comparison.

The 1-day moduli of elasticity for batches 1A and 2A were 44.2 GPa and 44.6 GPa (6400 and 6500 ksi), respectively. The 28-day moduli of elasticity for batches 1A and 2A were both 43.7 GPa (6350 ksi). The Bayshore 28-day modulus of elasticity was 38.9 GPa (5650 ksi). The 90-day moduli of elasticity for batches 1A and 2A were 44.6 GPa and 42.1 GPa (6500 and 6100 ksi), respectively.

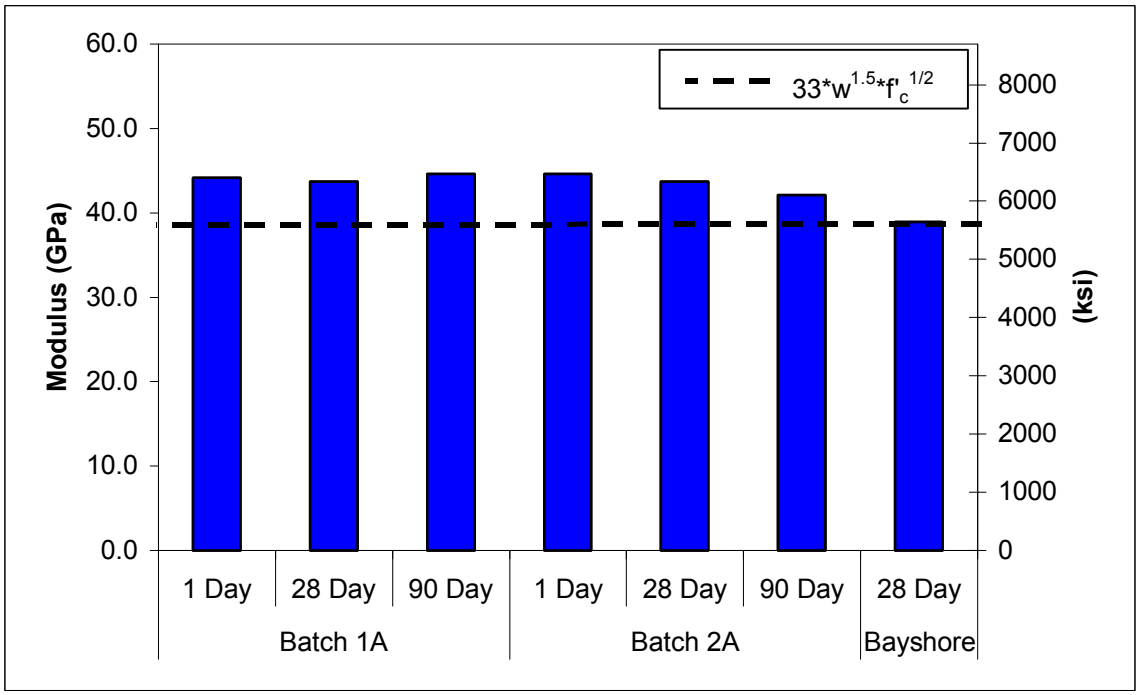

Figure 3 Accelerated Cure Modulus of Elasticity, HSC

Standard Cure

Figure 4 presents the HSC modulus of elasticity results for standard cure batches 3A and 4A. Measurements were taken on one specimen per batch at ages of 7, 28, 56, and 90 days. The AASHTO design modulus of elasticity of 39.3 GPa (5700 ksi) is shown for comparison.

The 7-day moduli of elasticity for batches 3A and 4A were 40.6 GPa and 43.0 GPa (5880 and 6240 ksi), respectively. The 28-day moduli of elasticity for batches 3A and 4A were 44.6 GPa and 46.2 GPa (6460 and 6700 ksi), respectively. The 56-day moduli of elasticity for batches 3A and 4A were 45.9 GPa and 45.5 GPa (6650 and 6600 ksi), respectively. The 90-day moduli of elasticity for batches 3A and 4A were 46.9 GPa and 45.7 GPa (6800 and 6600 ksi), respectively.

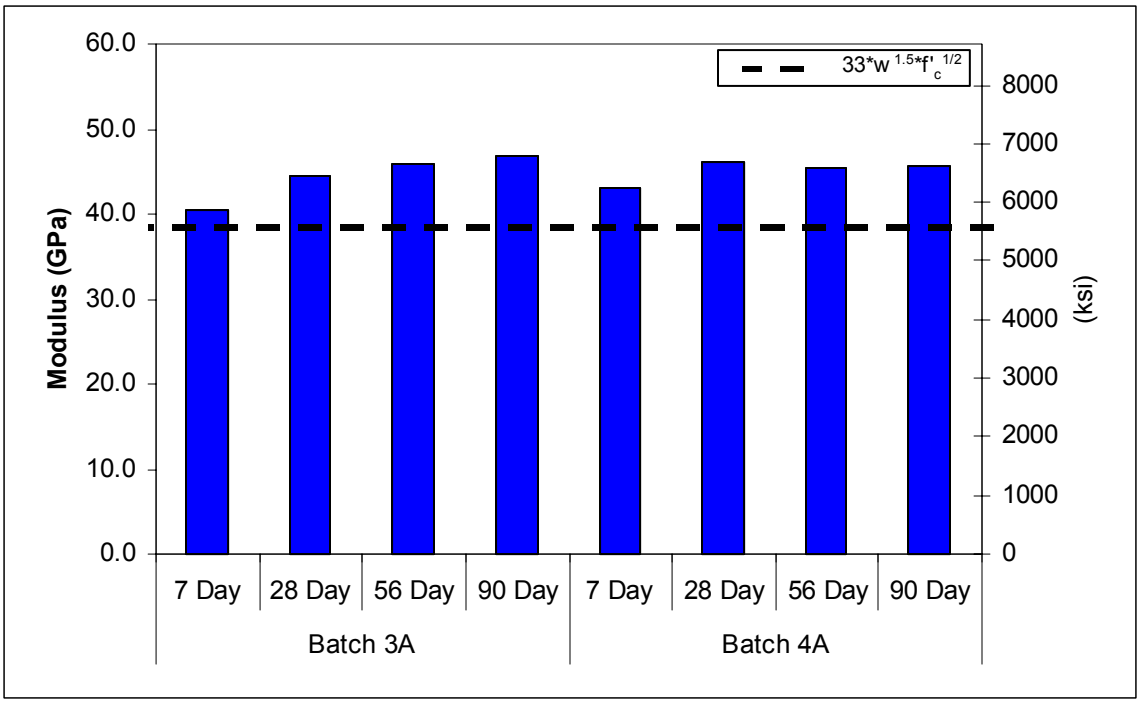

Figure 4 Standard Cure Modulus of Elasticity, HSC

Thermal Coefficient

The coefficient of thermal expansion for the HSC mixture was found to be 8.3 ± 0.7 microstrain per °C (4.6 ± 0.4 microstrain per °F) at a 95% confidence level.

Experimental and Predicted Strains

Figures 5 through 10 present the HSC experimental total strain, shrinkage, and creep measurements for accelerated cure and standard cure batches. Measurements were taken daily for 1 week after loading, then weekly thereafter; some measurements are not shown in the figures for clarity. For the accelerated cure batches, each curve represents an average of four specimens, and for the standard cure batches, each curve represents an average of three specimens. Each creep curve represents an average of four (accelerated cure) or three (standard cure) pairs of loaded and unloaded specimens. The figures also present 95% confidence intervals for each data point.

Figures 11 through 24 present the HSC total strain, shrinkage, and creep strains predicted by the models. The predicted strains were calculated using measured compressive strengths and elastic strains. The following models were considered:

- ACI 209R-92 (Mokhtarzadeh and French, 2000)
- ACI 209R-92, modified by Huo (Neville, 1970)
- Comite Euro-International Du Beton Model Code 1990 (Paulson et al., 1991)

- AASHTO-LRFD specification (Smadi et al., 1987)
- Gardner's and Lockman's GL2000 Model (Nawy, 2001)
- Tadros' revised AASHTO-LRFD (Collins, 1989)
- Bazant's B3 model (Shah and Ahmad, 1994).

The equations for prestress loss due to creep and shrinkage in the AASHTO Standard Specification are based on the ACI 209-92 model.

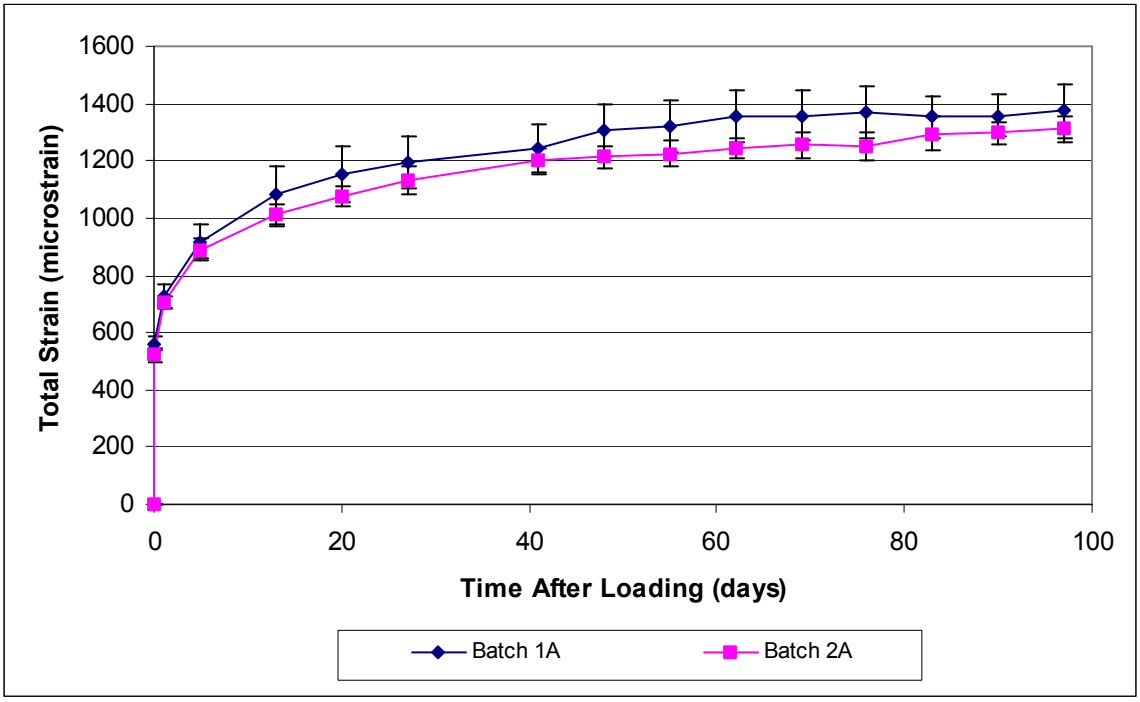

Figure 5 Accelerated Cure Experimental Total Strain, HSC

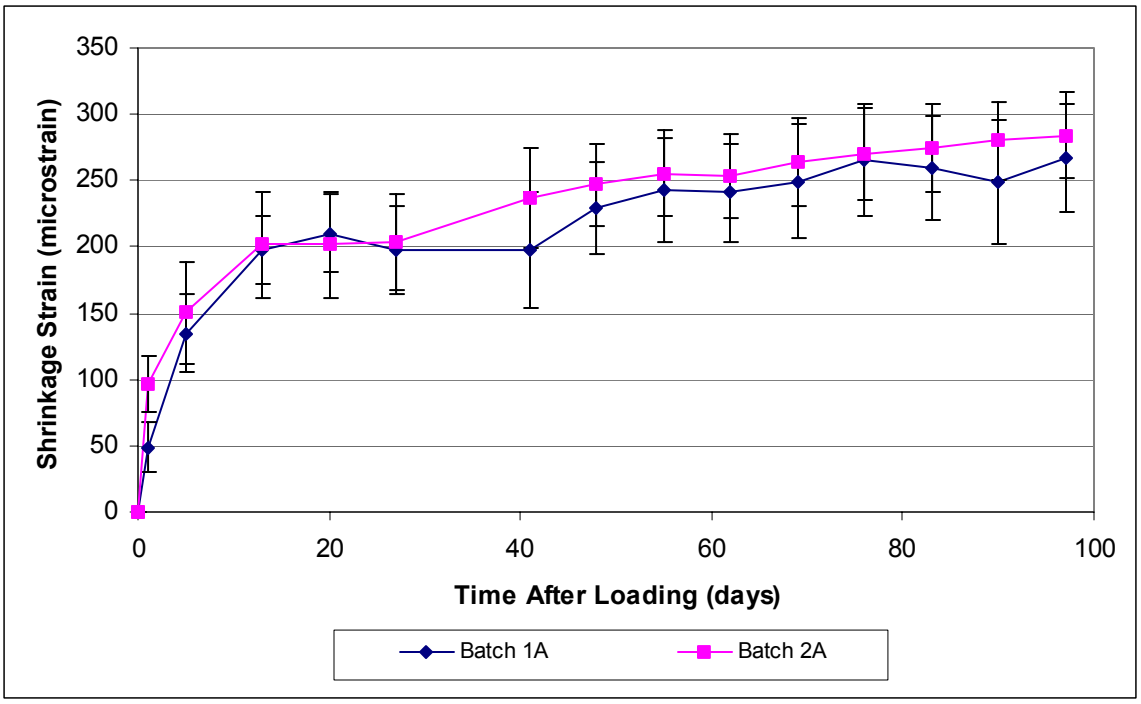

Figure 6 Accelerated Cure Experimental Shrinkage Strain, HSC

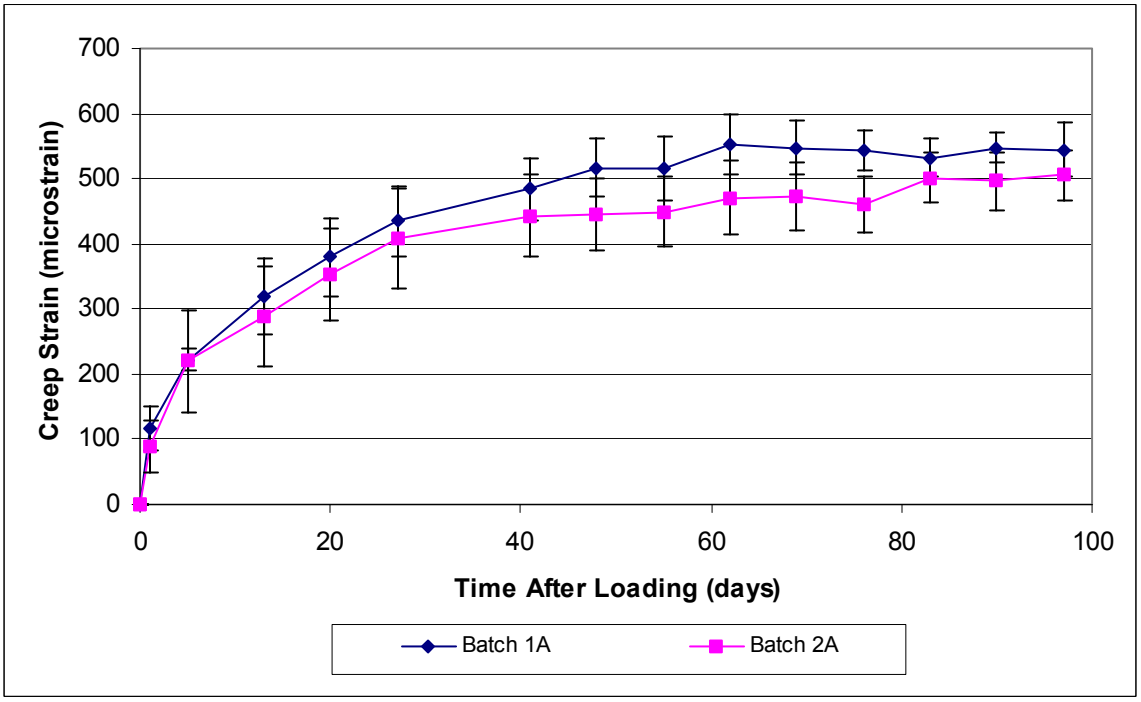

Figure 7 Accelerated Cure Experimental Creep Strain, HSC

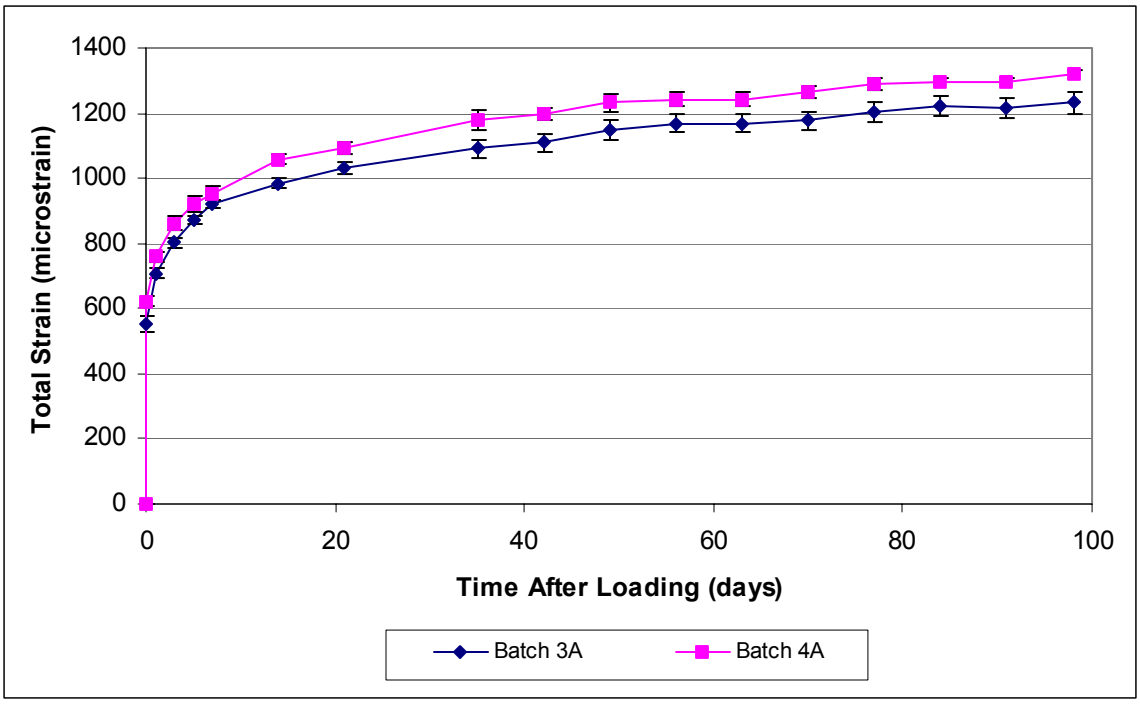

Figure 8 Standard Cure Experimental Total Strain, HSC

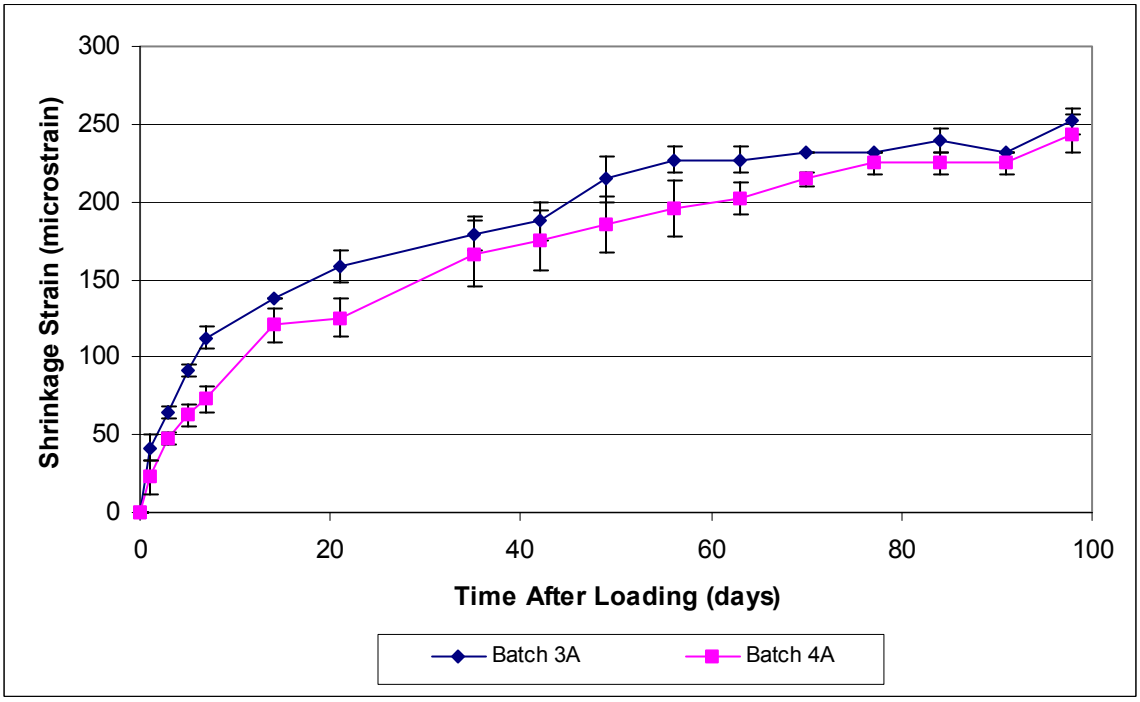

Figure 9 Standard Cure Experimental Shrinkage Strain, HSC

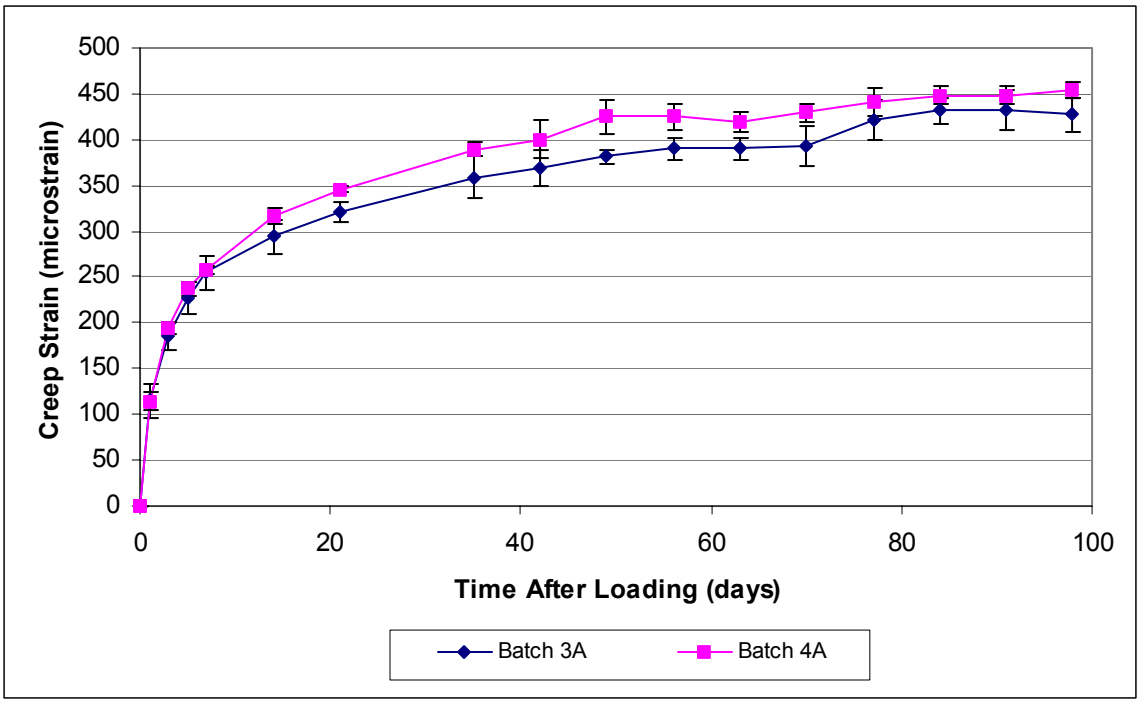

Figure 10 Standard Cure Experimental Creep Strain, HSC

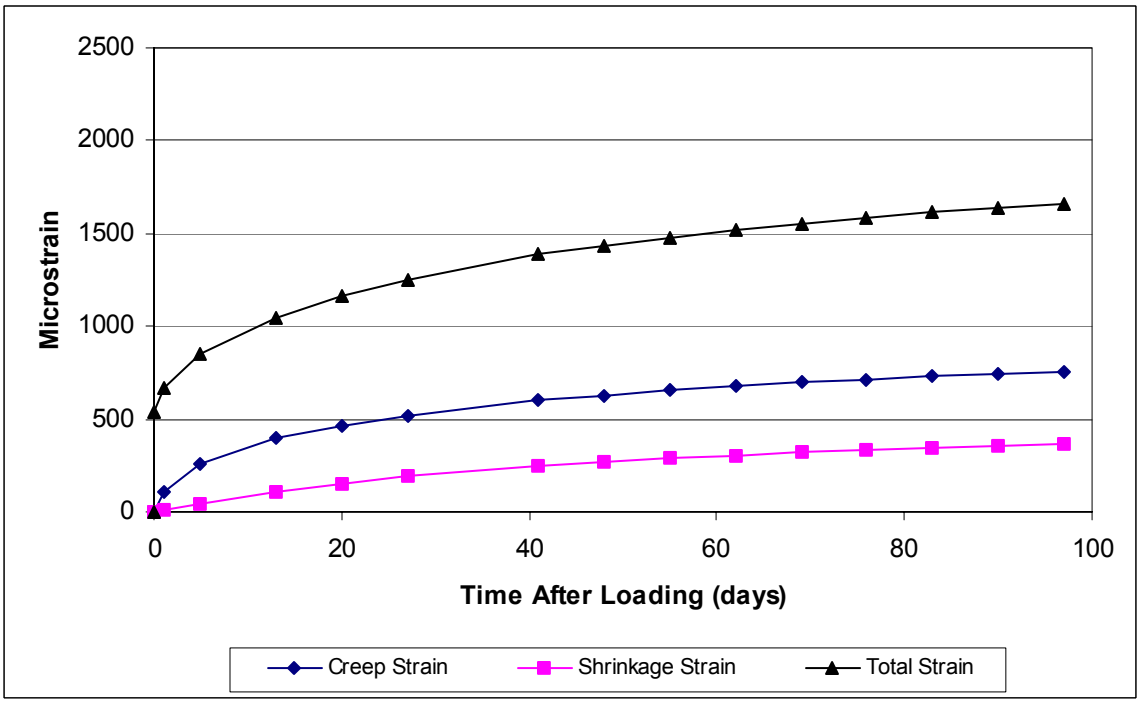

Figure 11 ACI 209 Accelerated Cure Predicted Strains, HSC

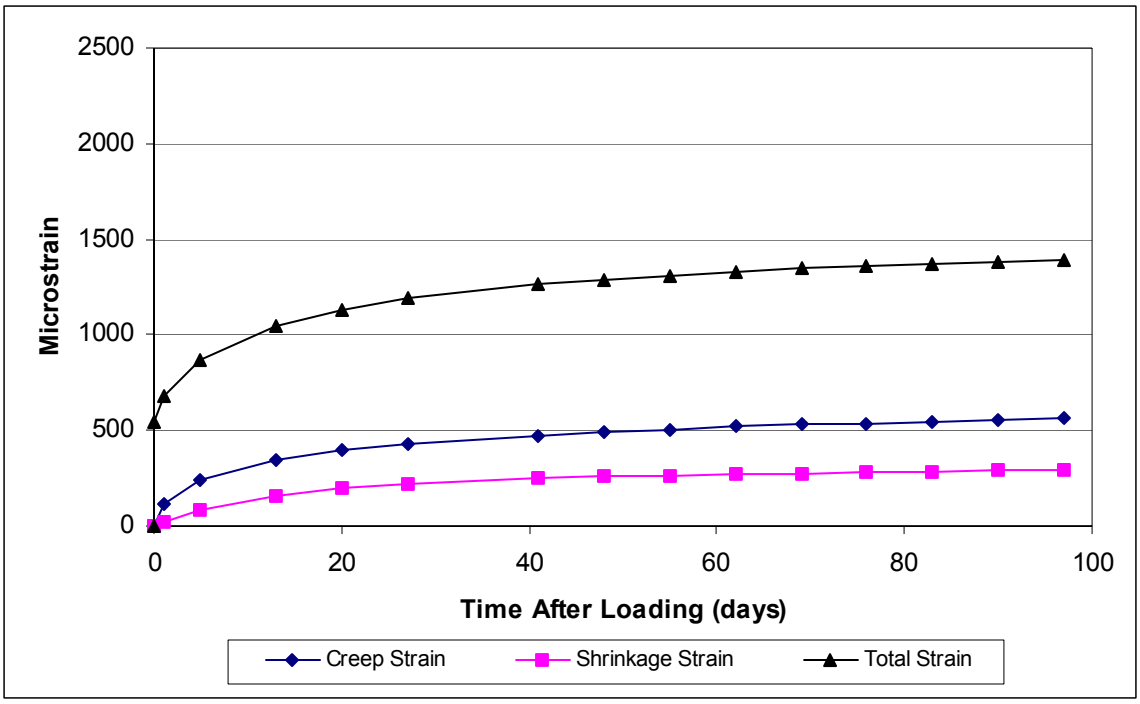

Figure 12 ACI 209 Modified Accelerated Cure Predicted Strains, HSC

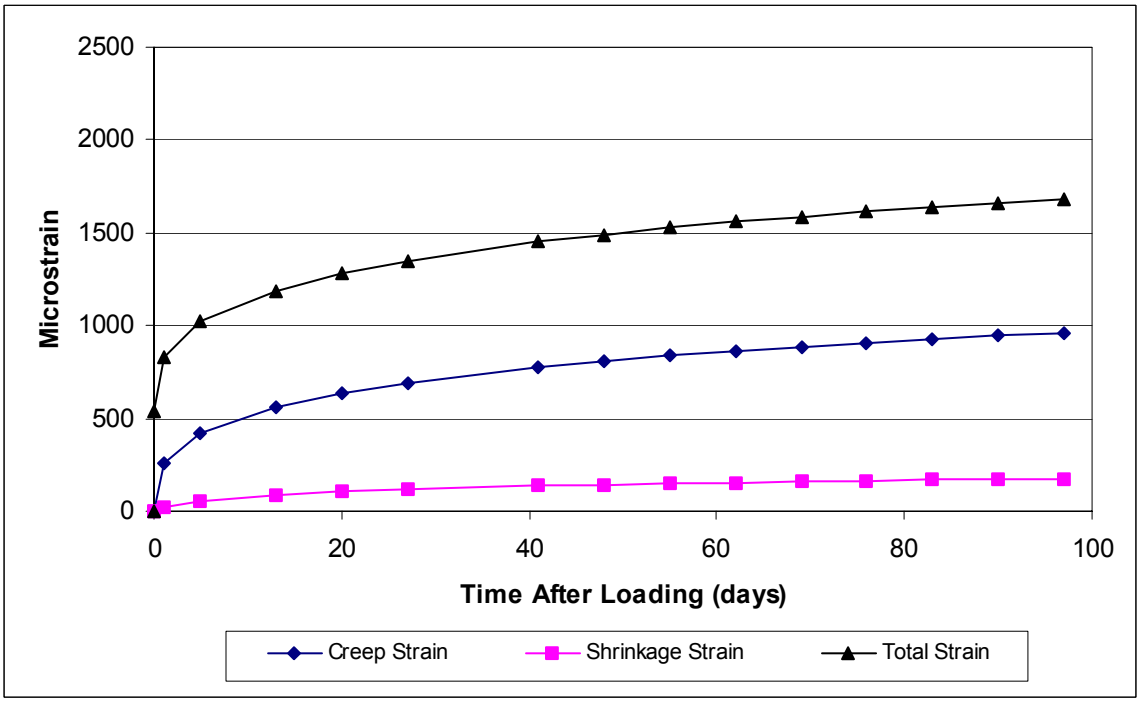

Figure 13 CEB-MC90 Accelerated Cure Predicted Strains, HSC

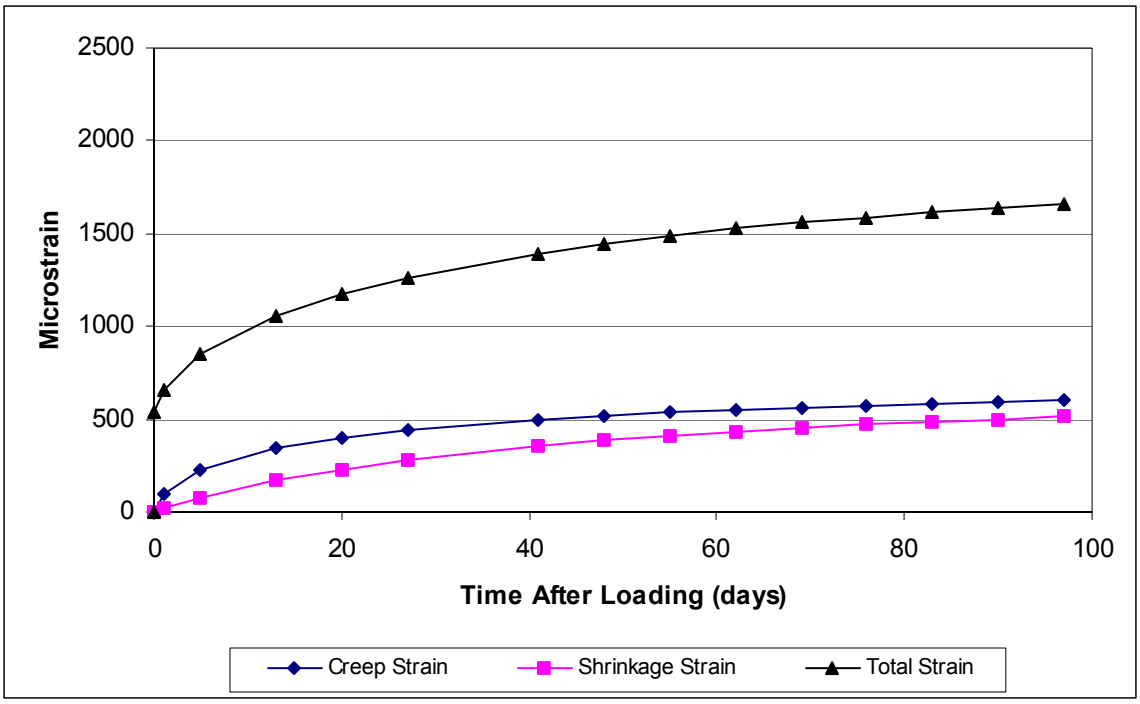

Figure 14 AASHTO-LRFD Accelerated Cure Predicted Strains, HSC

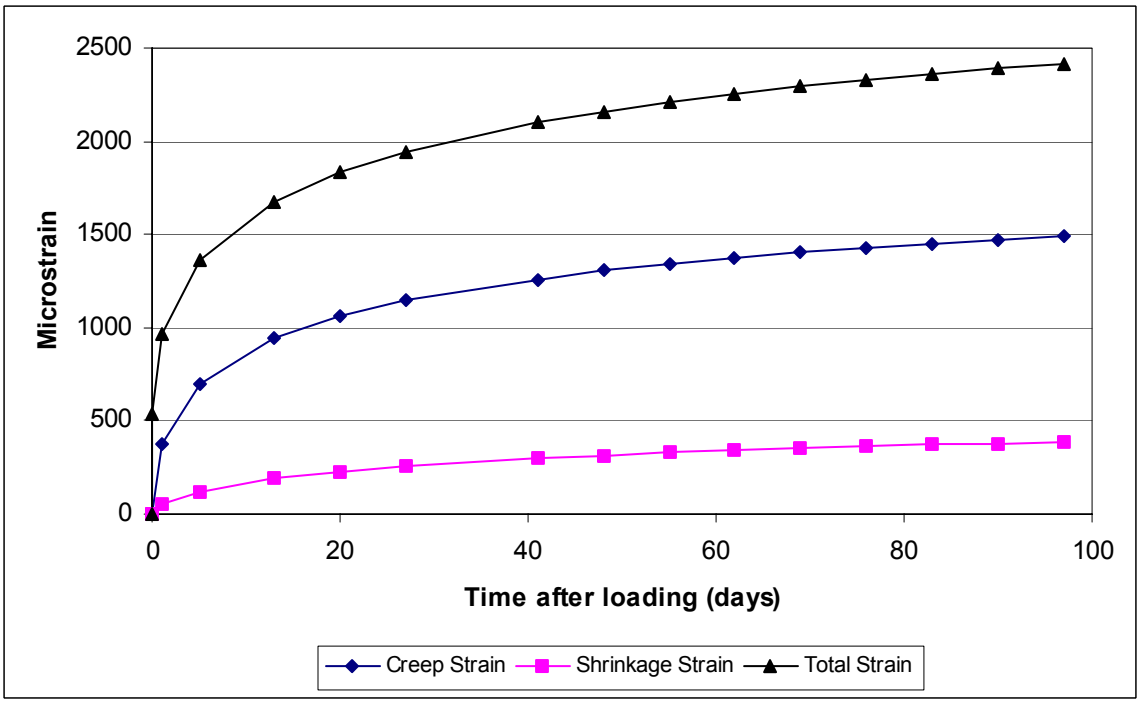

Figure 15 GL2000 Accelerated Cure Predicted Strains, HSC

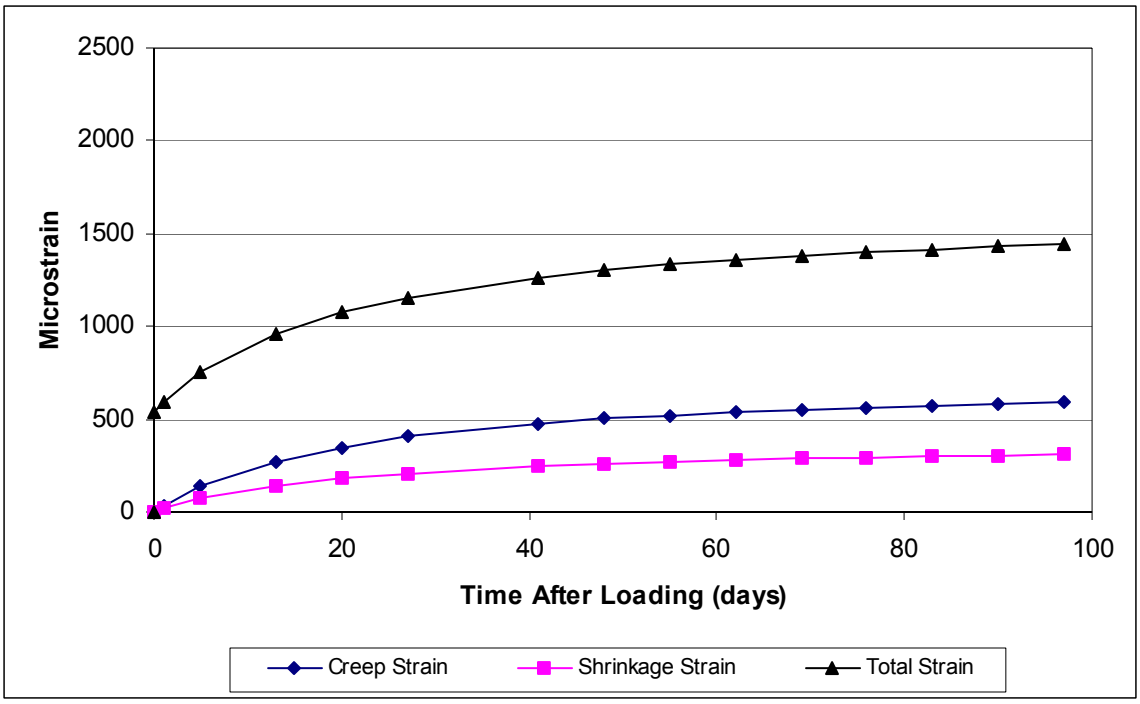

Figure 16 Tadros Accelerated Cure Predicted Strains, HSC

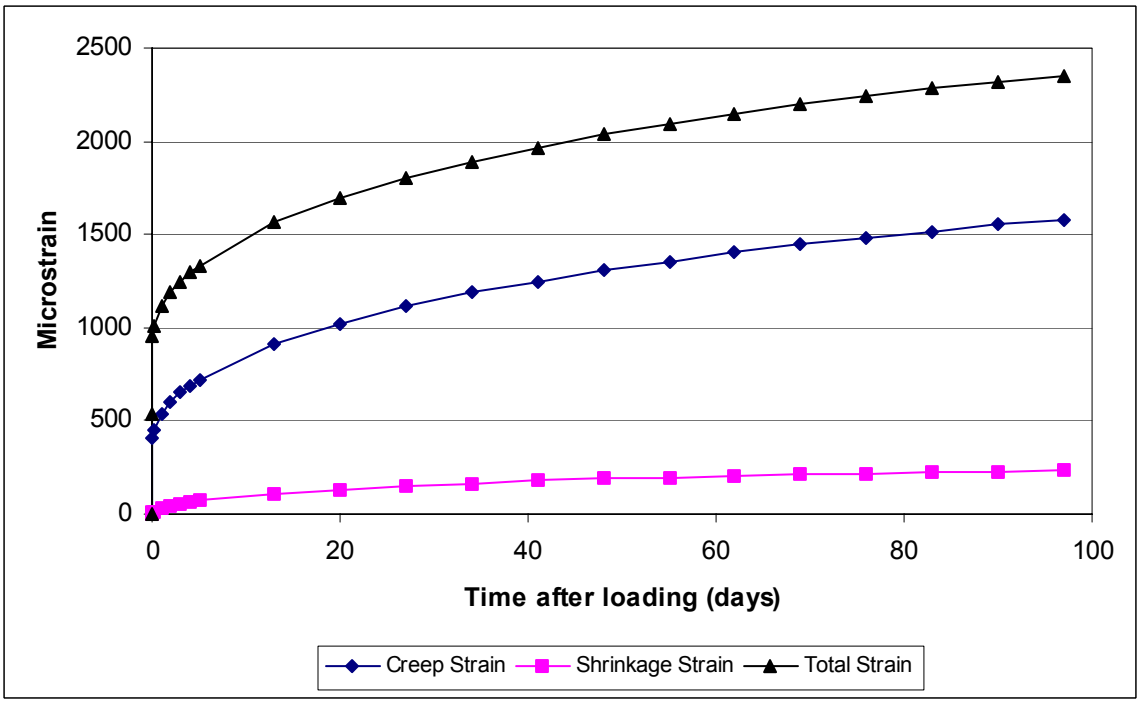

Figure 17 B3 Accelerated Cure Predicted Strains, HSC

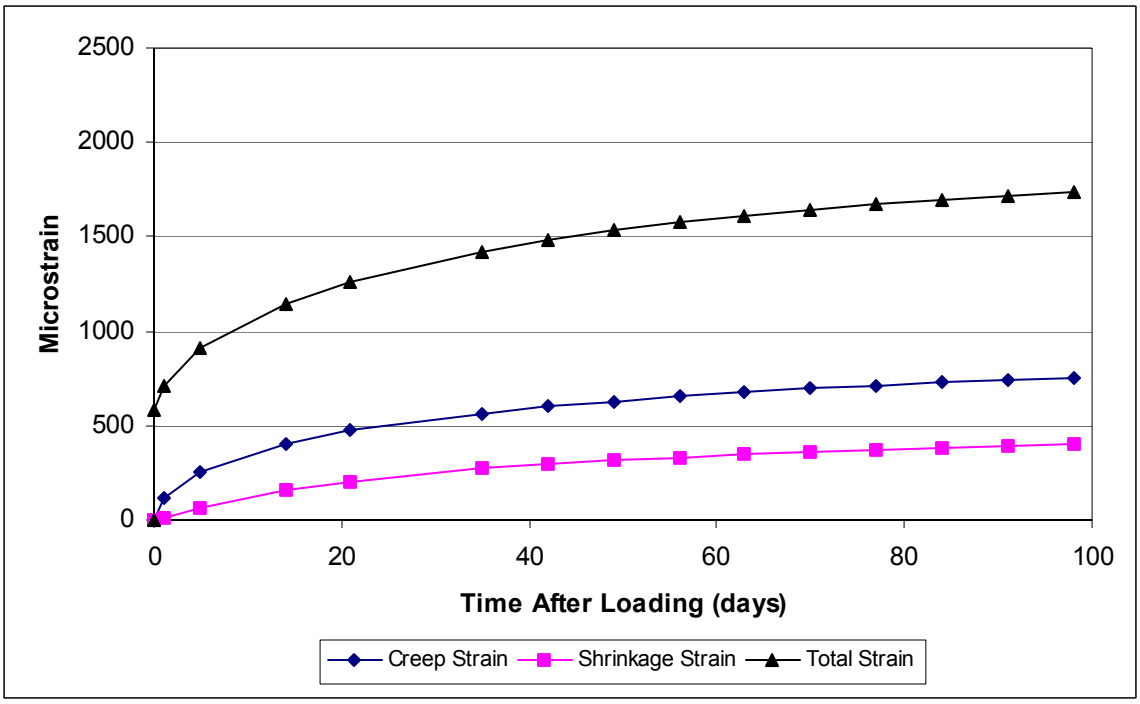

Figure 18 ACI 209 Standard Cure Predicted Strains, HSC

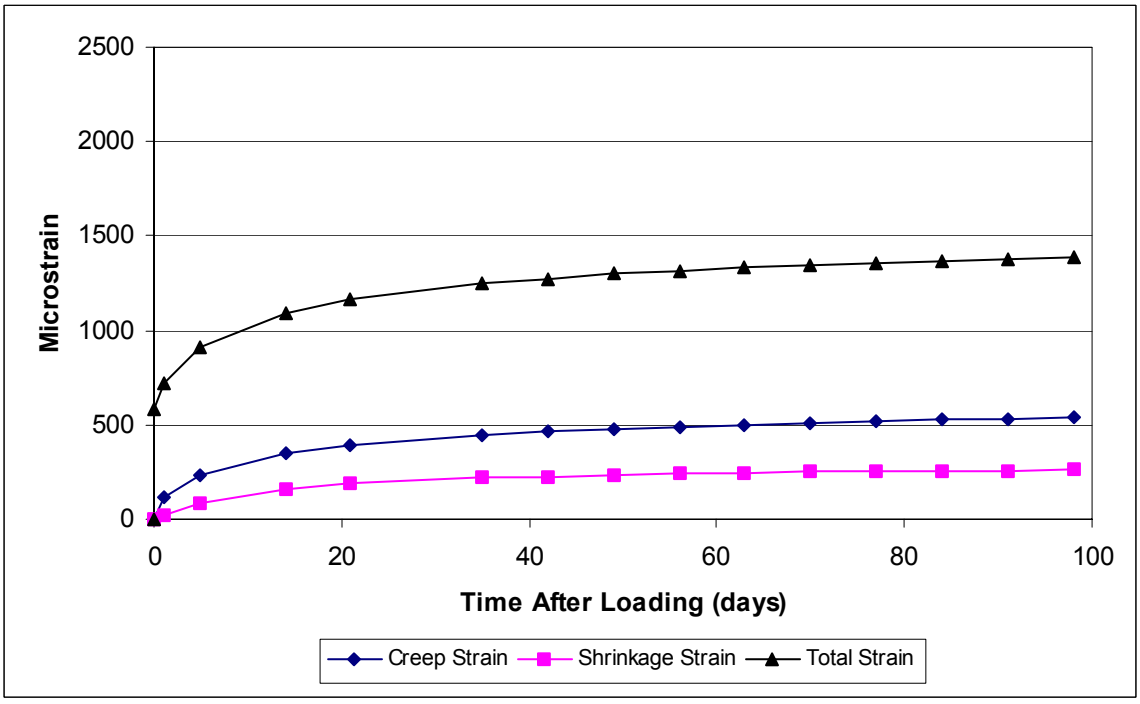

Figure 19 ACI 209 Modified Standard Cure Predicted Strains, HSC

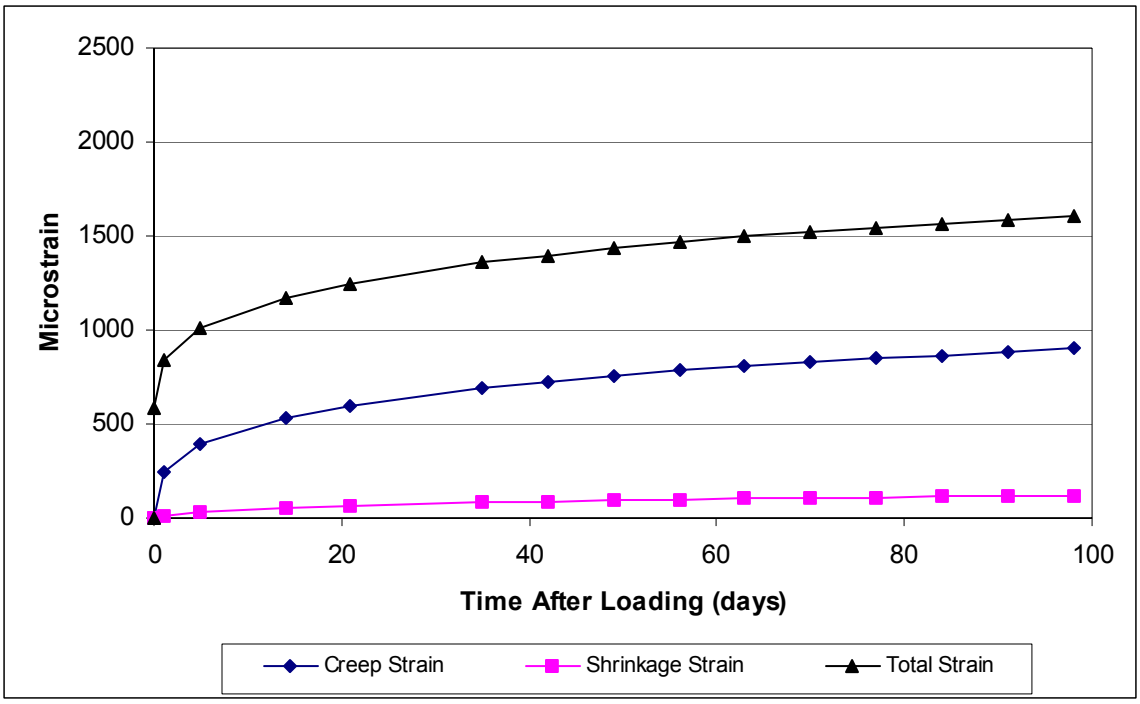

Figure 20 CEB-MC90 Standard Cure Predicted Strains, HSC

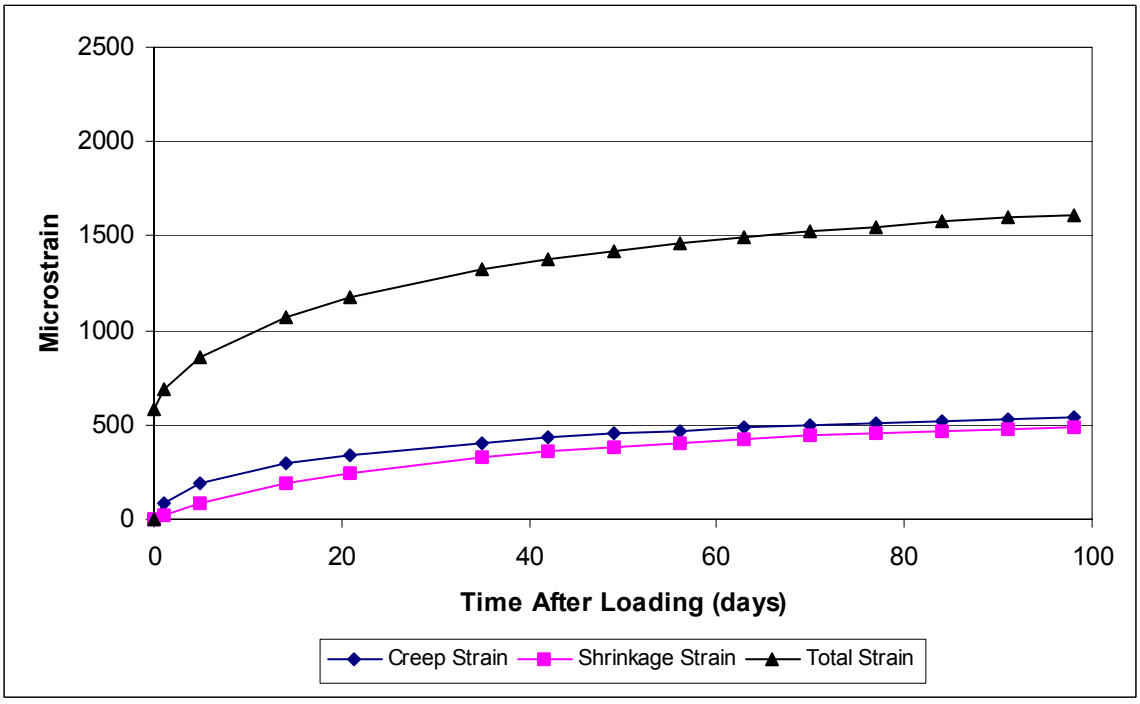

Figure 21 AASHTO-LRFD Standard Cure Predicted Strains, HSC

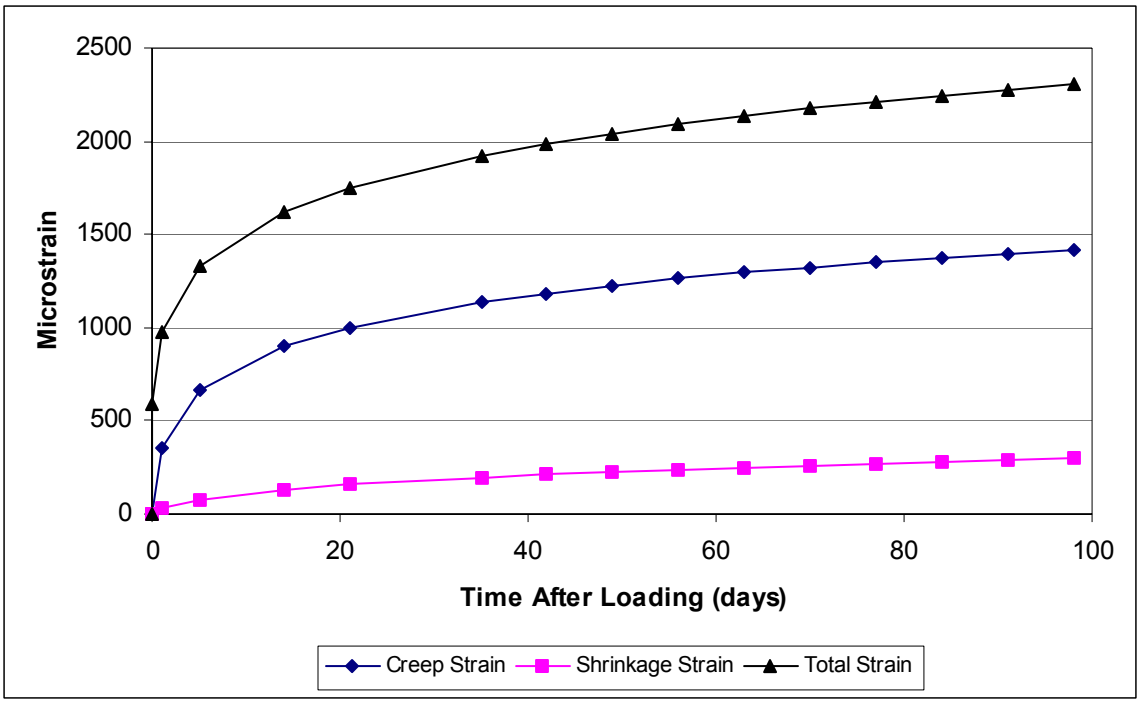

Figure 22 GL2000 Standard Cure Predicted Strains, HSC

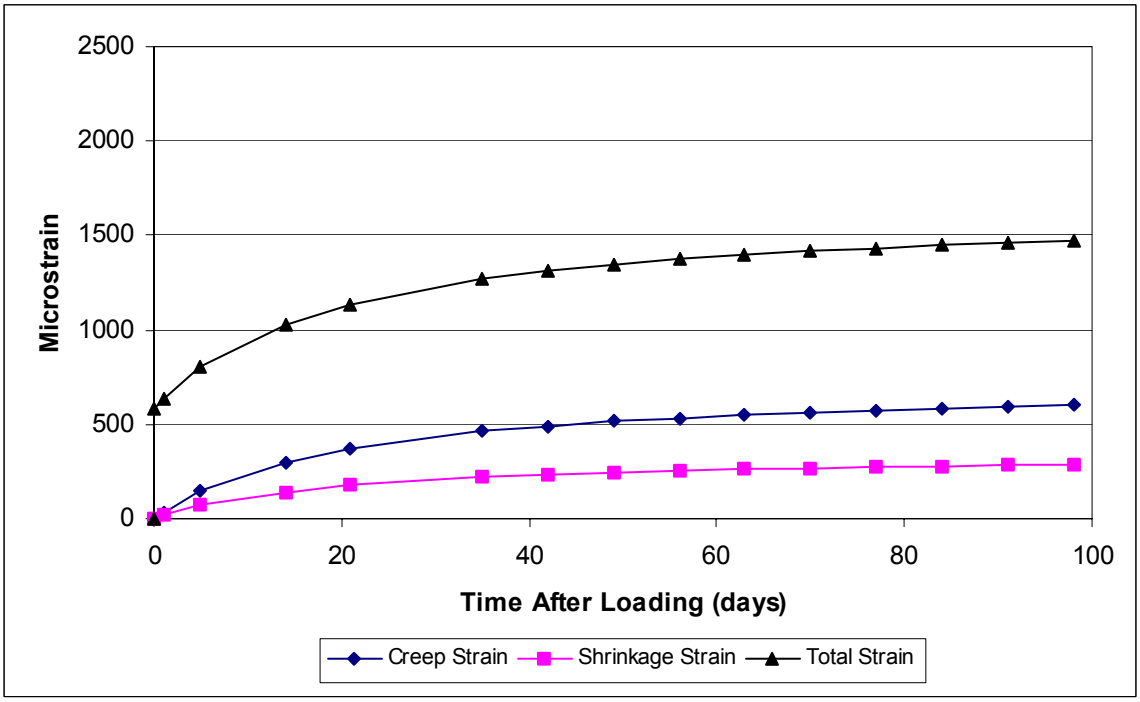

Figure 23 Tadros Standard Cure Predicted Strains, HSC

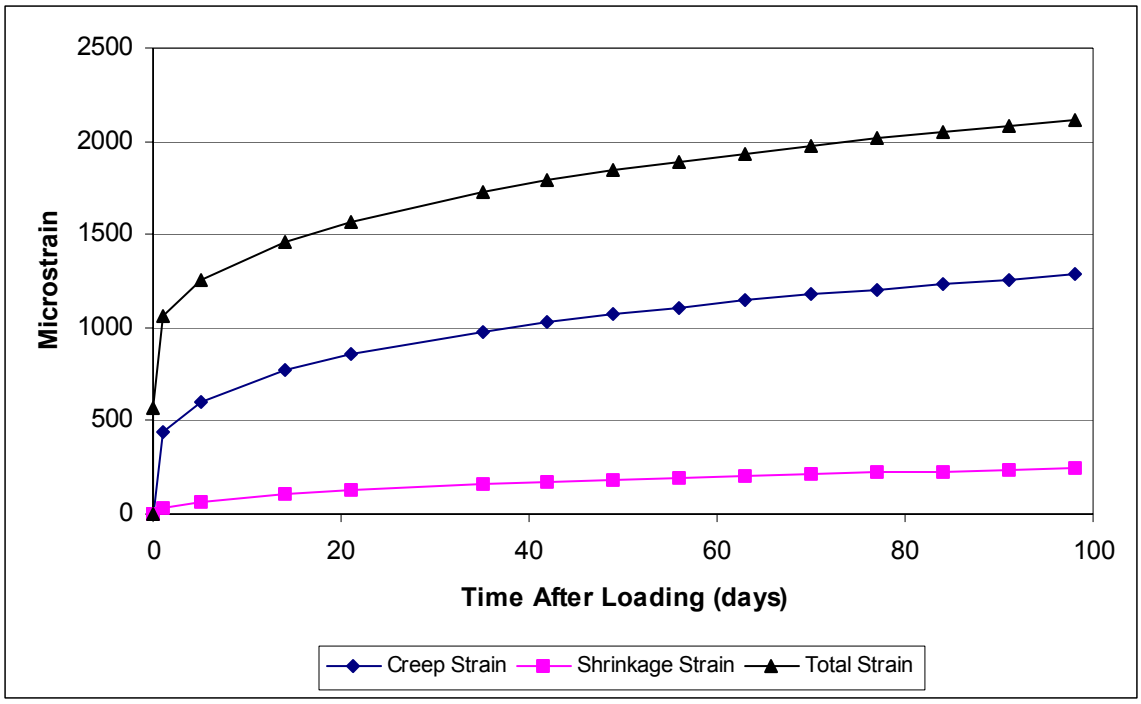

Figure 24 B3 Standard Cure Predicted Strains, HSC

Prediction Model Residuals

As shown in Figures 5 through 7 and 8 through 10, respectively, the experimental strains for the two accelerated cure batches were not significantly different, and likewise for the standard cure batches. Therefore, the two batches of HSC from each curing method were combined and treated as a single data set for comparison with the models. The accelerated cure and standard cure mean residuals and 95% confidence intervals are shown as a function of time for the eight accelerated cure specimens and six standard cure specimens. A residual is defined as the algebraic difference between a predicted value and an experimental value. A negative residual indicates that a model is underpredicting the experimental data, and a positive residual indicates the model is overpredicting the experimental data. Figures 25 through 28 present the total strain residuals of the prediction models for the accelerated cure and Figures 29 through 32 for the standard cure batches.

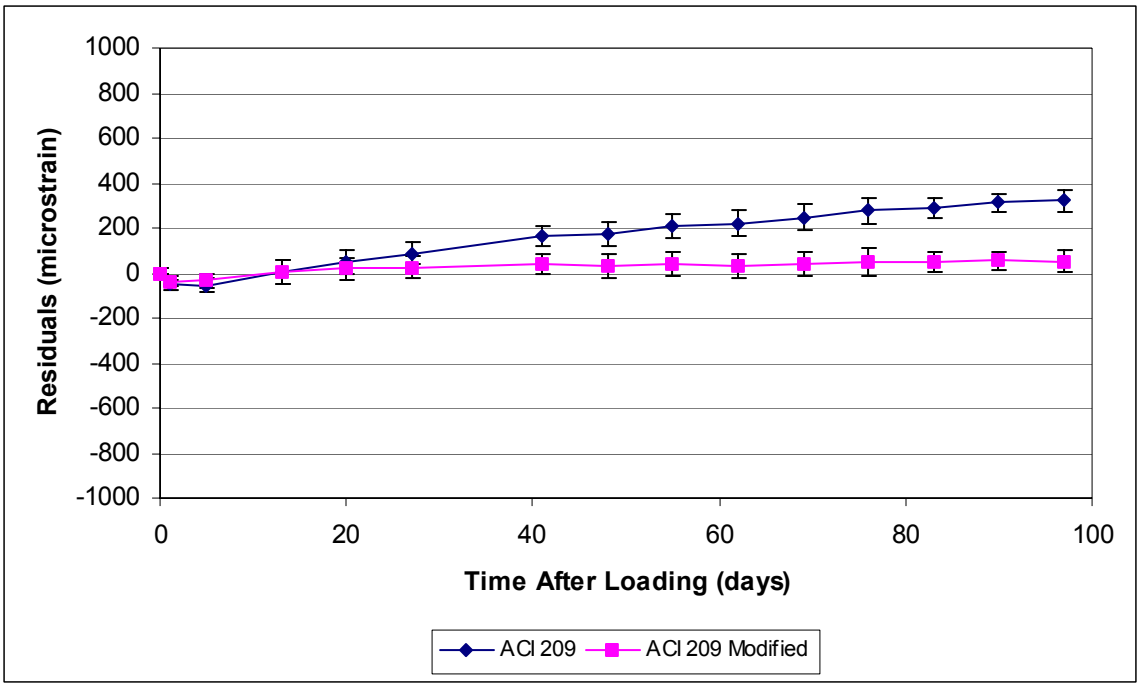

Figure 25 ACI 209 and ACI 209 Modified Accelerated Cure Total Strain Residuals, HSC

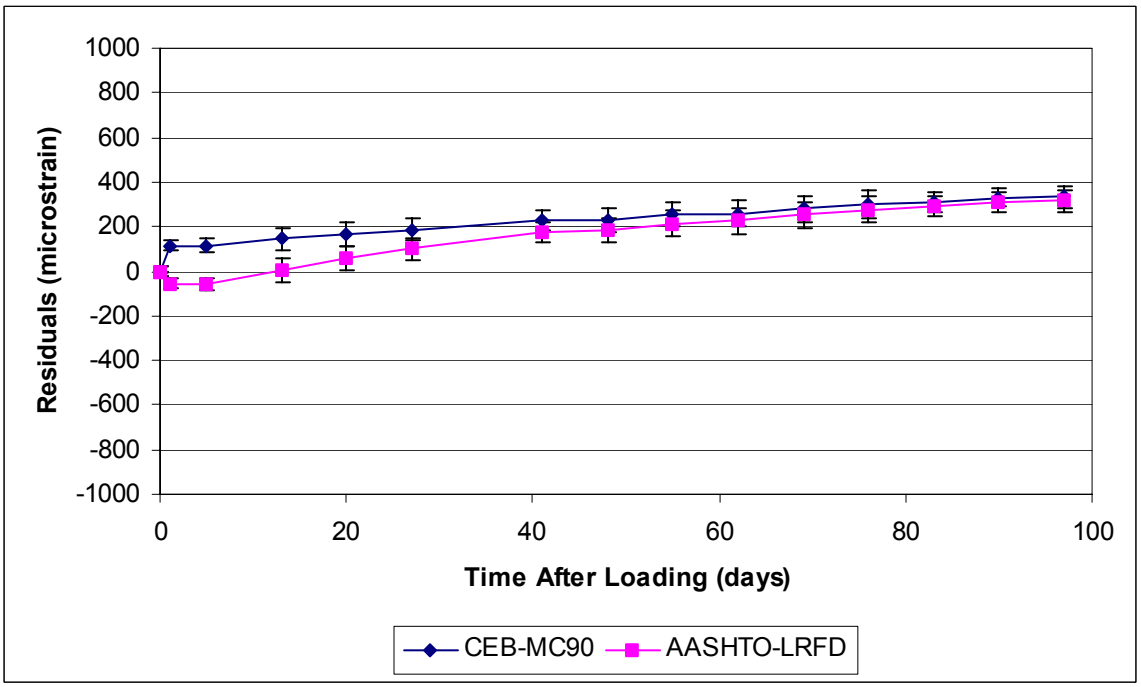

Figure 26 CEB-MC90 and AASHTO-LRFD Accelerated Cure Total Strain Residuals, HSC

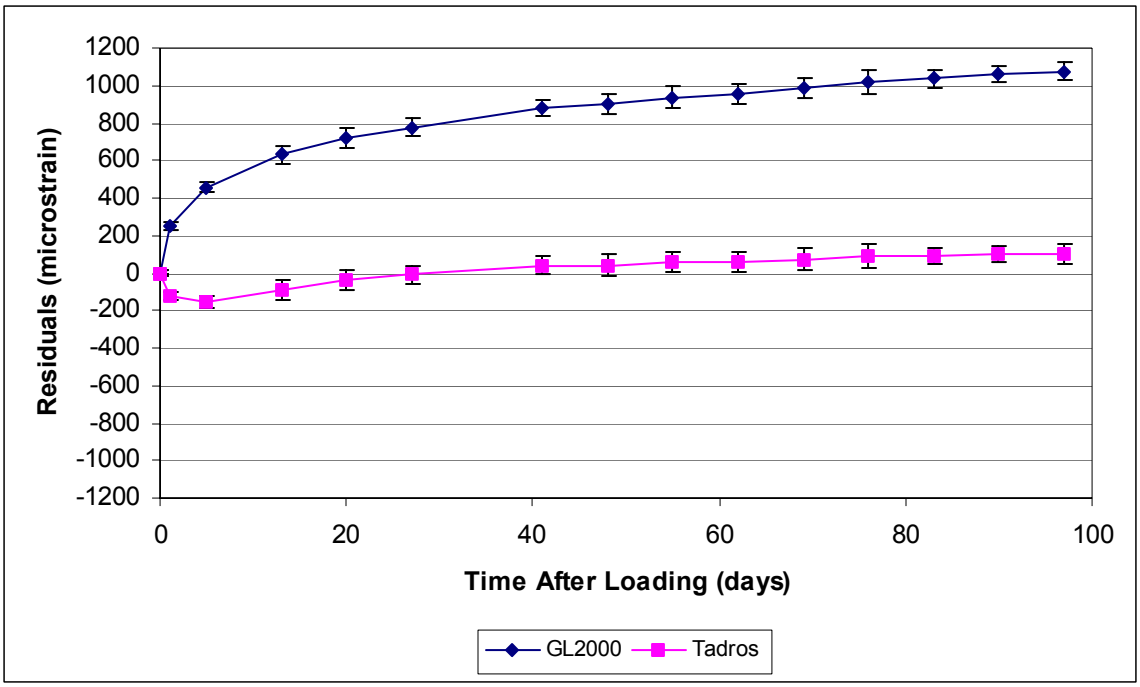

Figure 27 GL2000 and Tadros Accelerated Cure Total Strain Residuals, HSC

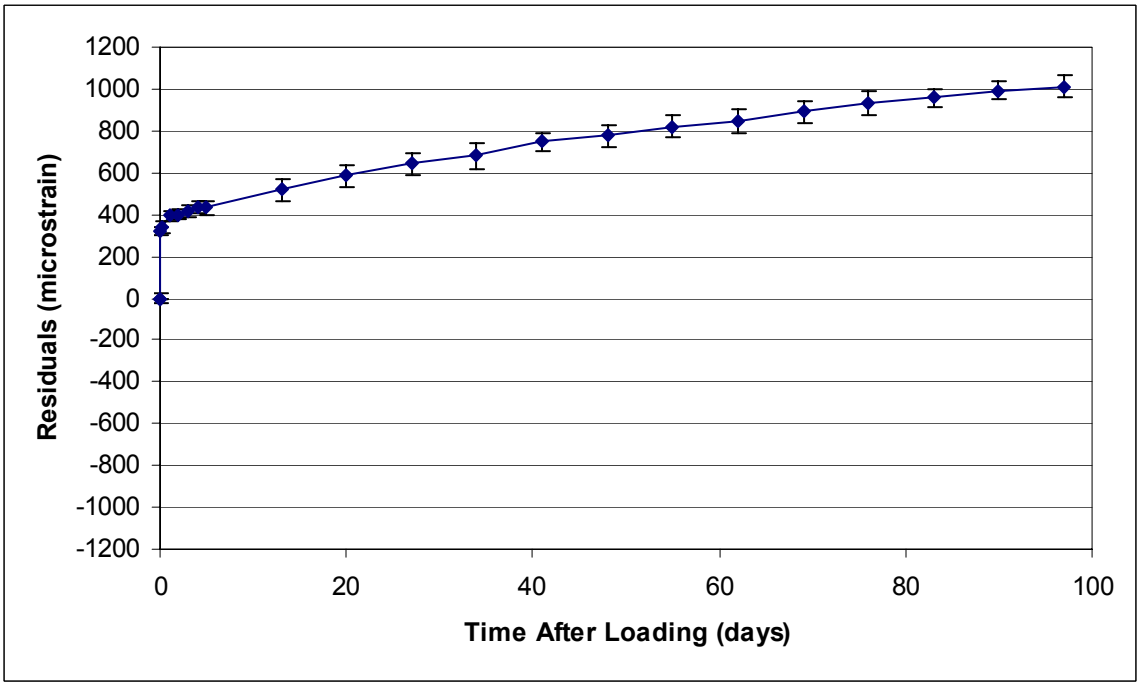

Figure 28 B3 Accelerated Cure Total Strain Residuals, HSC

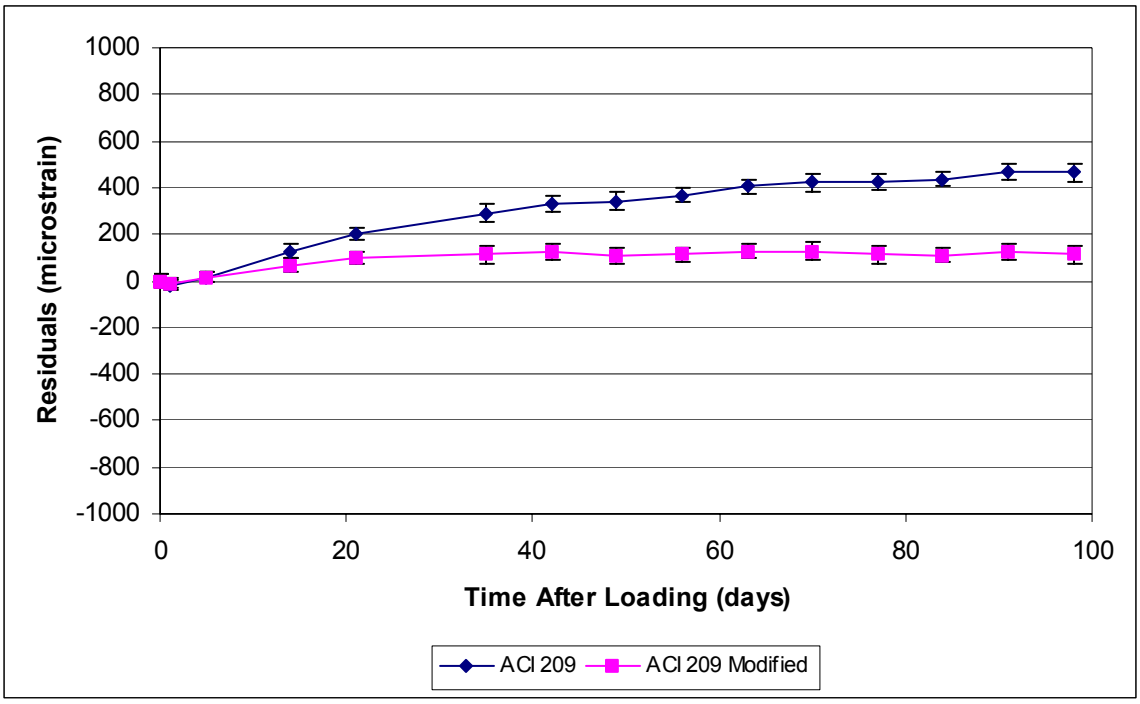

Figure 29 ACI 209 and ACI 209 Modified Standard Cure Total Strain Residuals, HSC

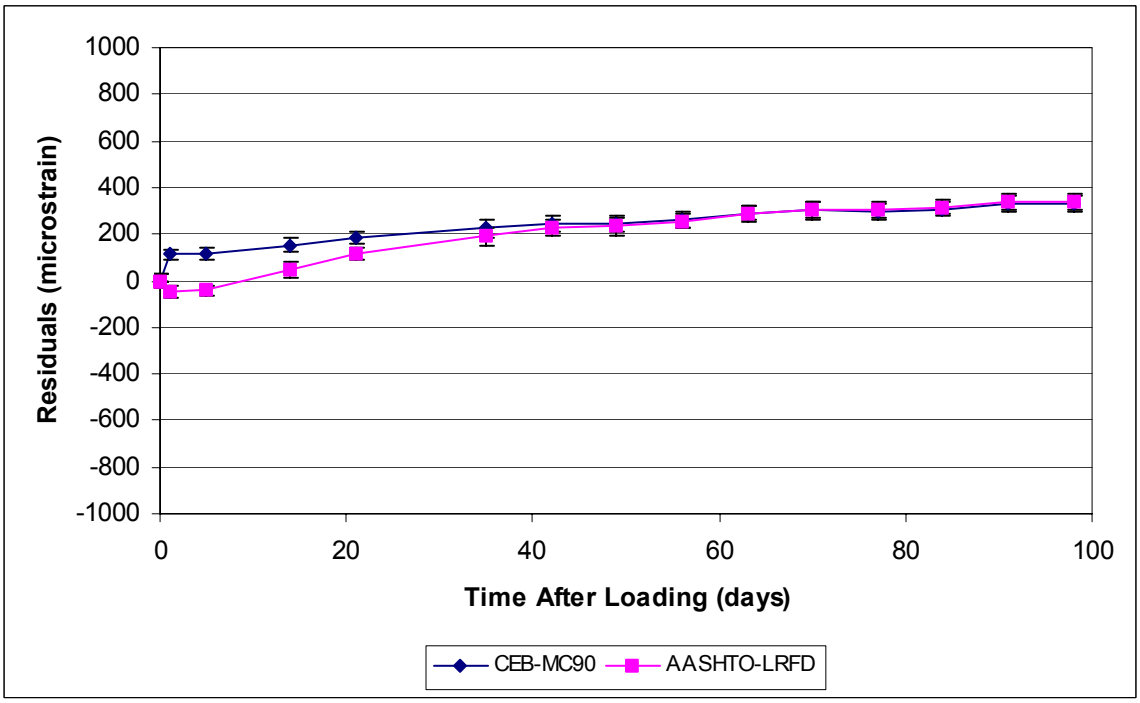

Figure 30 CEB-MC90 and AASHTO-LRFD Standard Cure Total Strain Residuals, HSC

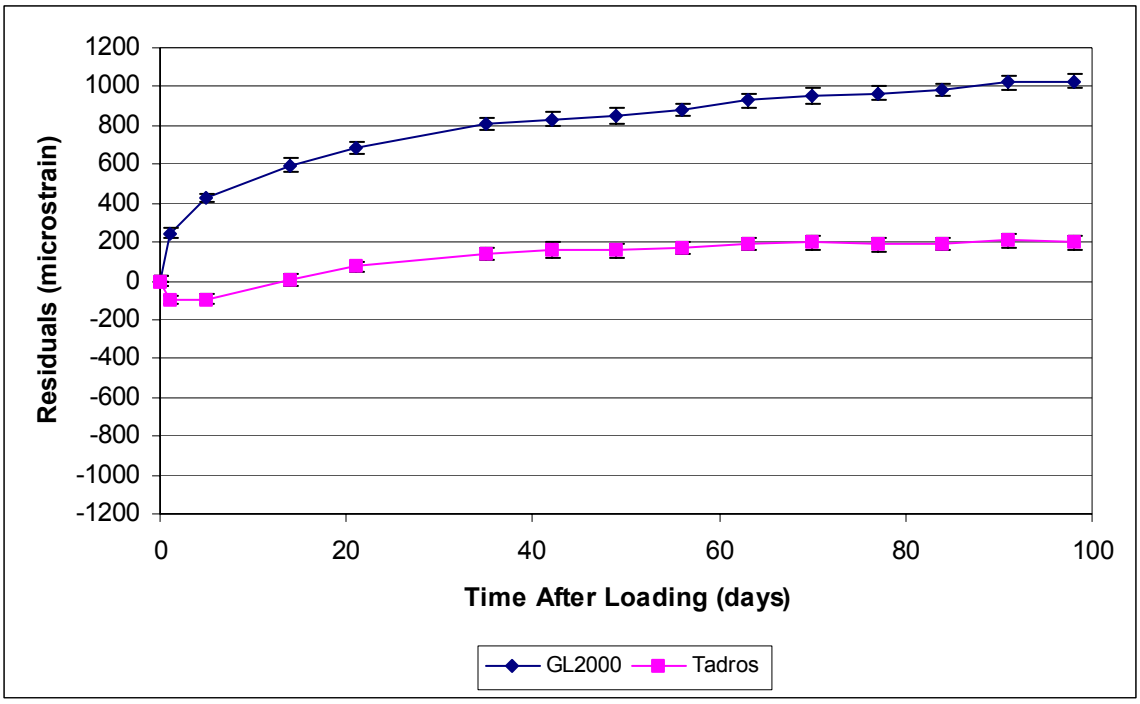

Figure 31 GL2000 and Tadros Standard Cure Total Strain Residuals, HSC

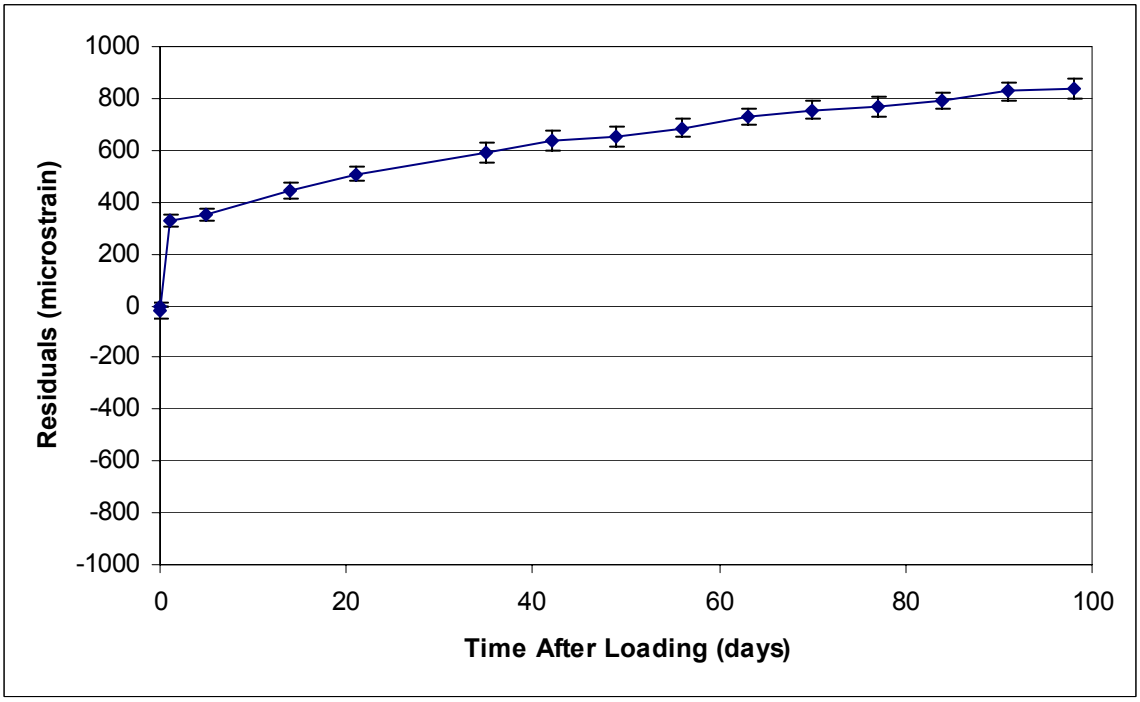

Figure 32 B3 Standard Cure Total Strain Residuals, HSC

Shrinkage Prisms

The data from standard cure HSC batches 3A and 4A were not significantly different and thus were combined for comparison purposes. The mean and 95% confidence interval of the six prisms are shown in Figures 33 through 36, along with the predicted values from the seven models. Shrinkage prism data are presented in terms of percent length change.

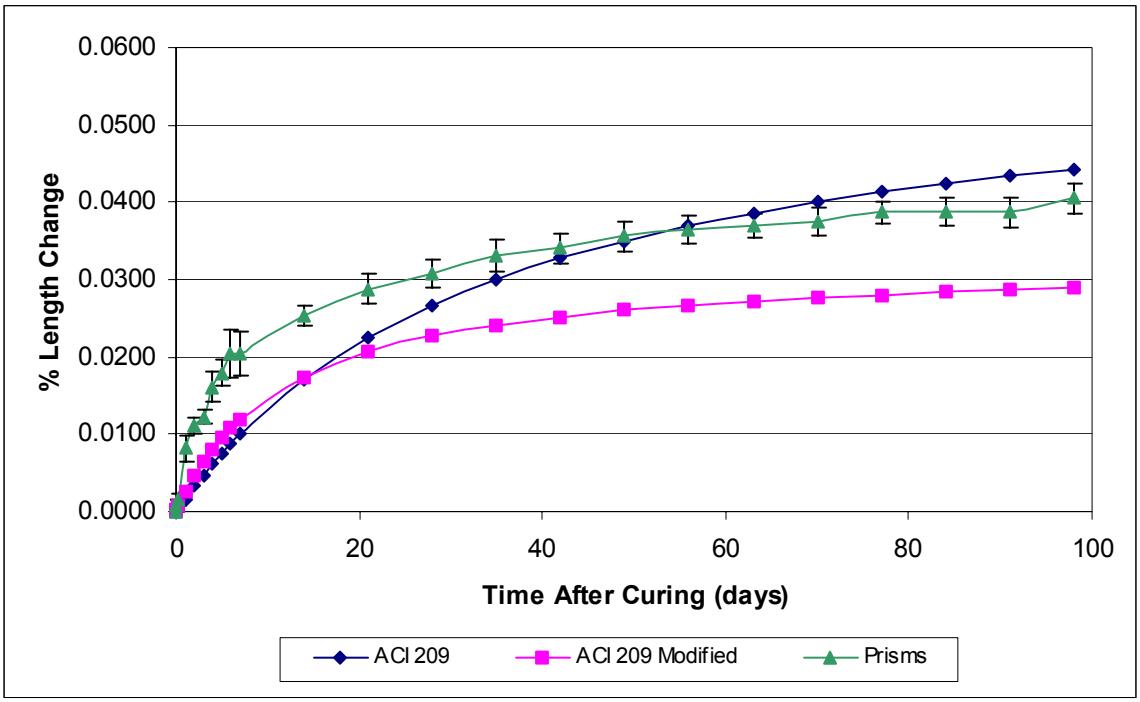

Figure 33 Shrinkage Prism Data with ACI 209 and ACI 209 Modified Models, HSC

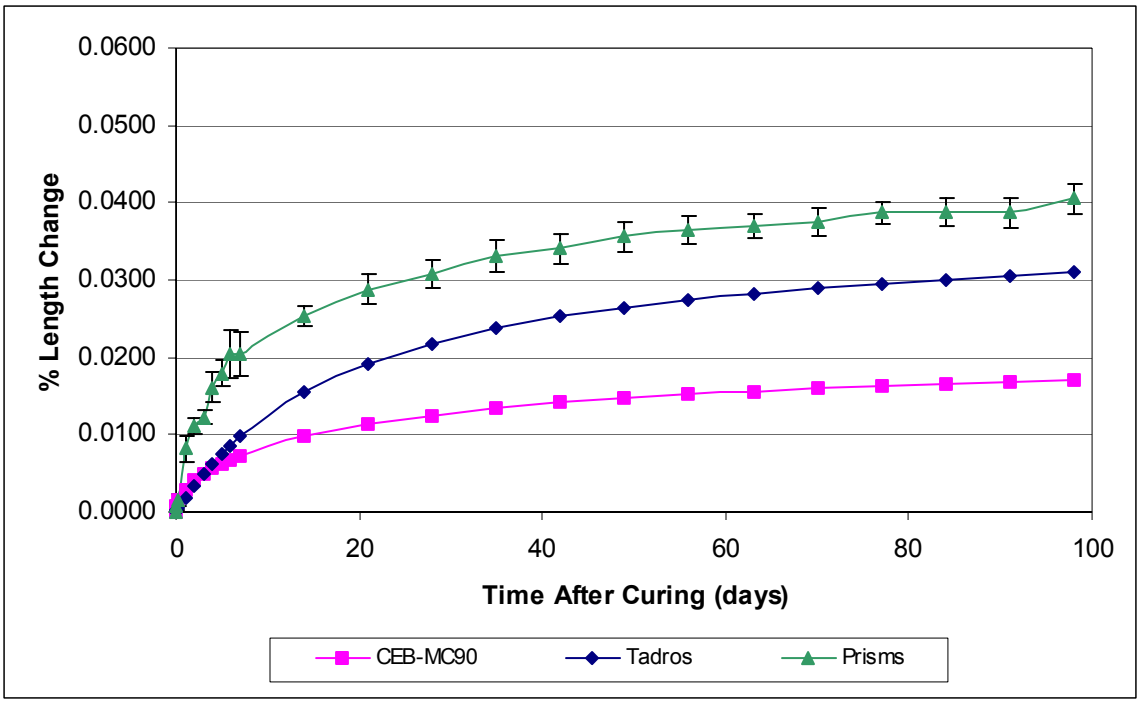

Figure 34 Shrinkage Prism Data with CEB-MC90 and Tadros Models, HSC

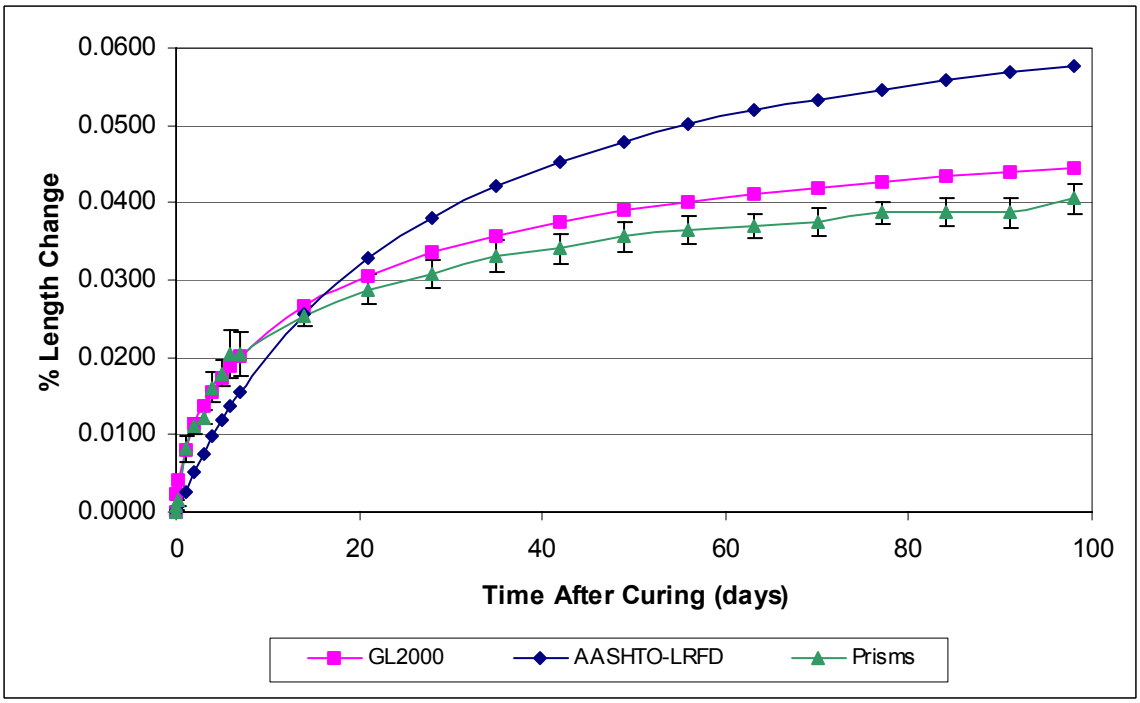

Figure 35 Shrinkage Prism Data with GL2000 and AASHTO-LRFD Models, HSC

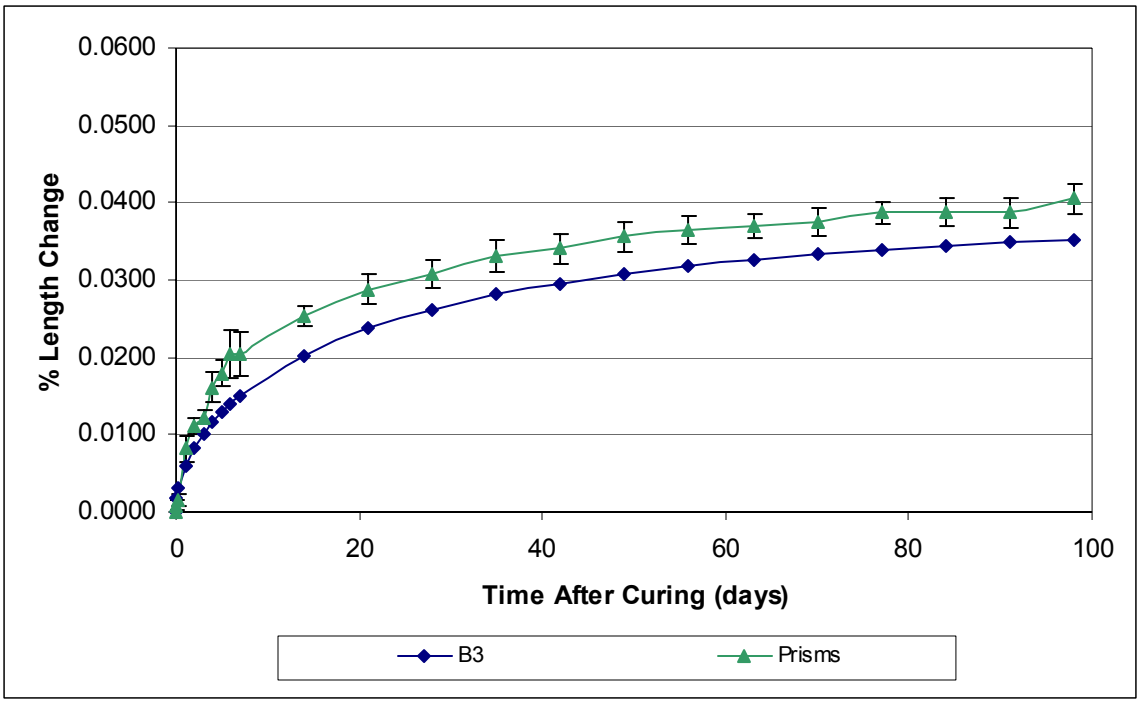

Figure 36 Shrinkage Prism Data with B3 Model, HSC

Vibrating Wire Gages

Figures 37 and 38 present the total strain measurements and Figures 39 and 40 present the shrinkage measurements of the specimens from accelerated batch 2A that had the embedded VWGs. The Whittemore gage and VWG measurements are shown. Each Whittemore measurement is an average of measurements taken on two diametrically opposite sides of the cylinder. Cylinders 2A-2 and 2A-4 are loaded creep specimens, and cylinders 2A-6 and 2A-8 are unloaded shrinkage specimens.

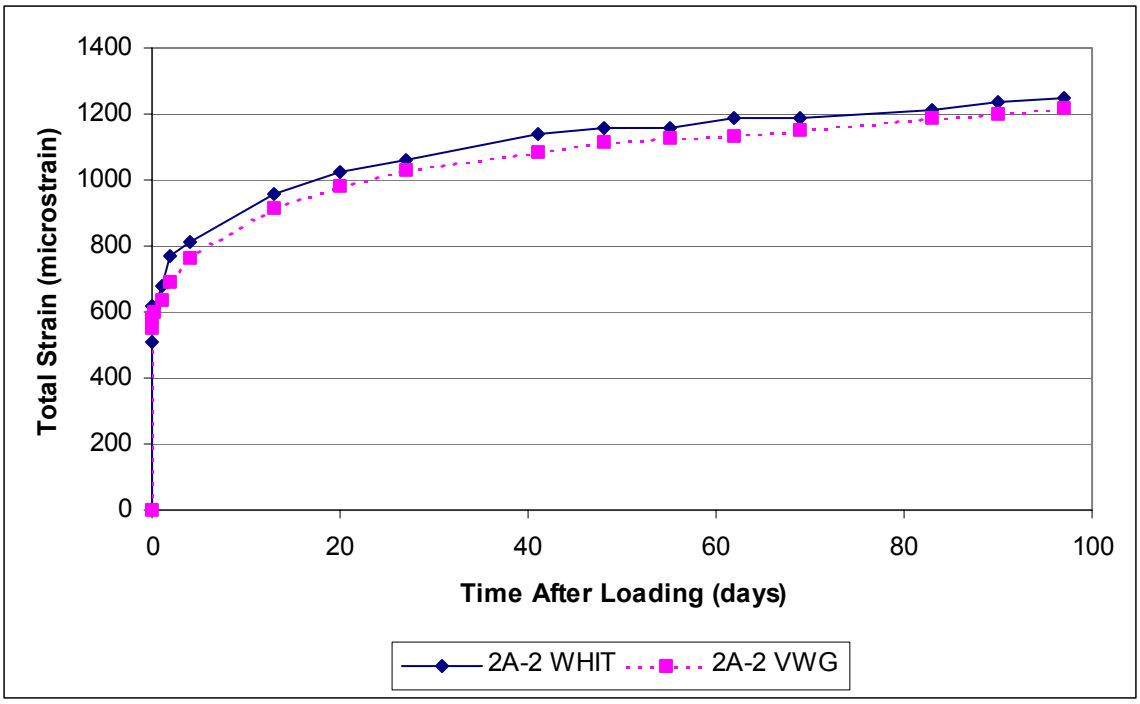

Figure 37 Cylinder 2A-2 Whittemore and VWG Total Strains, HSC

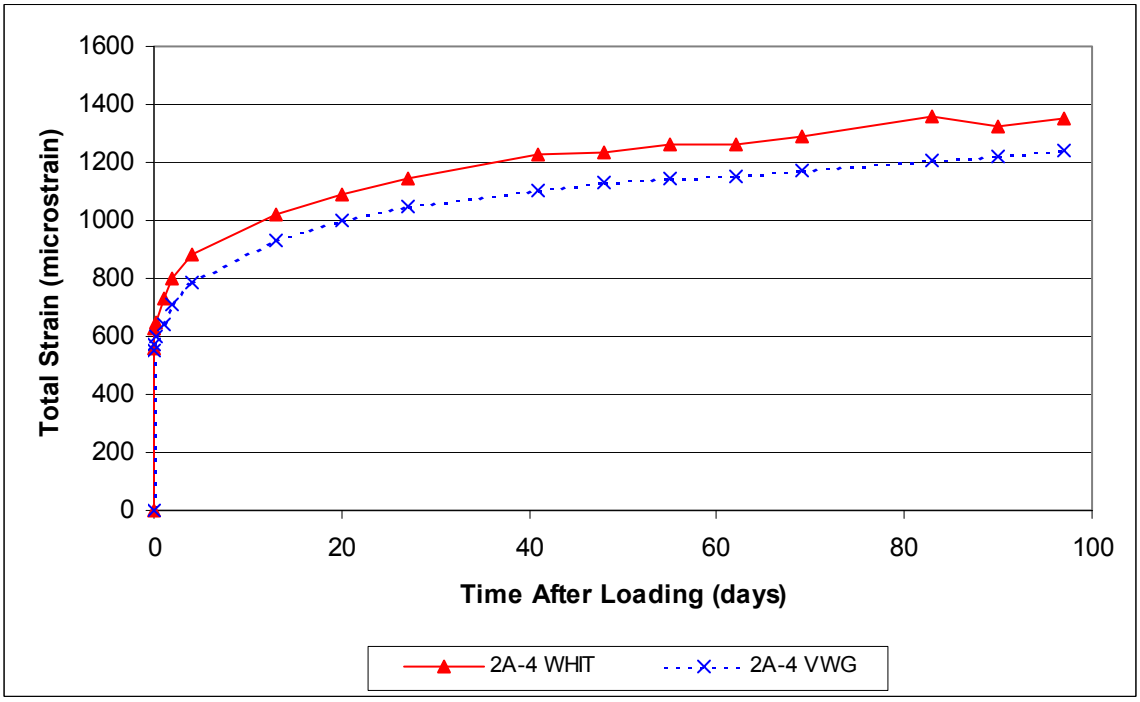

Figure 38 Cylinder 2A-4 Whittemore and VWG Total Strains, HSC

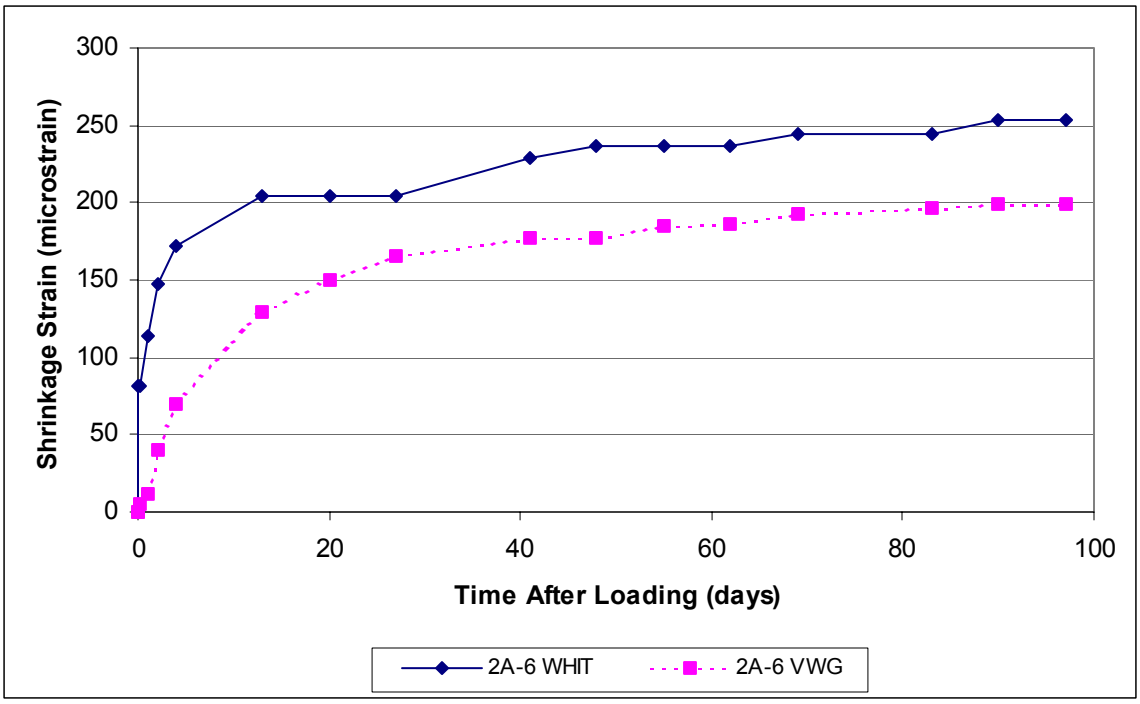

Figure 39 Cylinder 2A-6 Whittemore and VWG Shrinkage Strains, HSC

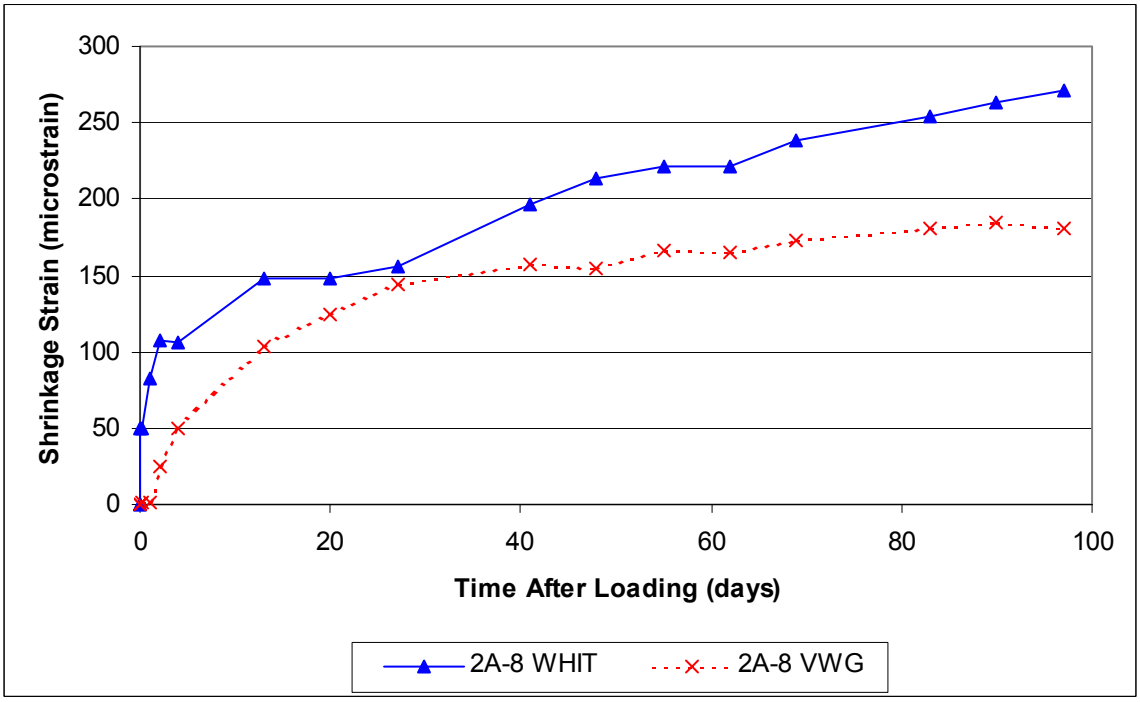

Figure 40 Cylinder 2A-8 Whittemore and VWG Shrinkage Strains, HSC

LTHSC

The compressive strength, tensile strength, modulus of elasticity, and thermal coefficient data for the LTHSC standard and accelerated cure batches are summarized in the following sections. The standard and accelerated experimental total strain, creep strain, and shrinkage strains per batch are presented along with the predicted values for the four models. The precision of the experimental values is examined as are the residuals of four prediction models.

Strength and modulus measurements for the LTHSC bridge beams (BB1 and BB2) are also presented. The compressive strength measurements are reported by Bayshore Concrete Products. Splitting tensile strength and modulus of elasticity were measured by the Virginia Transportation Research Council.

Compressive Strength

Standard Cure

Figure 41 presents the LTHSC standard cure compressive strengths at 7 and 28 days. The figure also presents the specified release strength, f'_{ci}, and the 28-day design compressive strength, f'_c. The f'_{ci} is 60% of the 28-day compressive design strength. The 7-day compressive strengths were 36 MPa and 35 MPa (5450 and 5100 psi) for batches 2 and 3, respectively. The 28-day compressive strengths were 43 MPa and 43 MPa (6210 psi and 6290 psi) for batches 2 and 3, respectively.

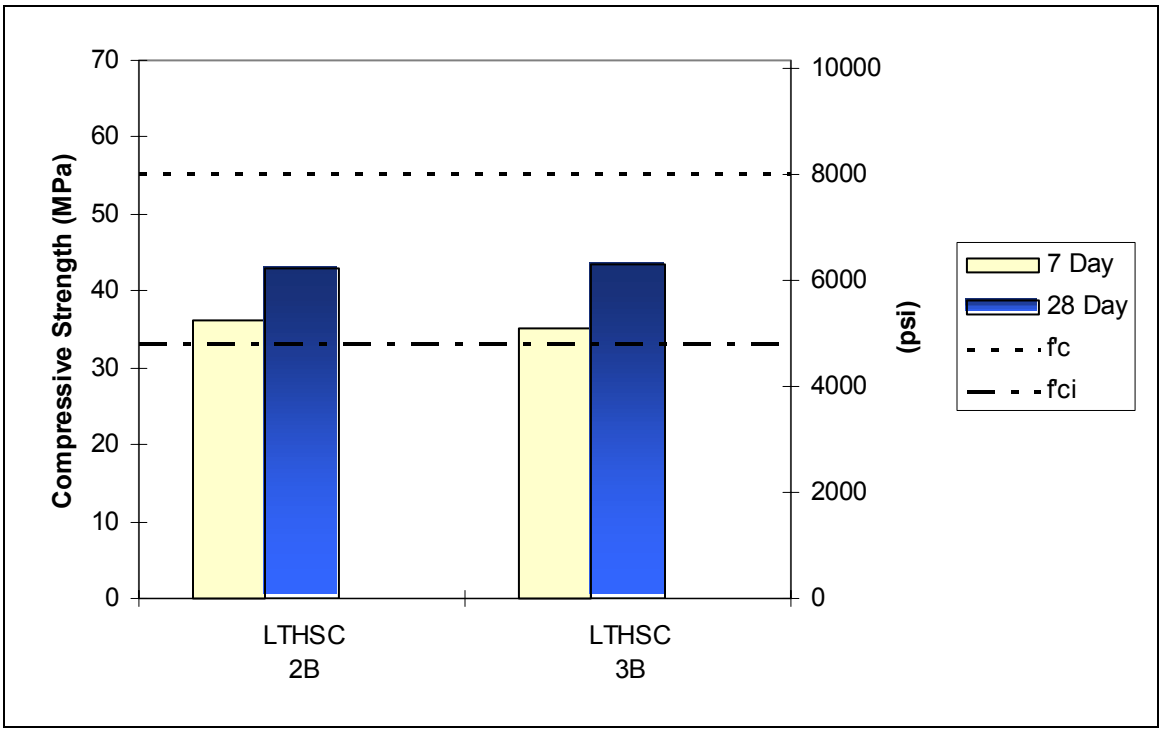

Figure 41 Standard Cure Compressive Strengths, LTHSC

Accelerated Cure

Figure 42 presents the LTHSC accelerated cure compressive strengths at 17 hours, 1 day, 7 days, and 28 days. The figure also presents f'_{ci}, the specified release strength, and f'_c, the 28-day design strength, for the Chickahominy River Bridge. The 17-hour compressive strengths were 44 MPa and 32 MPa (6300 psi and 4620 psi) for batches 4 and 5, respectively. The 17-hour compressive strength was 30 MPa (4350 psi) for Bayshore beam 1. The 1-day compressive strengths were 33 MPa and 32 MPa (4800 psi and 4620 psi) for Bayshore beams 1 and 2, respectively. The 7-day compressive strengths were 43 MPa and 38 MPa (6250 psi and 5570 psi) for batches 4 and 5, respectively. The 7-day compressive strengths were 49 MPa and 48 MPa (7110 psi and 6900 psi) for Bayshore beams 1 and 2, respectively. The 28-day compressive strengths were 50 MPa and 38 MPa (7320 psi and 5470 psi) for batches 4 and 5, respectively. The 28-day compressive strengths were 57 MPa and 55 MPa (8310 psi and 7900 psi) for Bayshore beams 1 and 2, respectively.

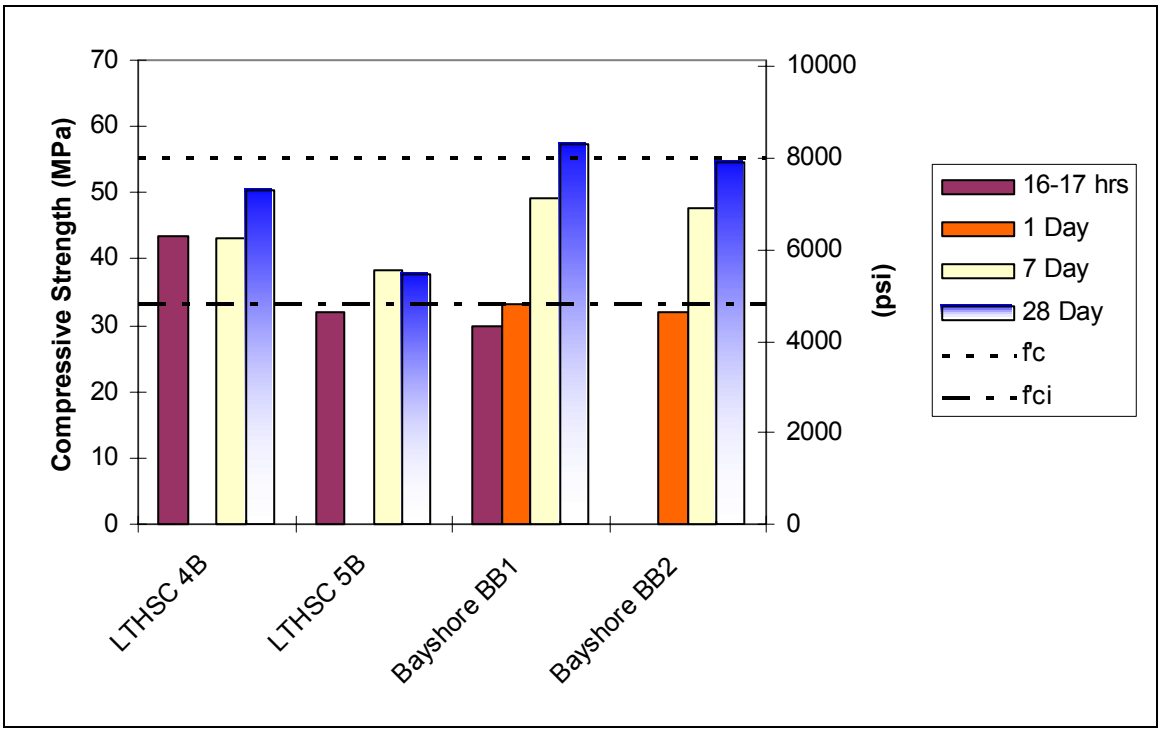

Figure 42 Accelerated Cure Compressive Strengths, LTHSC

Tensile Strength

Standard Cure

Figure 43 presents the LTHSC tensile strengths for the standard and accelerated cure batches. The figure also presents the AASHTO allowable design stress of 200 psi at release and the 28-day design cracking stress of 492 psi for lightweight aggregate concretes. The 7-day tensile strengths were 4.0 MPa and 3.4 MPa (580 psi and 500 psi) for batches 2 and 3,

respectively. The 28-day tensile strengths were 4.7 MPa, 4.5 MPa and 4.5 MPa (690 psi and 650 psi, 650 psi) for batches 2 and 3, respectively.

Accelerated Cure

The 17-hour tensile strengths were 4.1 MPa and 3.2 MPa (590 psi and 470 psi) for batches 4 and 5, respectively. The 28-day tensile strengths were 4.5 MPa and 4.0 MPa (650 and 580 psi) for batches 4 and 5, respectively. The 28-day tensile strengths were 4.8 MPa and 4.0 MPa (690 psi and 580 psi) for Bayshore beams 1 and 2, respectively.

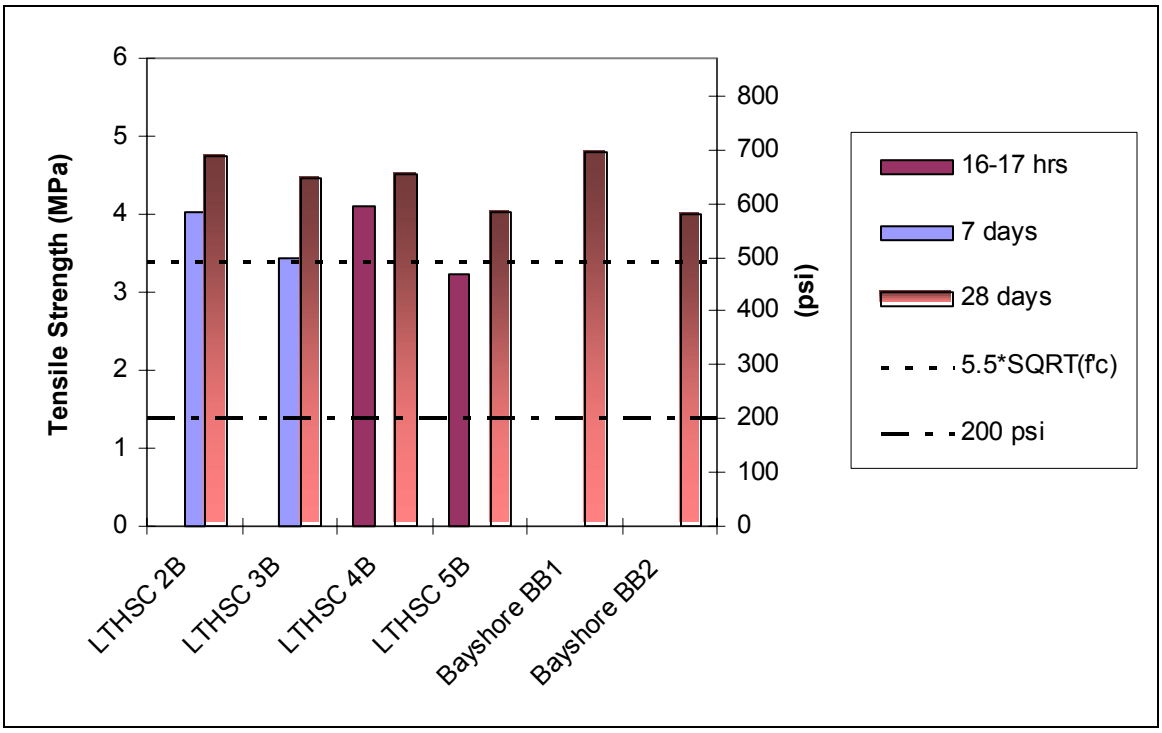

Figure 43 Tensile Strength, LTHSC

Modulus of Elasticity

Standard Cure

Figure 44 presents the LTHSC standard cure moduli of elasticity at 7, 28, 56, and 90 days. The figure also presents the computed AASHTO moduli of elasticity for lightweight aggregate concretes. The 7-day moduli of elasticity were 20 GPa and 19 GPa (2.90 $x10^6$ psi and 2.74 $x10^6$ psi) for batches 2 and 3, respectively. The 28-day moduli of elasticity were 20 GPa and 19 GPa (2.96 $x10^6$ psi and 2.74 $x10^6$ psi) for batches 2 and 3, respectively. The 56-day moduli of elasticity were 21 GPa and 18 GPa (3.04 $x10^6$ psi and 2.64 $x10^6$ psi) for batches 2 and 3, respectively. The 90-day moduli of elasticity were 20 GPa and 20 GPa (2.94 $x10^6$ psi and 2.84 $x10^6$ psi) for batches 2 and 3, respectively.

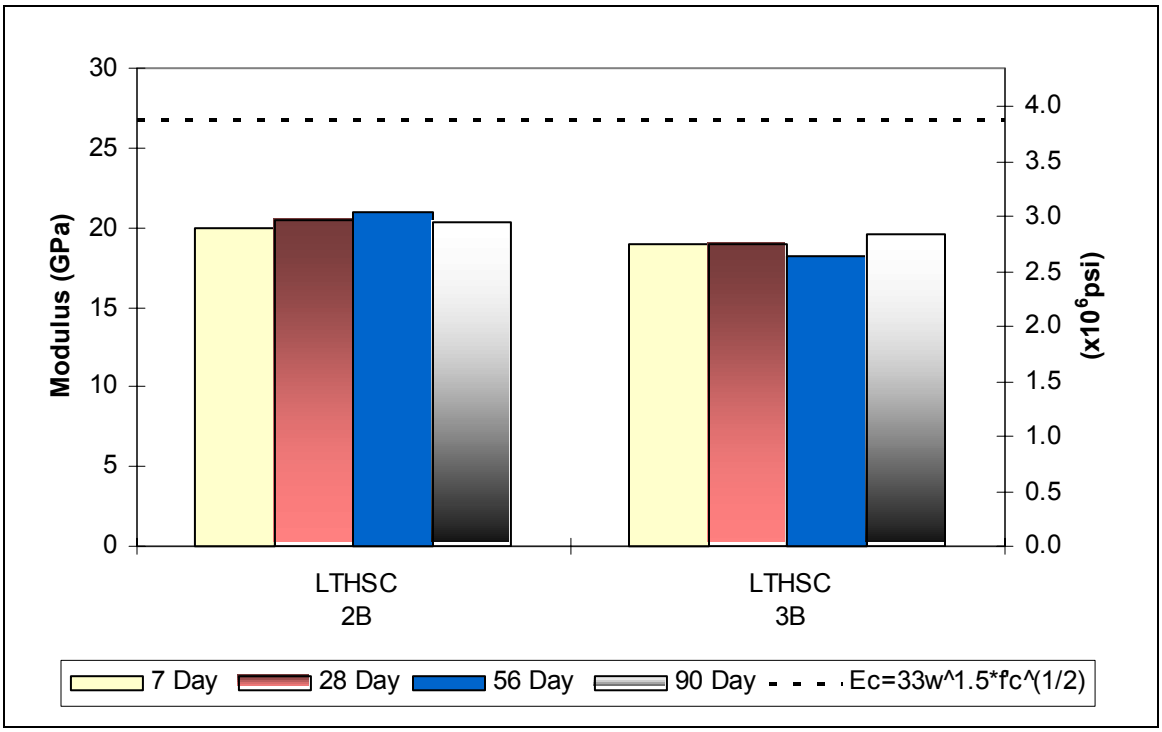

Figure 44 Standard Cure Modulus of Elasticity, LTHSC

Accelerated Cure

Figure 45 presents the LTHSC accelerated cure moduli of elasticity at 17 hours, 7 days, 28 days, 56 days, and 90 days. The figure also presents the computed AASHTO moduli of elasticity for lightweight aggregate concretes. The 17-hour moduli of elasticity were 22 GPa and 19 GPa (3.23 x10^6 psi and 2.70 x10^6 psi) for batches 4 and 5, respectively. The 7-day moduli of elasticity were 18 GPa and 19 GPa (2.67 x10^6 psi and 2.82 x10^6 psi) for batches 4 and 5, respectively. The 28-day moduli of elasticity were 18 GPa and 20 GPa (2.64 x10^6 psi and 2.94 x10^6 psi) for batches 4 and 5, respectively. The 28-day moduli of elasticity were 20 GPa and 21 GPa (2.91 x10^6 psi and 3.04 x10^6 psi) for the Bayshore beams 1 and 2, respectively. The 56-day moduli of elasticity were 21 GPa and 18 GPa (3.07 x10^6 psi and 2.62 x10^6 psi) for batches 4 and 5, respectively. The 90-day moduli of elasticity were 20 GPa and 16 GPa (2.85 x10^6 psi and 2.32 x10^6 psi) for batches 4 and 5, respectively.

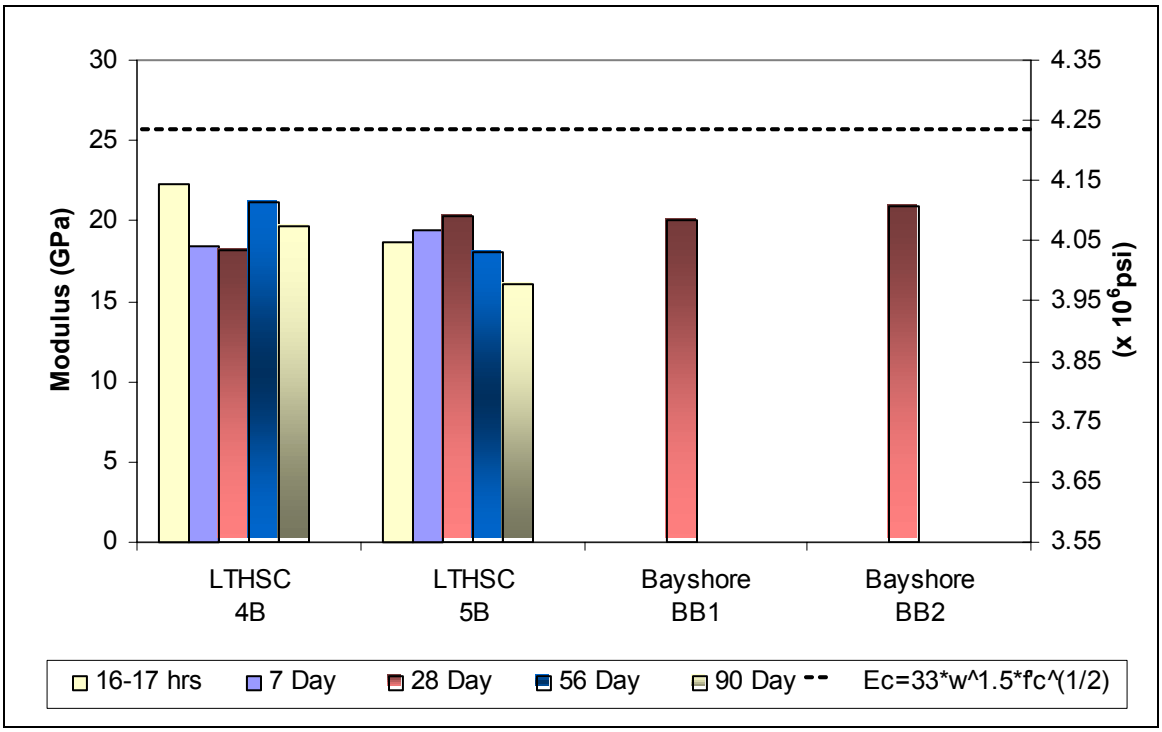

Figure 45 Accelerated Cure Modulus of Elasticity, LTHSC

Thermal Coefficient

The coefficient of thermal expansion for the LTHSC mixture was found to be 9.5 microstrain per ^{o}C (5.3 microstrain per ^{o}F) with a confidence interval of ±0.24 microstrain per ^{o}C (± 0.13 microstrain microstrain per ^{o}F).

Experimental and Predicted Strains

Figures 46 through 49 present the experimental strains from two standard cure and two accelerated cure batches. At a given time, each strain value is the average value from three specimens with the error bars representing the 95% confidence limits. Total strain specimens for each batch are in the same load frame so there is no deviation in the applied stress within a batch. The accelerated and standard cure batches were initially loaded to 40% of the 1-day and 7-day compressive strengths, respectively. The applied stress of 40% of the compressive strength was maintained by increasing the load at 7 and 28 days for the accelerated cure batches and at 28 days for the standard cure batches.

The total, shrinkage, and creep strains were predicted with the four most-cited creep and shrinkage prediction models:

1. ACI 209R-92
2. Comite Euro-International Du Beton Model Code 1990
3. Bazant's B3 model (B3)
4. Gardner's and Lockman's GL2000 model.

However, of the previously presented seven models, only ACI 209 considers lightweight aggregate in its development, whereas GL2000 considers aggregate stiffness and B3 and CED 90 were developed for normal weight aggregate.

Figures 46 and 47 present the standard cure batch strain results, and Figures 48 and 49 the accelerated batch results.

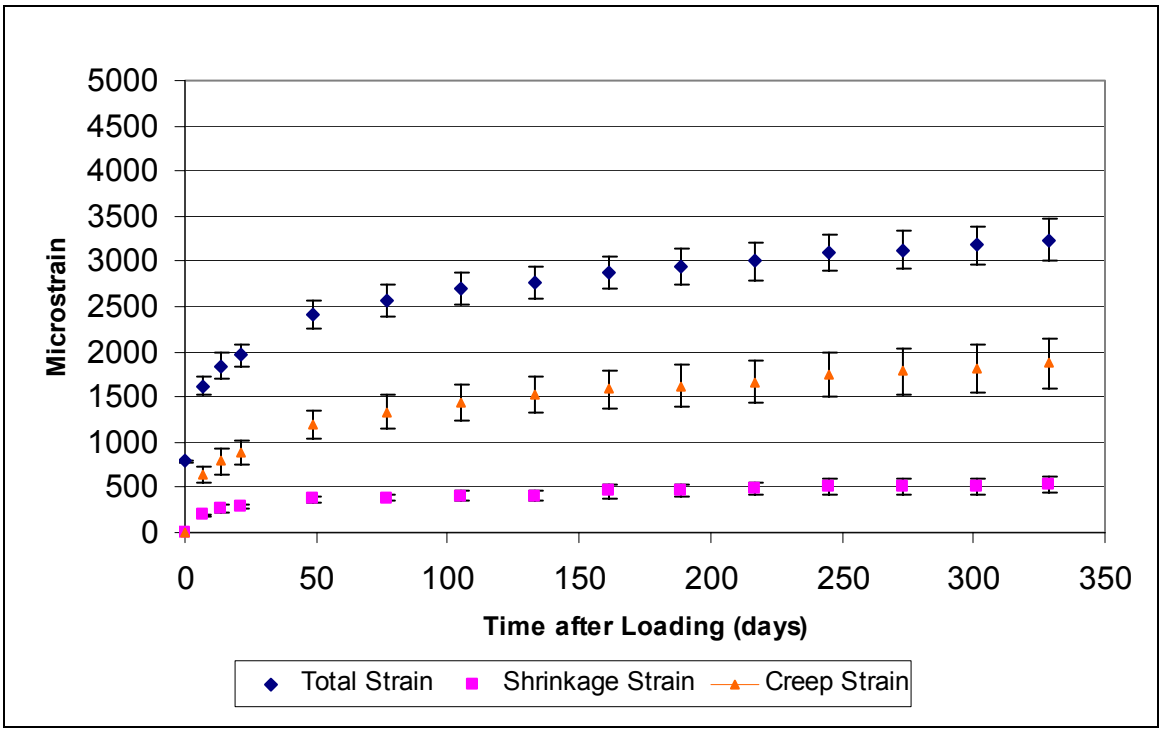

Figure 46 Standard Cure Batch 2: Total, Creep, and Shrinkage Strain, LTHSC

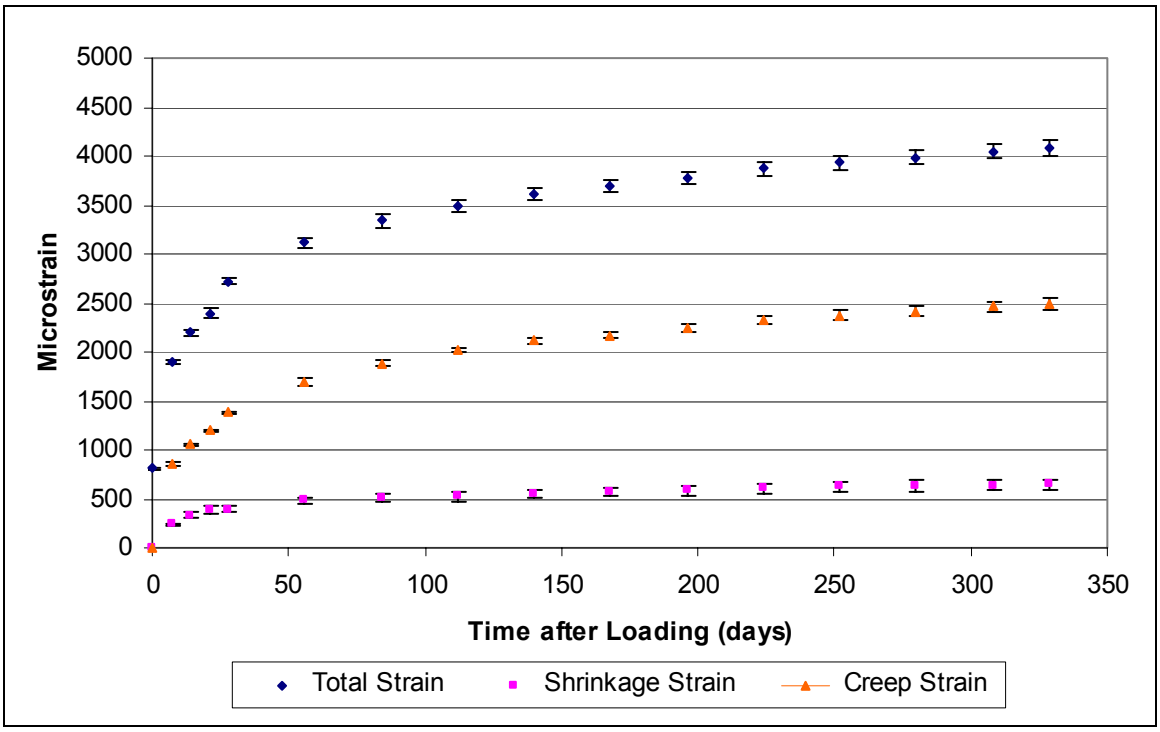

Figure 47 Standard Cure Batch 3: Total, Creep, and Shrinkage Strain, LTHSC

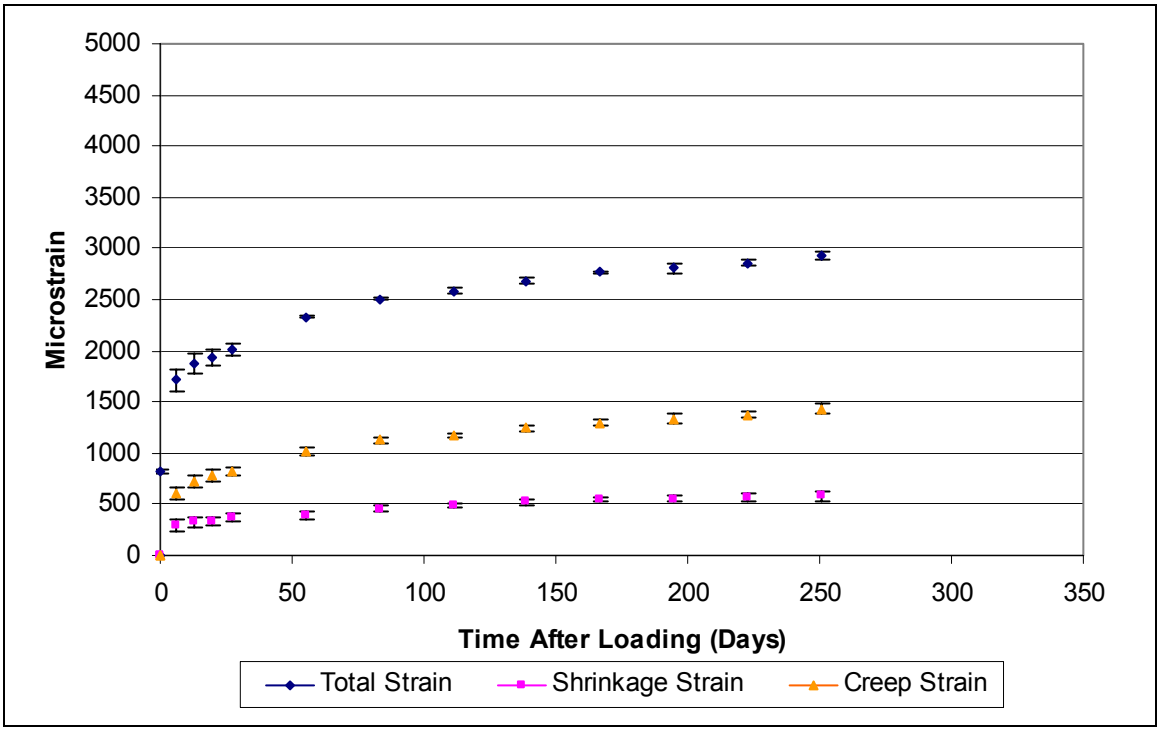

Figure 48 Accelerated Cure Batch 4: Total, Creep, and Shrinkage Strain, LTHSC

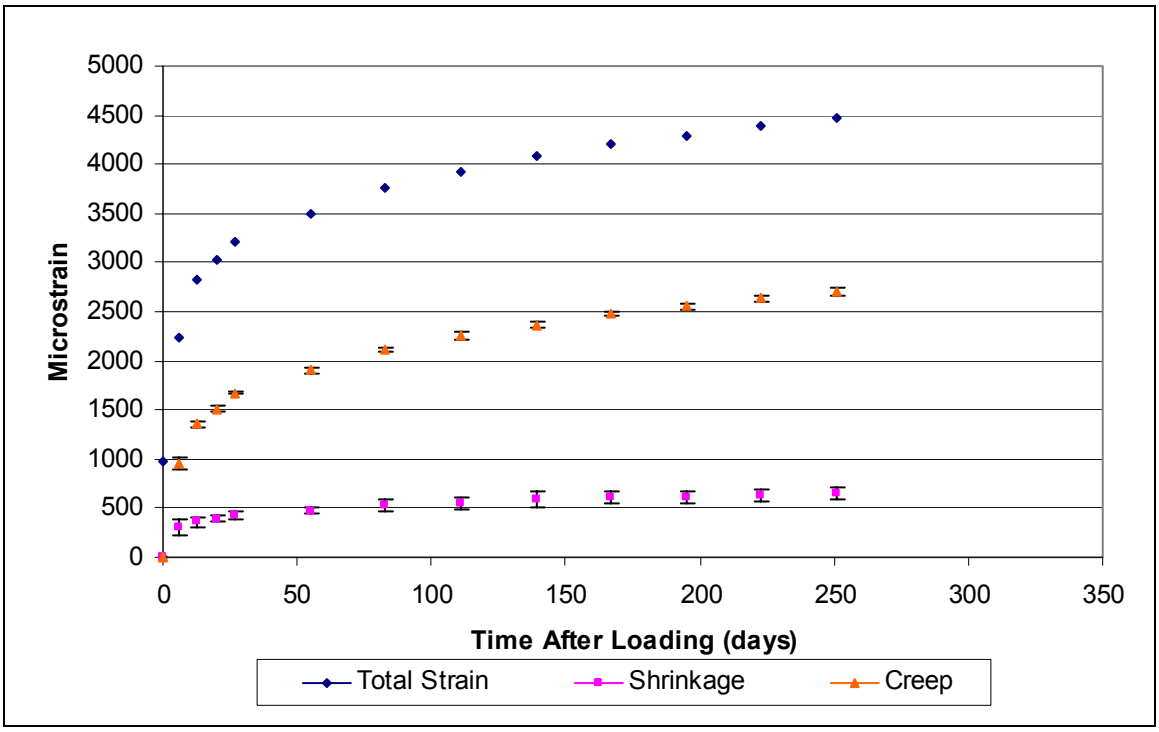

Figure 49 Accelerated Cure Batch 5: Total, Creep, and Shrinkage Strain, LTHSC

The ACI 209 model was used to predict the prestressed losses for the Virginia Route 106 bridge over the Chickahominy River.

Figures 50 through 53 present the standard cure and 54 through 57 the accelerated cure model-predicted total, shrinkage, and creep strains. The values were predicted using the experimentally measured compressive strengths and modulus of elasticity for each batch. If the LTHSC design strength was used, the elastic strain would have been underpredicted based on the measured values and current prediction equations. Time-dependent deformation would also be underpredicted based on the strength because a strong cement paste matrix is more resistant to time-dependent losses than is a weaker matrix.

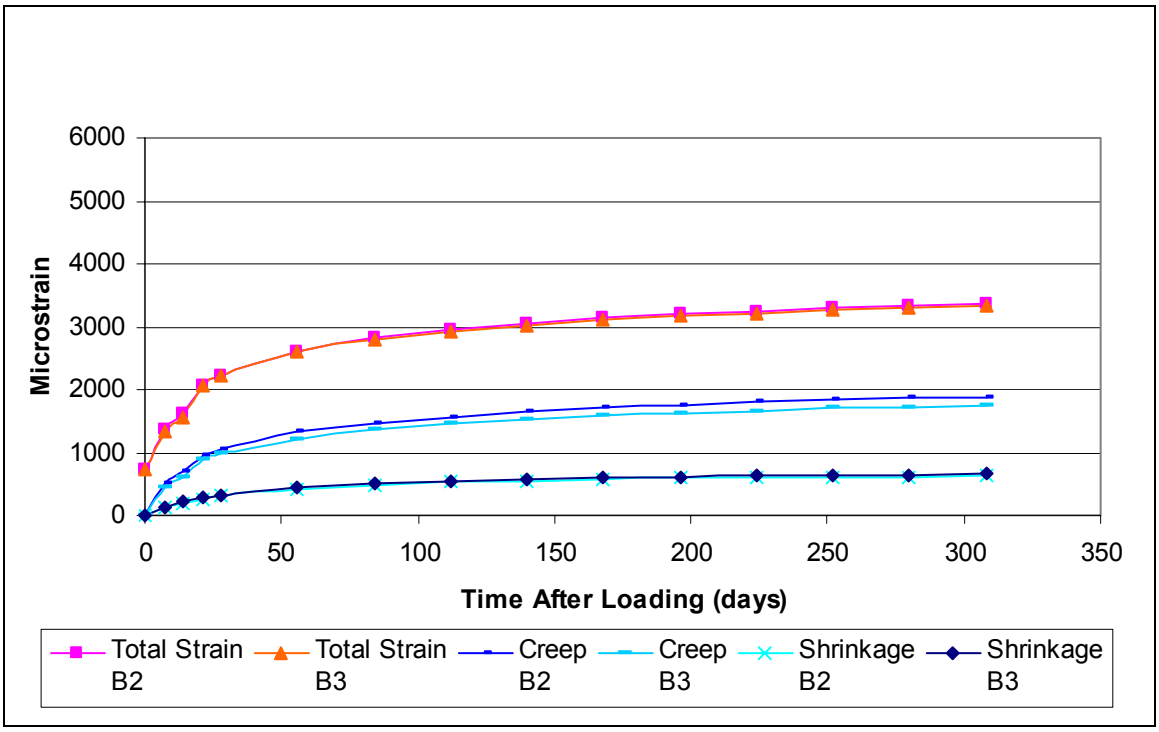

Figure 50 ACI 209 Standard Cure, LTHSC

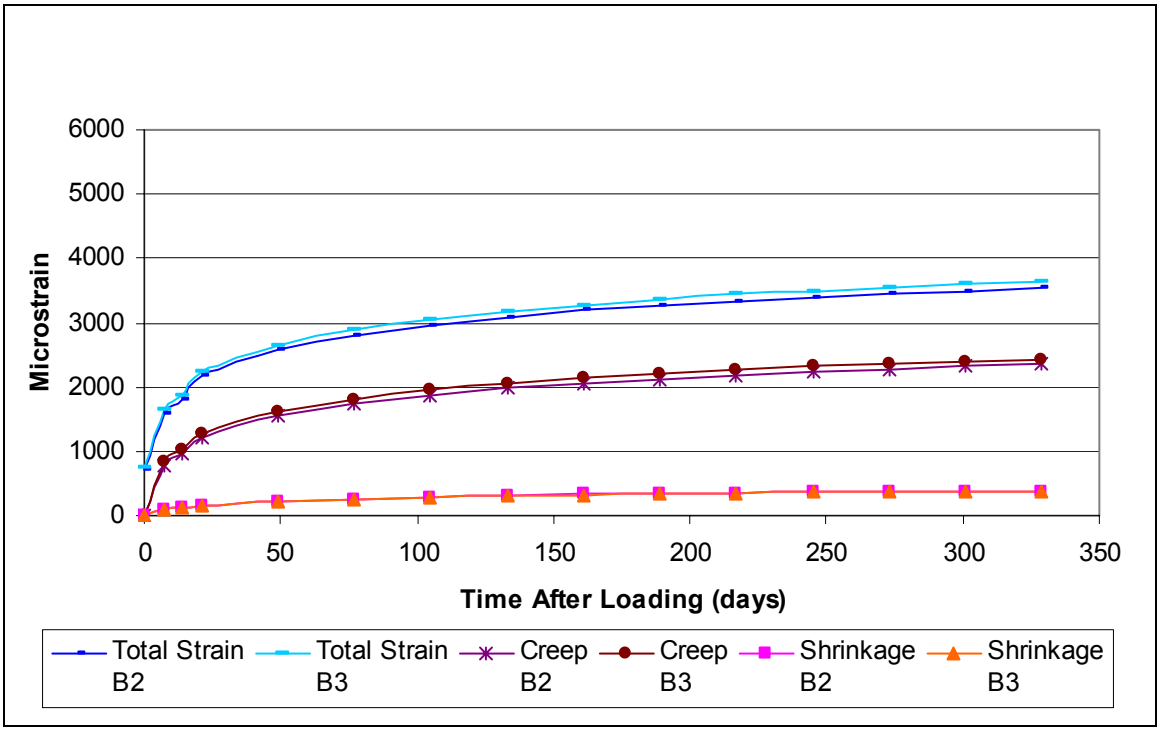

Figure 51 CEB 90 Standard Cure, LTHSC

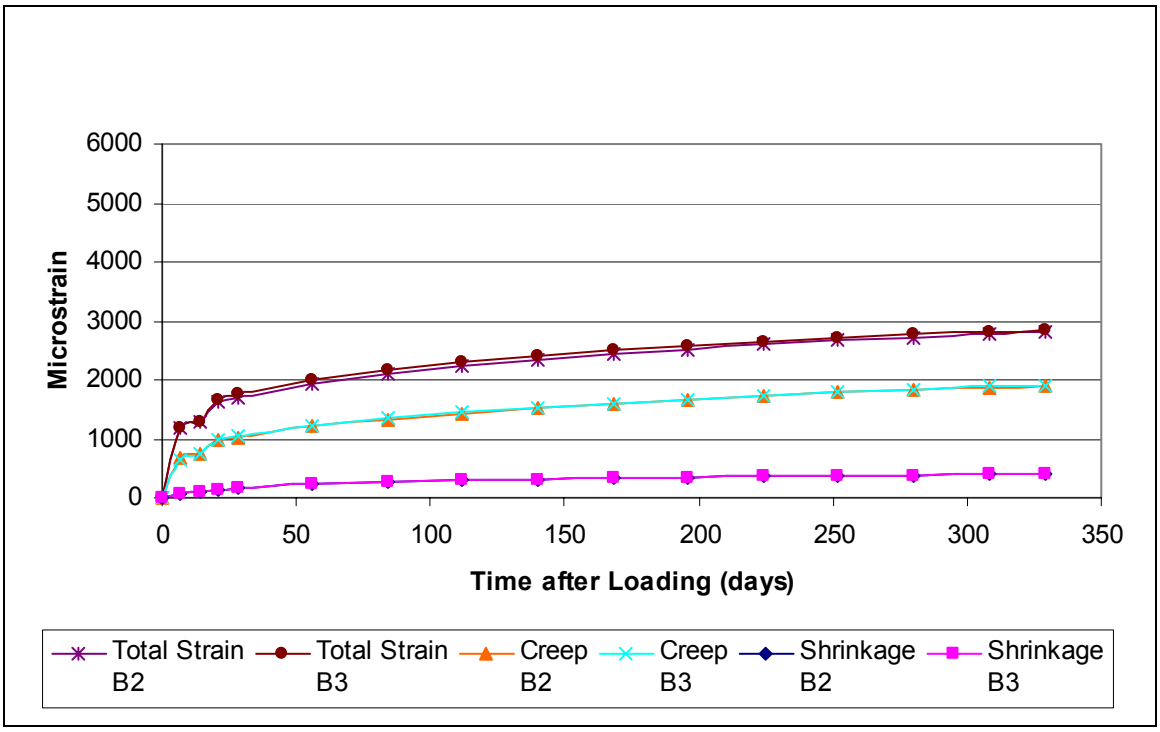

Figure 52 B3 Standard Cure, LTHSC

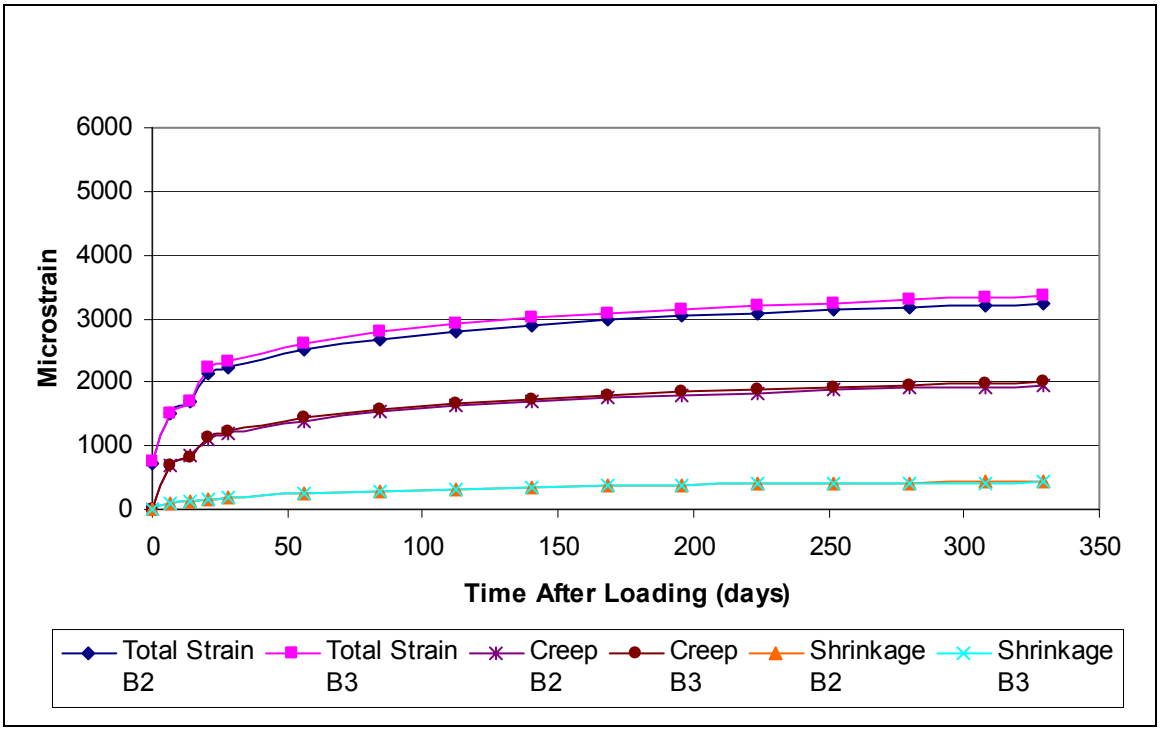

Figure 53 GL2000 Standard Cure, LTHSC

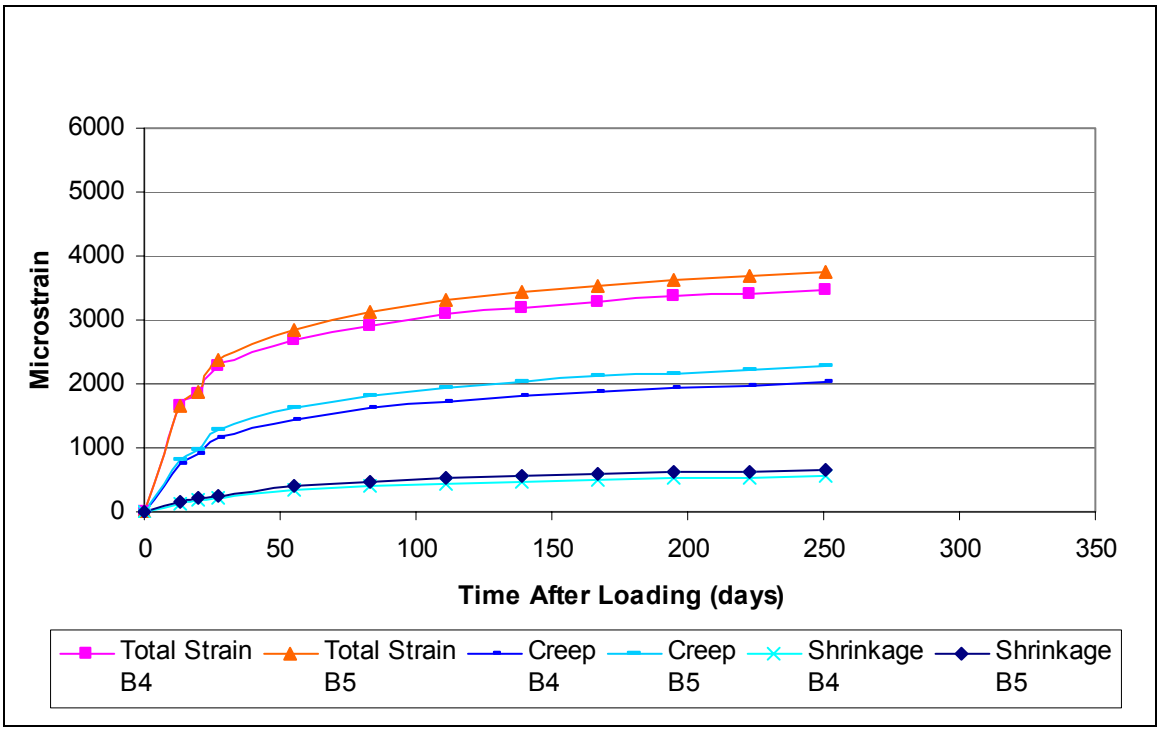

Figure 54 ACI 209 Accelerated Cure, LTHSC

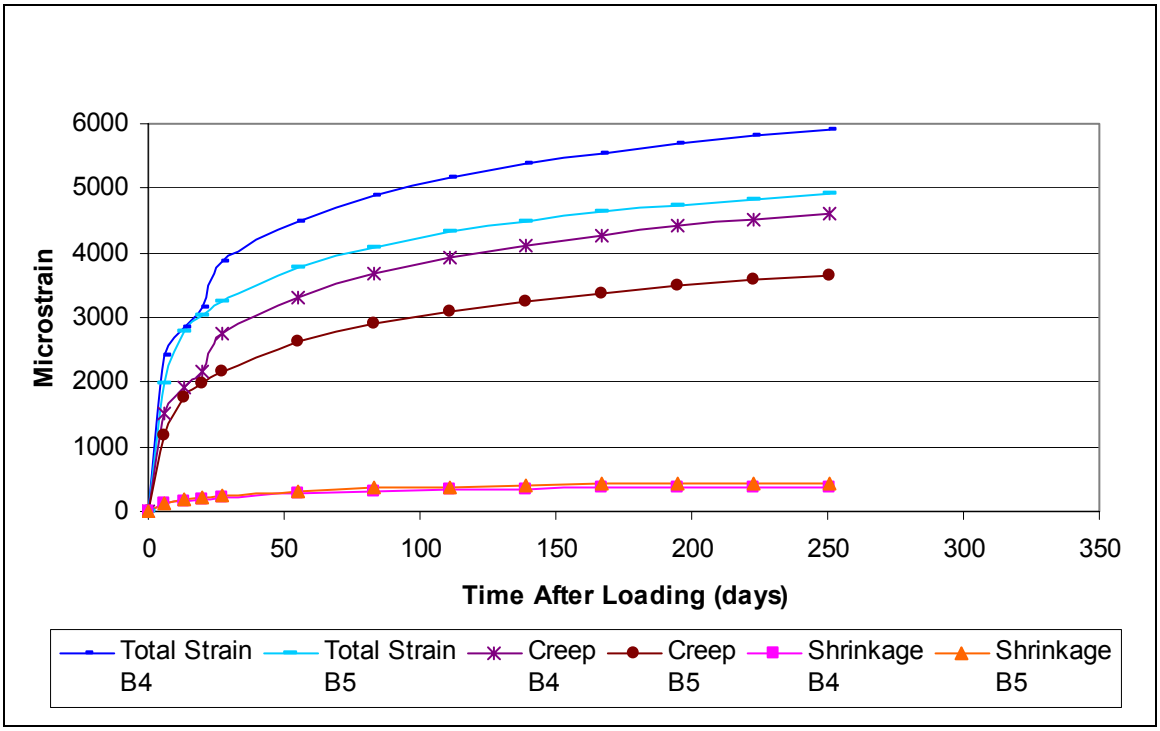

Figure 55 CEB 90 Accelerated Cure, LTHSC

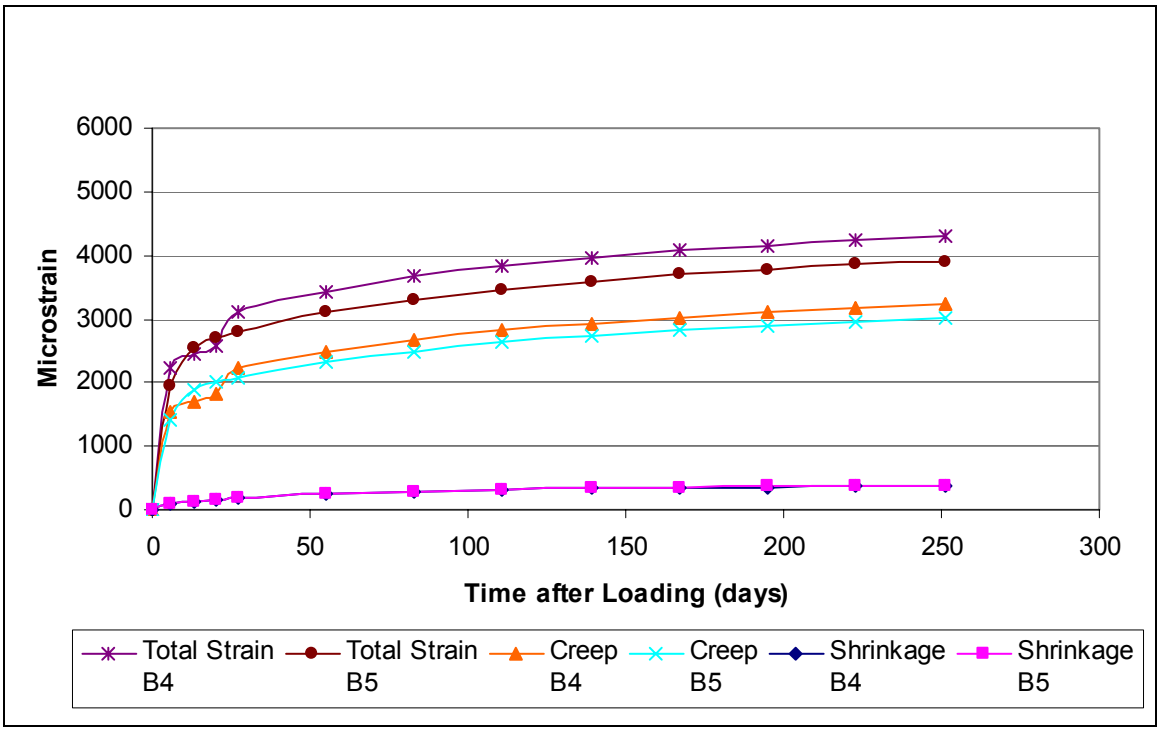

Figure 56 B3 Accelerated Cure, LTHSC

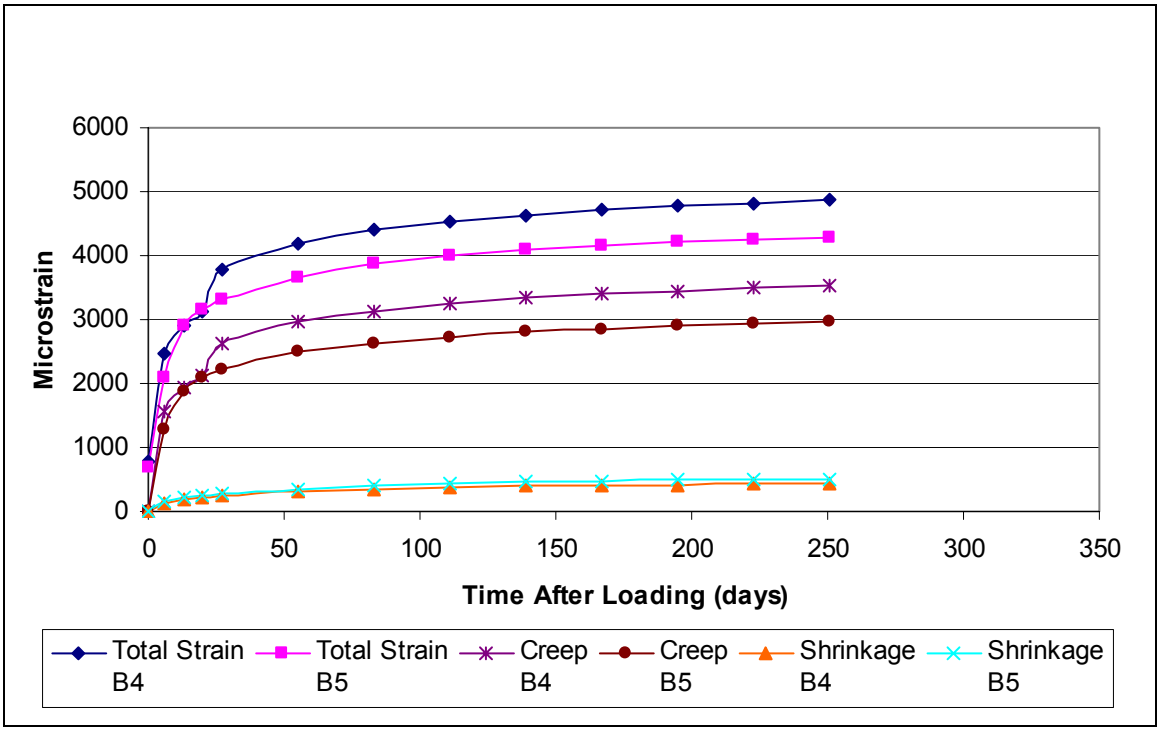

Figure 57 GL2000 Accelerated Cure, LTHSC

Prediction Model Residuals

A residual is the difference between a model and the experimental value at a given time. Residuals identify a model as either overpredicting, a positive value, or underpredicting, a negative value. The residuals are calculated as the predicted model mean for a batch minus the experimental value for a test specimen at a given time.

Figures 58 through 61 present the residuals for the standard cure total strain, and Figures 62 through 65 for the accelerated cure batches. The residuals are plotted as the mean and the 95% confidence limits at the given test time. The standard cure residuals are for batches 2 and 3 combined for a total of six test values because the strain results were not significantly different. The accelerated cure residuals are for batches 4 and 5 separately because they were significantly different.

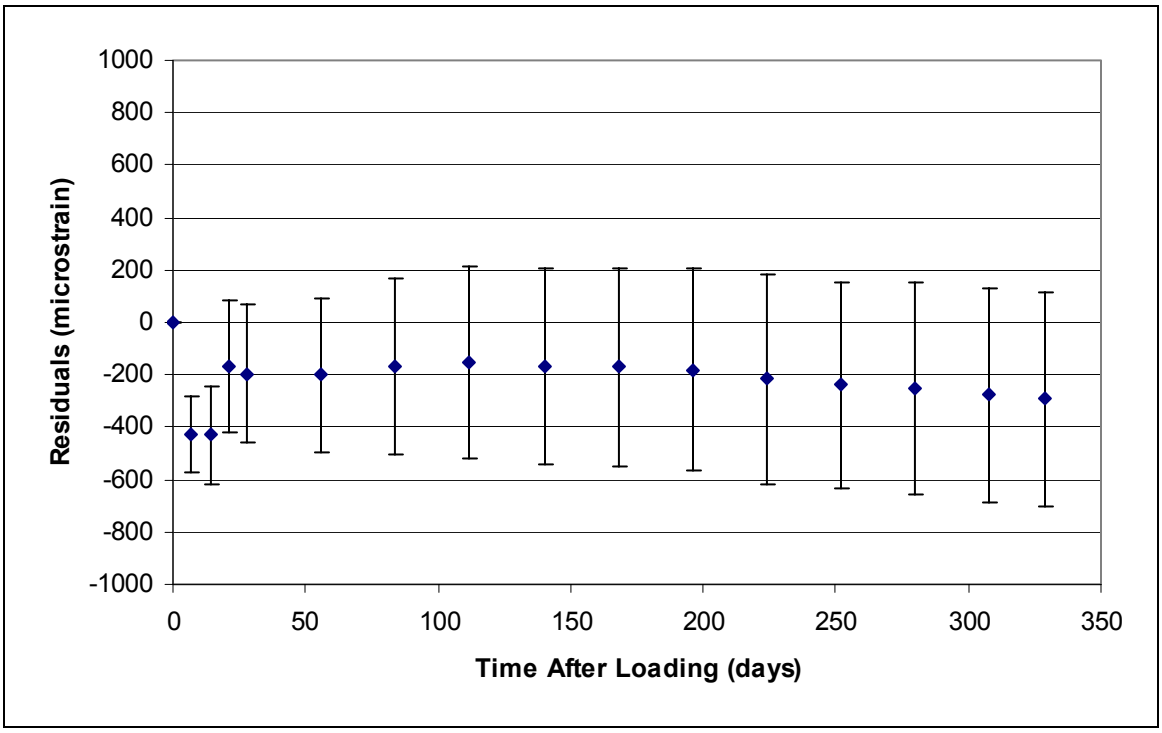

Figure 58 ACI 209 and Standard Cure Total Strain Residuals, LTHSC

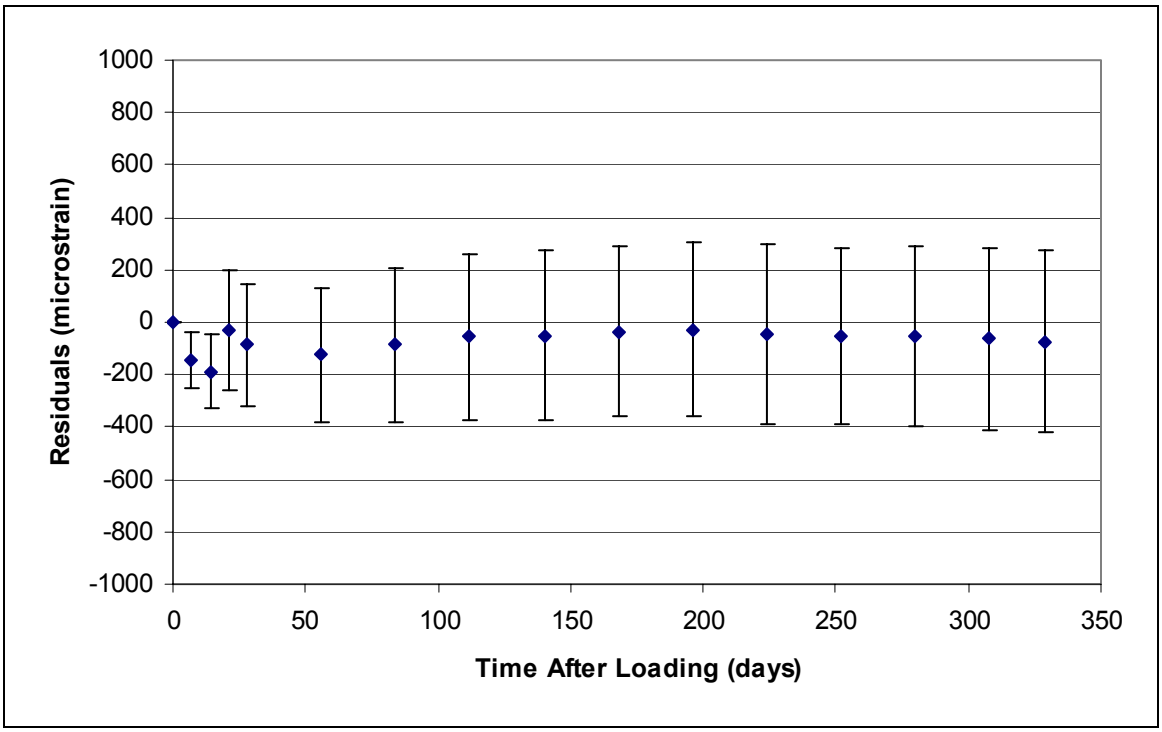

Figure 59 CEB 90 and Standard Cure Total Strain Residuals, LTHSC

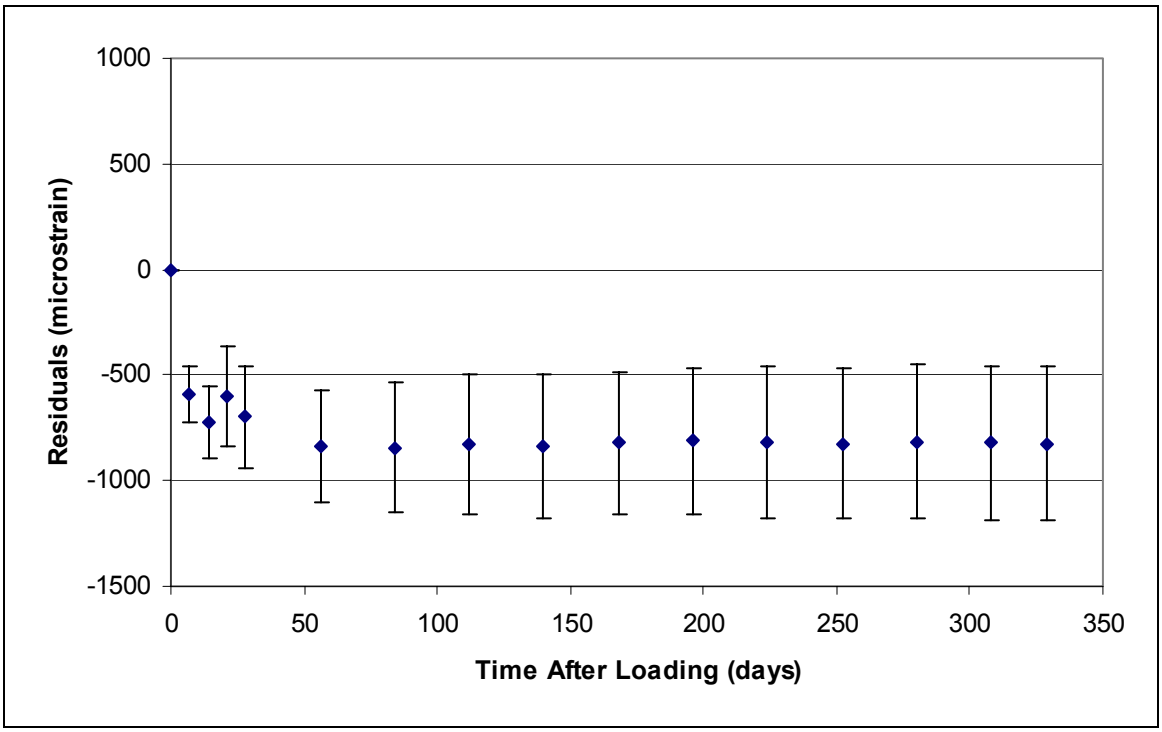

Figure 60 B3 and Standard Cure Total Strain Residuals, LTHSC

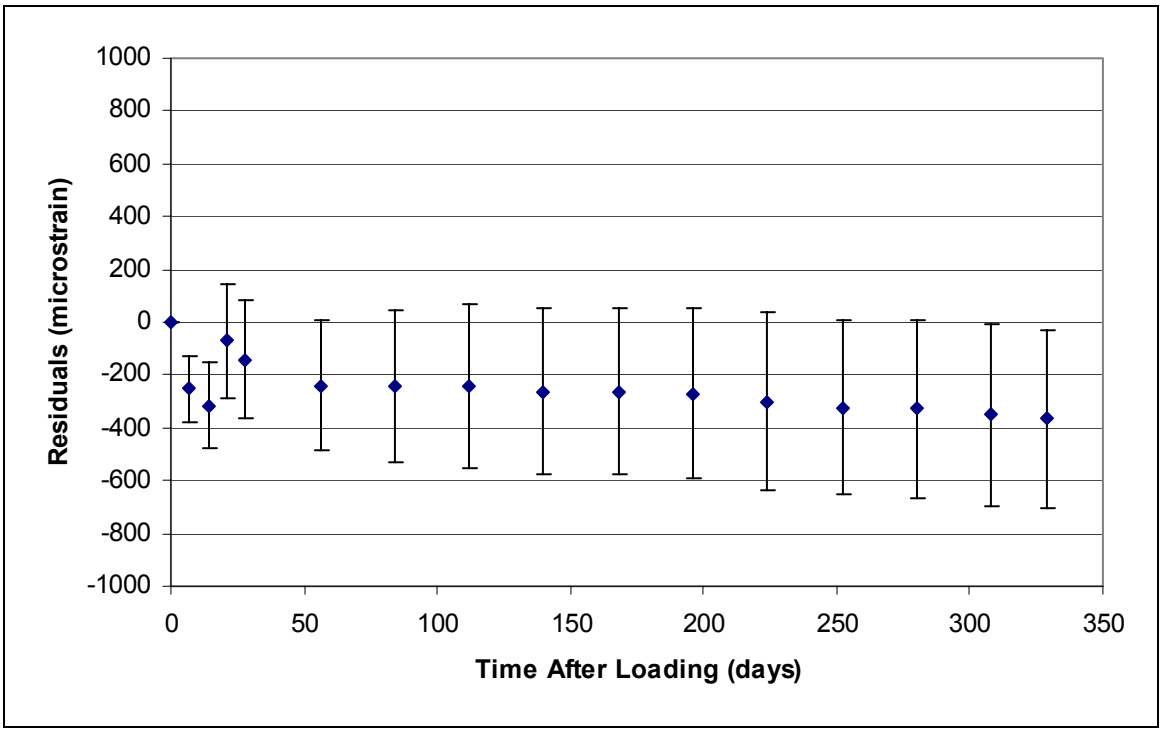

Figure 61 GL2000 and Standard Cure Total Strain Residuals, LTHSC

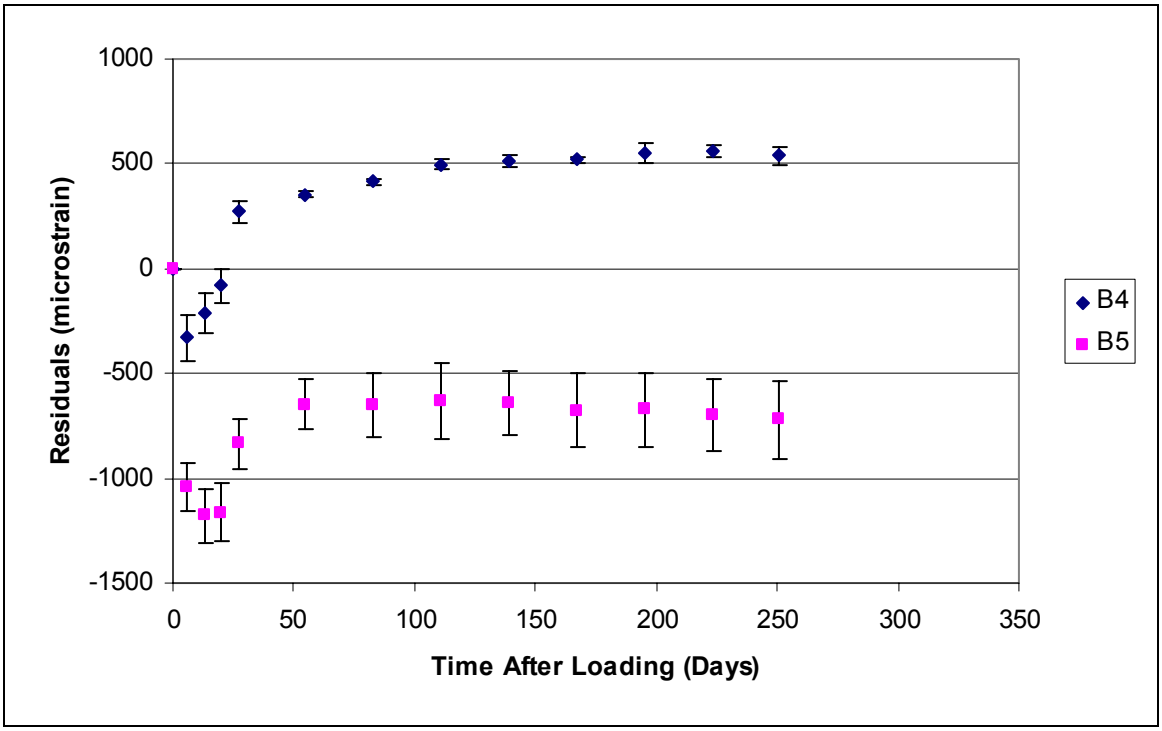

Figure 62 ACI 209 and Accelerated Cure Total Strain Residuals per Batch, LTHSC

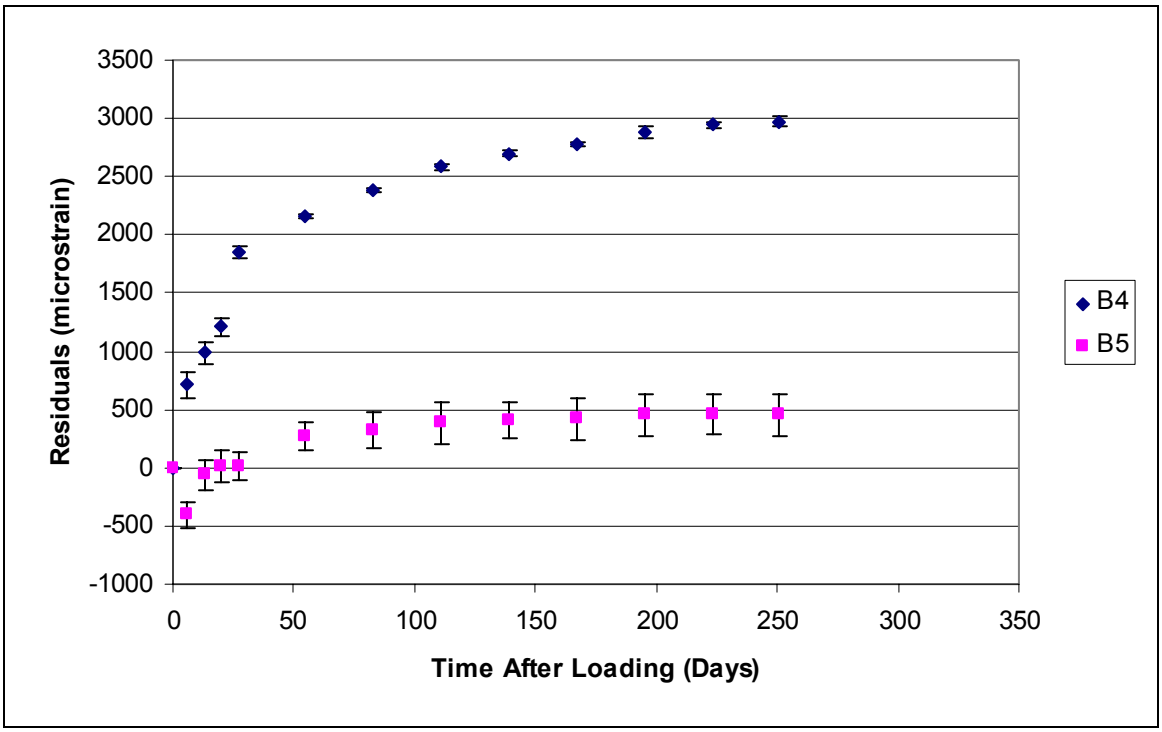

Figure 63 CEB 90 and Accelerated Cure Total Strain Residuals per Batch, LTHSC

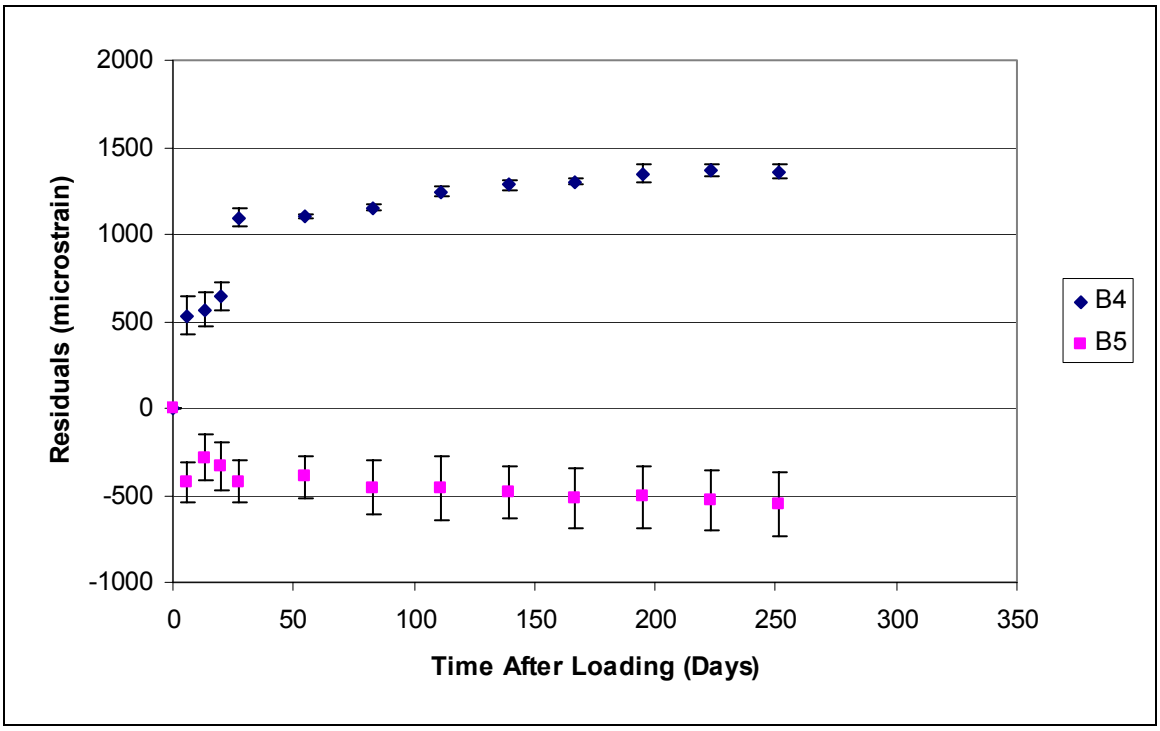

Figure 64 B3 and Accelerated Cure Total Strain Residuals per Batch, LTHSC

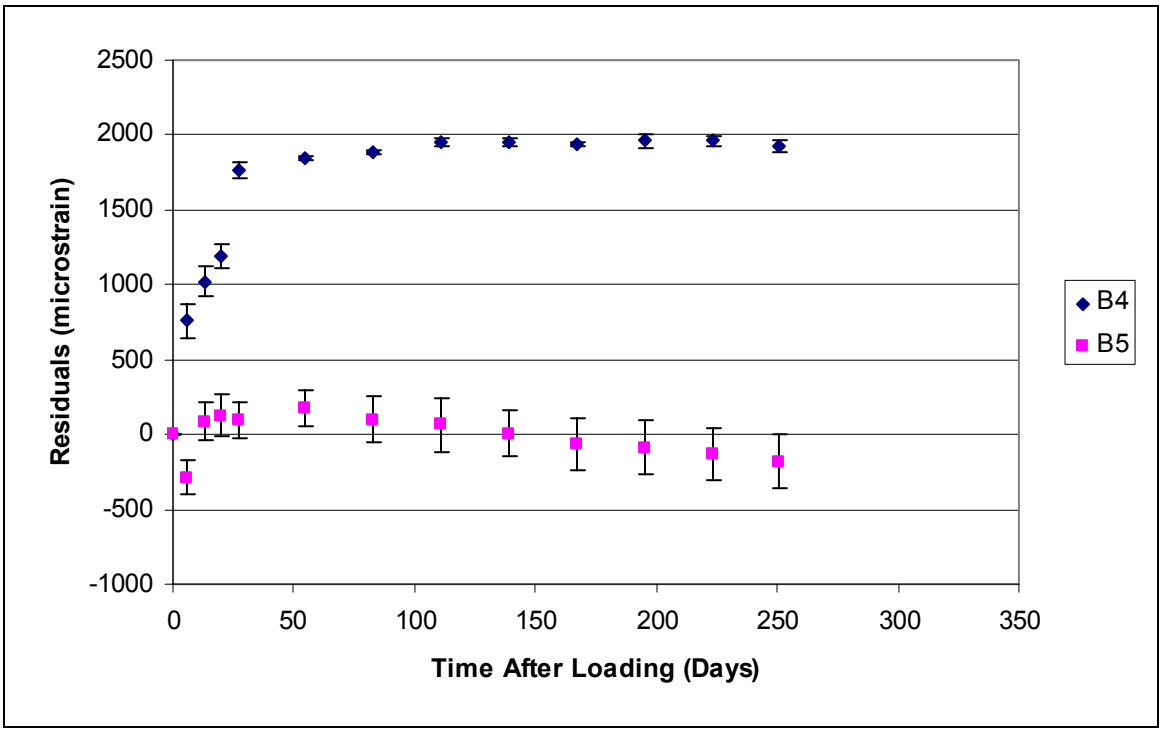

Figure 65 GL2000 and Accelerated Cure Total Strain Residuals per Batch, LTHSC

Shrinkage Prisms

Figure 66 presents the shrinkage prism mean percent length change with 95% confidence limits and the ACI 209 and the CEB 90 predictions. The ACI 209 model initially underpredicted shrinkage and overpredicted after 50 days. The CEB 90 model was the best early age predictor but underpredicted shrinkage after 28 days.

Figure 67 presents the percent length change for the shrinkage prisms with 95% confidence limits and the B3 and GL2000 predictions. The B3 model initially underpredicted shrinkage up to 80 days and then was within the prisms' 95% confidence limits thereafter. The GL2000 model underpredicted shrinkage throughout the test period.

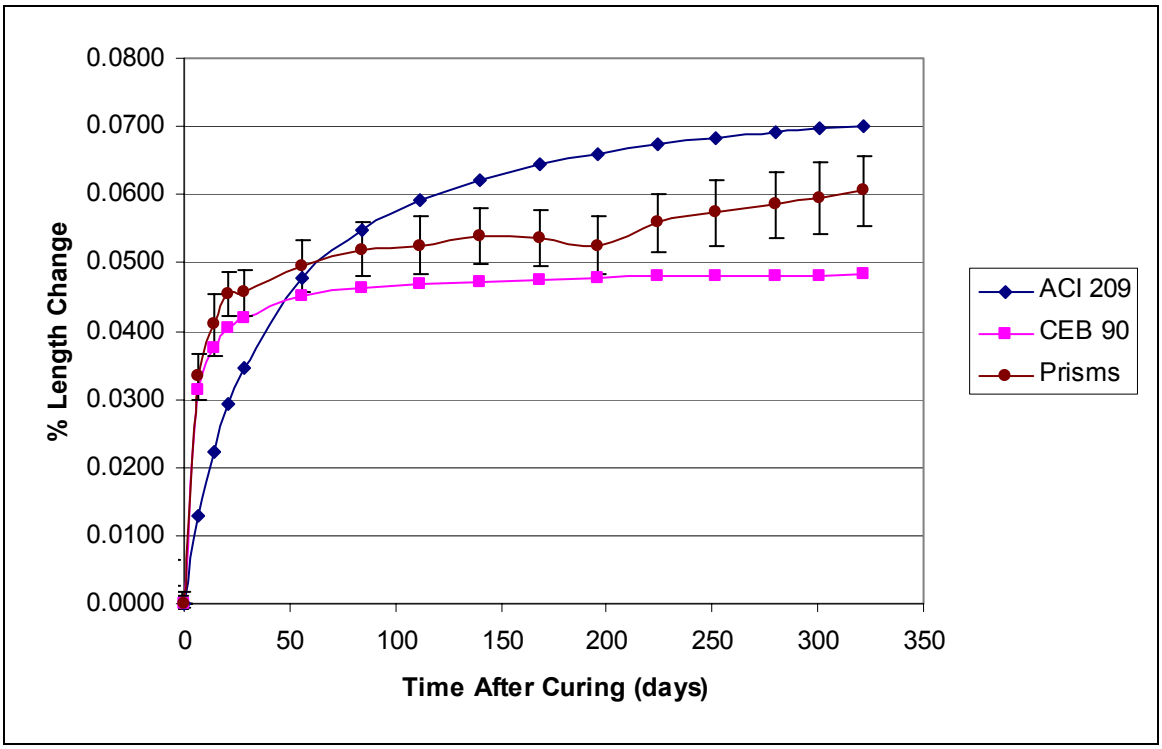

Figure 66 Prism Data with ACI 209 and CEB 90 Models, LTHSC

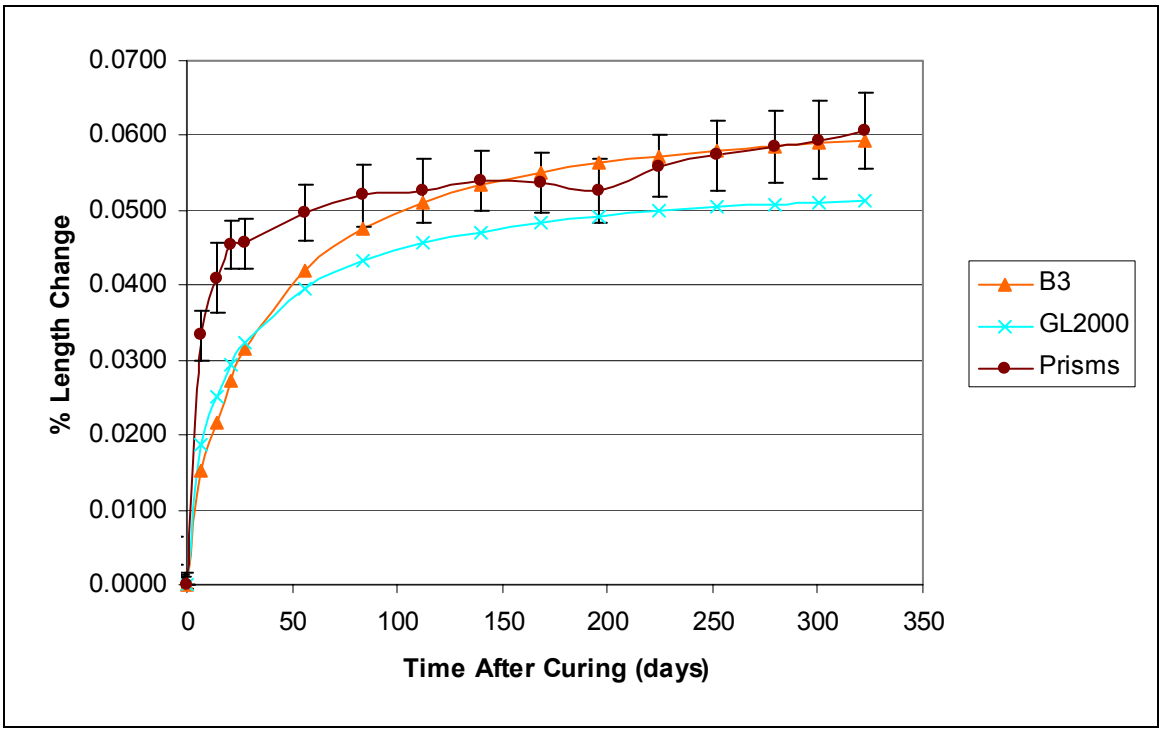

Figure 67 Prism Data with B3 and GL2000 Models, LTHSC

DISCUSSION AND ANALYSIS

HSC

Compressive Strength

The average 7-day strengths for the two curing methods were similar, but the standard cure batches had significantly higher strength gain with time. During the accelerated curing procedure the specimens consumed more water and thus created a more porous hydrated cement matrix than did standard curing. The standard cure specimens contained more excess water after the initial moist curing, which allowed for continued hydration and thus densification of the cement matrix. The use of accelerated curing allows for rapid initial strength gain but significantly decreases the potential for continued strength gain after curing.

As seen in Figure 1, the Bayshore compressive strengths were 30% lower than the laboratory accelerated cure strengths. This disparity is due in part to differences in the amounts of water in the concrete mixtures. The aggregate for the laboratory mixtures was dried before mixing, whereas the aggregate in Bayshore's mixtures was likely in SSD condition. Aggregate absorption was not accounted for in the laboratory mixtures, resulting in a w/cm of 0.30. The w/cm should have been 0.33 with the aggregate in SSD condition. A decrease in w/cm from 0.33 to 0.30 would cause a compressive strength increase of at most 13.8 MPa (2000 psi), which is half of the observed strength difference (Chern and Chan, 1989). The Bayshore concrete also had a higher air content than did the laboratory mixtures, but the differences in air content and w/cm do not fully explain the strength differences. A possible explanation is that the Bayshore mixture contained more water than the amount specified in the mixture proportions. The fact that the Bayshore mixture had a higher air content than the laboratory mixtures supports this explanation in that a higher water content increases fluidity and air content of a mixture.

Tensile Strength

On average, the end-of-cure of all tensile strengths equaled 9.8% of the end-of-cure of all compressive strengths. All 28-day tensile strengths equaled 8.5% of all the 28-day compressive strengths, on average. The ratio of tensile strength to compressive strength decreases as the compressive strength increases, which is an expected trend (Alexander, 1996).

Modulus of Elasticity

Figure 68 presents the relationship between the modulus of elasticity and compressive strength results for the standard cure specimens. The AASHTO design equation overpredicted modulus of elasticity at all ages.

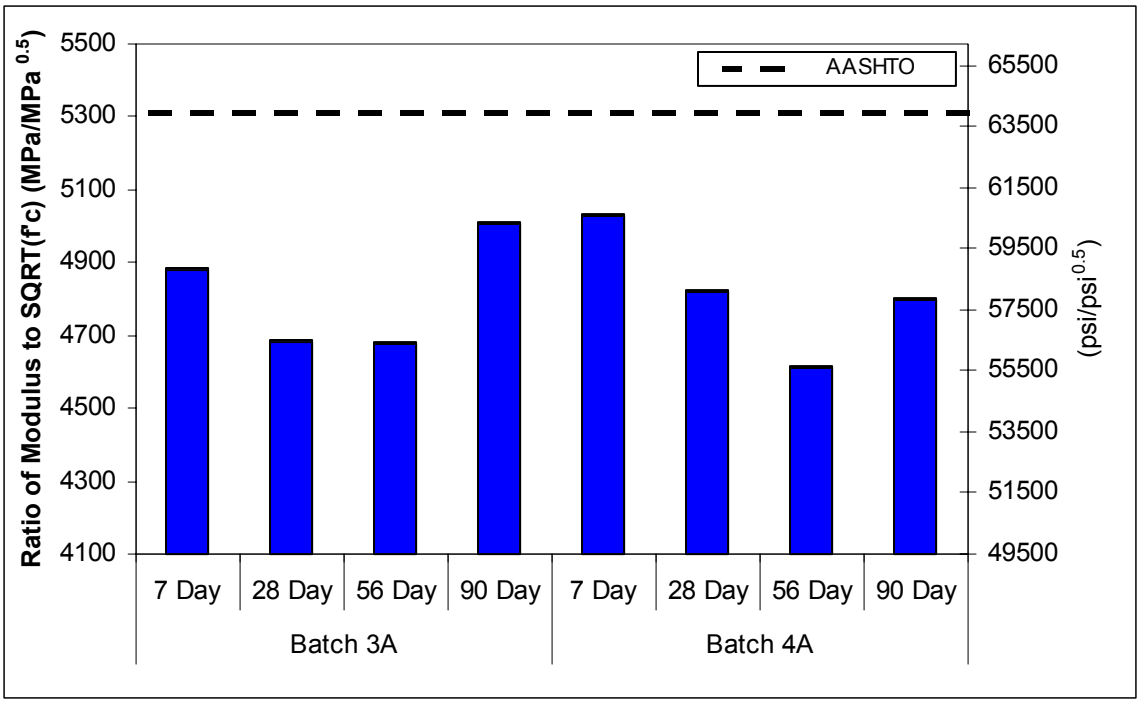

Figure 68 Standard Cure Ratio of Elastic Modulus to SQRT(f'_c), HSCS

The Bayshore modulus of elasticity was significantly lower than those of the laboratory accelerated cure batches. This is expected since the Bayshore compressive strengths were lower than the laboratory accelerated cure strengths. The Bayshore modulus was within 1% of the AASHTO design value and thus was in agreement with the AASHTO design equation.

Thermal Coefficient

The coefficient of thermal expansion for the HSC mixture was found to be 4.6 ± 0.4 microstrain per °F (8.3 ± 0.7 microstrain per °C) at a 95% confidence level. This is within the published range of 3.5 to 5 microstrain per °F (6.3 to 9.0 microstrain per °C) (Alexander, 1996).

Experimental and Predicted Strains

A noticeable difference is observed between the accelerated cure and standard cure curves in that the standard cure curves have much smaller 95% confidence intervals. This indicates that the accelerated cure batches had larger within-batch variation, which is likely a result of the following factors:

- Curing conditions. More variability is inherent with accelerated curing than standard curing. This is corroborated by the LTHSC results.
- Gage lengths. The standard cure specimens have a 203 mm (8 in.) gage length, whereas the accelerated cure gage length is 152 mm (6 in.). Equal length measurement errors result in 33% more strain variation for the smaller gage length than for the larger one.

- Learning error. The standard cure batches were tested last, so the standard cure results may contain less measurement error than the accelerated cure results.

The GL2000 and B3 models predicted the largest creep strain and total strain, and the AASHTO-LRFD model predicted the largest shrinkage strain

Accelerated Cure vs. Standard Cure

Accelerated and standard cure specimens can be expected to behave differently over time because of differences in specimen size, curing method, and compressive strength. Larger specimens generally have less drying creep and shrinkage, especially early on, because it is more difficult for water to move from the center of the specimen to the outside surface. Accelerated curing forms larger hydration products than standard curing. As a result, standard cure specimens have a denser concrete matrix that is more resistant to water movement, thus reducing drying creep and shrinkage. The standard cure specimens had greater compressive strength gain with time than the accelerated cure specimens. As a result, the standard cure creep specimens were loaded to a smaller fraction of their compressive strength at later ages, since the applied stress was kept constant for both curing methods. The following figures do not include any adjustment factors for size or compressive strength. The accelerated cure and standard cure data sets are averages of eight and six specimens, respectively.

The relationship between average accelerated cure and standard cure total strains is presented in Figure 69. The two data sets are nearly equivalent early on, but the accelerated cure strains are slightly higher at later ages.

The relationship between average accelerated cure and standard cure creep strains is presented in Figure 70. The accelerated cure creep strain is significantly higher at later ages. The smaller specimen size resulted in higher drying creep. In addition, the accelerated cure specimens had a less dense cement matrix and less strength gain with time.

The relationship between average accelerated cure and standard cure shrinkage strains is presented in Figure 71. Shrinkage strain is higher for the accelerated cure specimens due to smaller specimen size and a less dense concrete matrix.

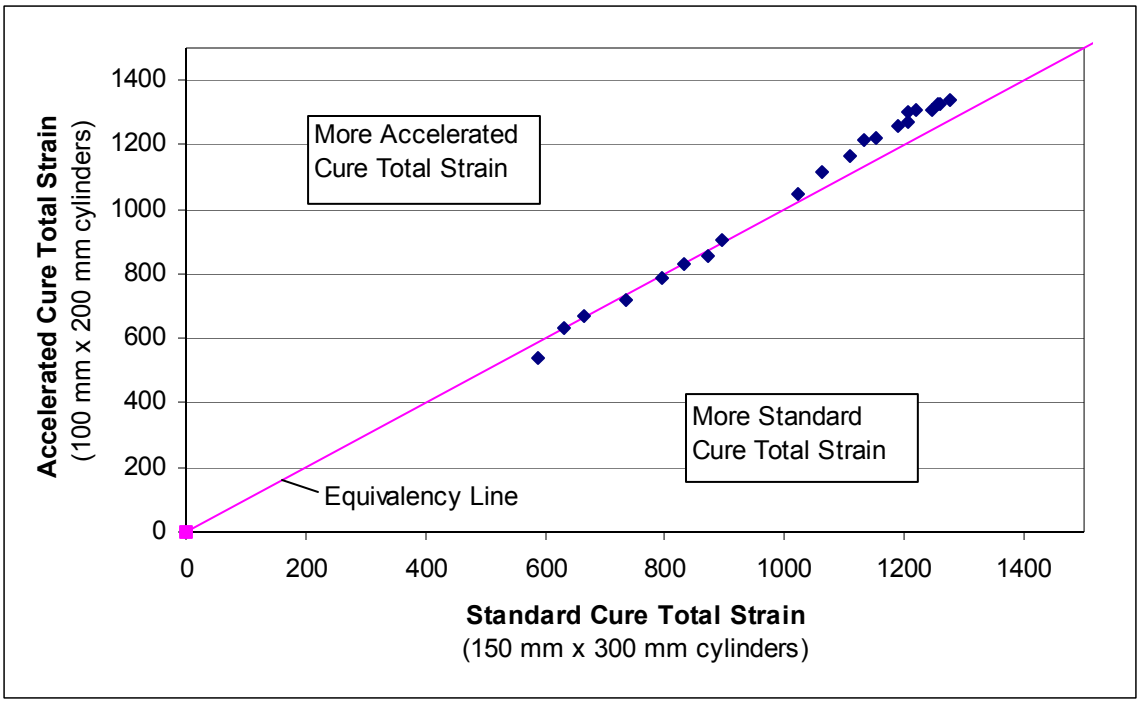

Figure 69 Accelerated Cure vs. Standard Cure Total Strain (microstrain), HSC

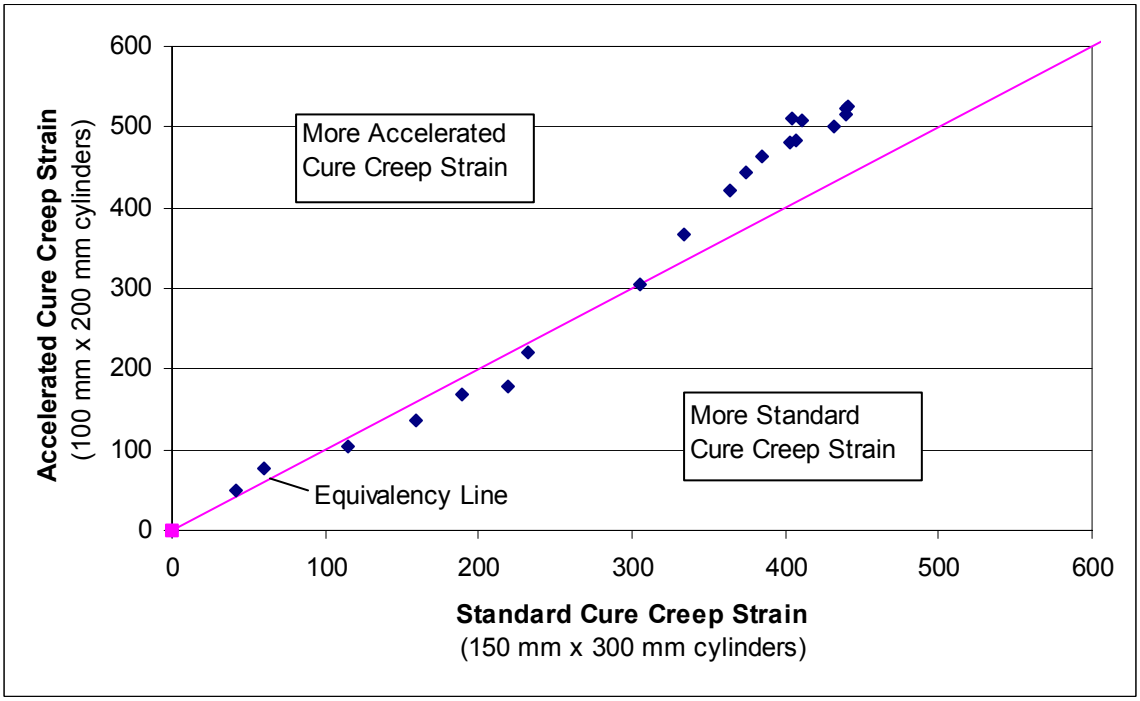

Figure 70 Accelerated Cure vs. Standard Cure Creep (microstrain), HSC

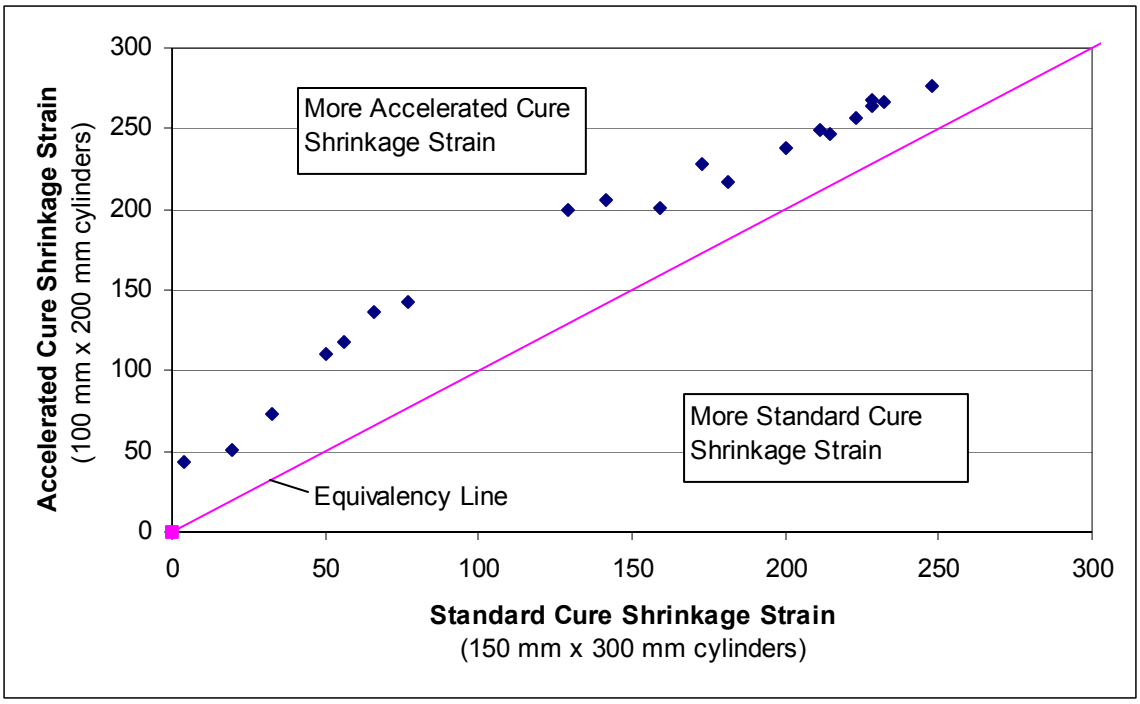

Figure 71 Accelerated Cure vs. Standard Cure Shrinkage (microstrain), HSC

Shrinkage Prisms vs. Cylinders

Figure 72 presents the relationship between shrinkage strains of the 75 mm x 75 mm x 285 mm (3 in. x 3 in. x 11.25 in.) prisms and the 150 mm x 300 mm (6 in. x 12 in.) cylinders. No adjustment was made for specimen size. The prisms had significantly higher shrinkage strains, mainly due to the size difference. The prisms and cylinders had an exposed surface area to volume ratios of 1.5 and 0.67, respectively.

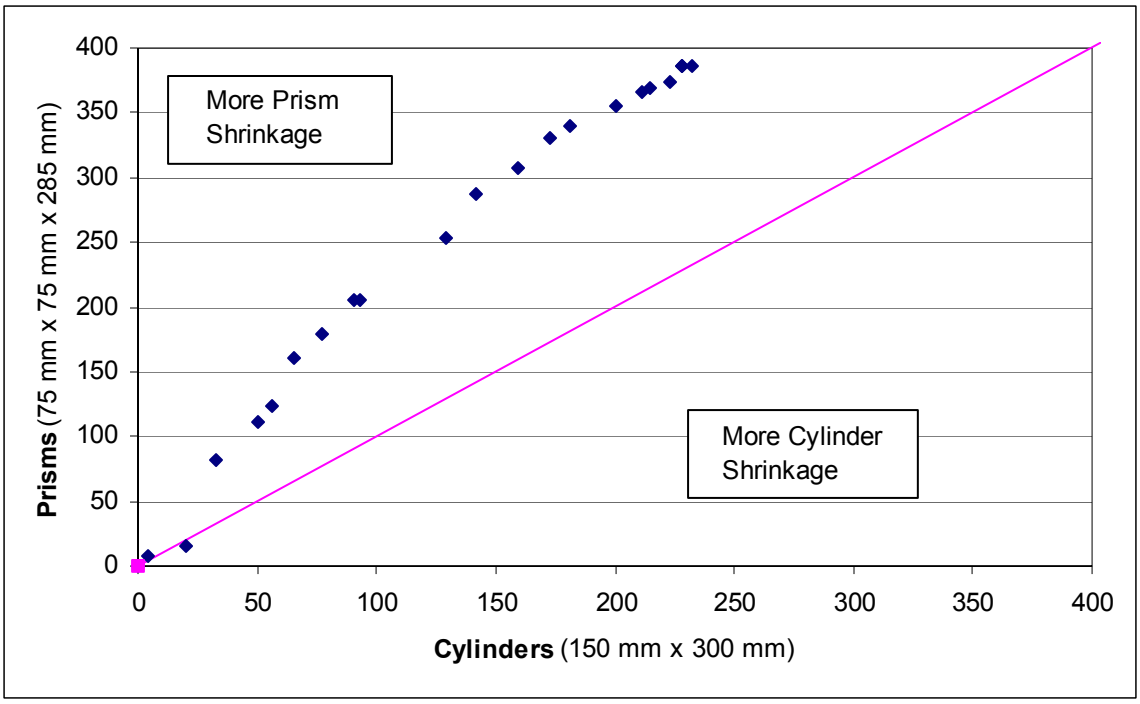

Figure 72 Prism vs. Cylinder Shrinkage Strain (microstrain), HSC

Field vs. Laboratory

Figure 73 presents the relationship between time-dependent strains measured on test girders at Bayshore and those measured in the laboratory. The strain measurements are divided by applied stress, which is not a constant for the two data sets. The field stress is calculated as the initial elastic stress minus estimated prestress losses over time. The field data represent the average total strain at the center of prestressing for three test girders (Meyerson, 2001). The laboratory data represent the average total strain of eight accelerated cure specimens. The data are not adjusted for parameters such as specimen size, compressive strength, and relative humidity.

The laboratory specimens had significantly higher time-dependent deformations than the test girders. This is to be expected due to the following factors:

- Size effects: The field measurements were taken in the center of a large girder, where drying creep and shrinkage are limited.
- Ambient conditions: The average relative humidity at Bayshore is over 70%, compared to the laboratory relative humidity of 50%. Relative humidity has a significant effect on drying creep and shrinkage.

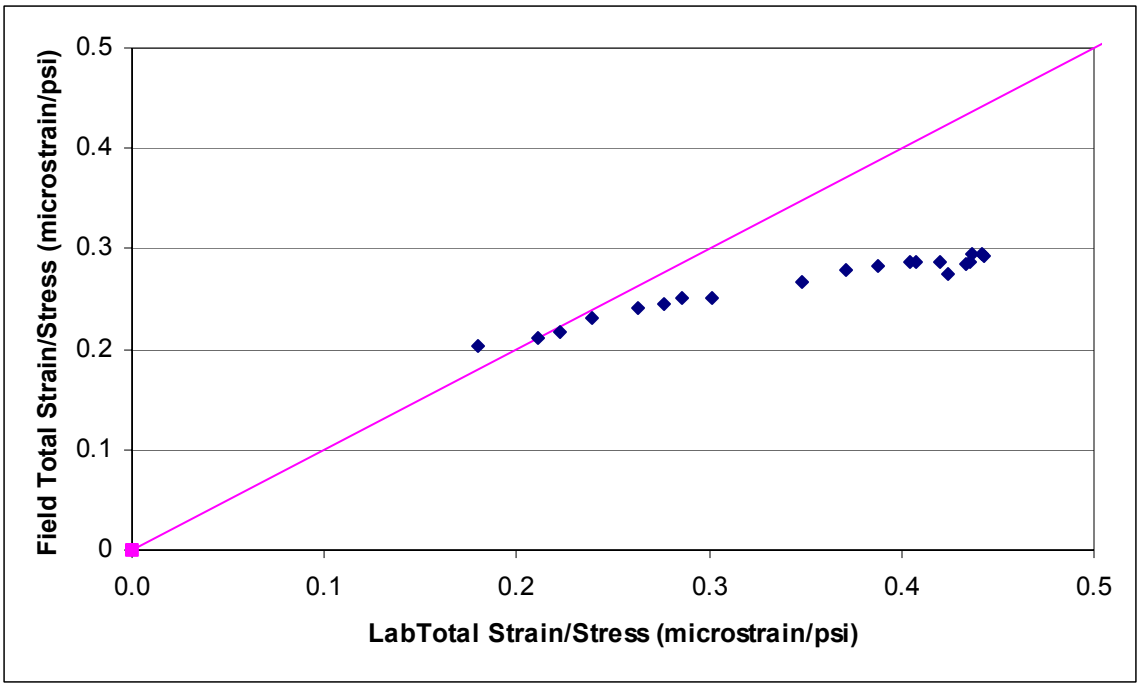

Figure 73 Field vs. Laboratory Accelerated Cure Total Strains, HSC

Prediction Model Residuals

Tables 9 and 10 summarize the accelerated cure and standard cure residuals, respectively. The models are identified as overpredicting or underpredicting. Model predicted values that have residuals of zero within the 95% confidence limits are identified with parentheses ().

Accelerated Cure Residuals

The ACI 209 modified and Tadros models predicted all time-dependent strains within the 95% confidence limits. All of the models were overpredicting, except that CEB-MC90 and B3 underpredicted shrinkage strains. The AASHTO-LRFD predicted creep was within the 95% confidence limits.

Table 9 Accelerated Cure Residuals Summary, HSC

Model	Total Strain	Creep	Shrinkage
ACI 209	Overpredicting	Overpredicting	Overpredicting
ACI 209 Modified	(Overpredicting)	(Overpredicting)	(Overpredicting)
CEB MC-90	Overpredicting	Overpredicting	Underpredicting
AASHTO-LRFD	Overpredicting	(Overpredicting)	Overpredicting
GL2000	Overpredicting	Overpredicting	Overpredicting
Tadros	(Overpredicting)	(Overpredicting)	(Overpredicting)
B3	Overpredicting	Overpredicting	Underpredicting

Standard Cure Residuals

For the standard cure batches, all strains were overpredicted in all cases, with the exceptions that the CEB MC-90 and B3 models underpredicted shrinkage strain. Because the standard cure variability was less than the accelerated cure variability, it was less likely that the predicted strains would fall in the experimental 95% confidence limits.

Table 10 Standard Cure Residuals Summary, HSC

Model	Total Strain	Creep	Shrinkage
ACI 209	Overpredicting	Overpredicting	Overpredicting
ACI 209 Modified	Overpredicting	Overpredicting	Overpredicting
CEB MC-90	Overpredicting	Overpredicting	Underpredicting
AASHTO-LRFD	Overpredicting	Overpredicting	Overpredicting
GL2000	Overpredicting	Overpredicting	Overpredicting
Tadros	Overpredicting	Overpredicting	Overpredicting
B3	Overpredicting	Overpredicting	(Underpredicting)

Prediction Model Rankings

The prediction model rankings based on residuals squared analysis were summed to determine the best overall predictor. The accelerated cure and standard cure rankings are determined at 97 and 98 days after loading, respectively.

Accelerated Cure Rankings

Table 11 presents the accelerated cure prediction model rankings. The ACI 209 modified was the most accurate model for each strain type.

Table 11 Accelerated Cure Prediction Model Rankings. HSC

Model	Total Strain	Creep	Shrinkage	Sum
ACI 209 Modified	1	1	1	3
Tadros	2	2	2	6
ACI 209	4	4	4	12
AASHTO-LRFD	3	3	7	13
B3	6	6	3	15
CEB MC-90	5	5	6	16
GL2000	7	7	5	19

Standard Cure Rankings

Table 12 presents the standard cure prediction model rankings. The ACI 209 modified was the best total strain and overall predictor. AASHTO-LRFD was the best predictor of creep strain, and B3 was the best predictor of shrinkage strain.

Table 12 Standard Cure Prediction Model Rankings, HSC

Model	Total Strain	Creep	Shrinkage	Sum
ACI 209 Modified	1	2	2	5
Tadros	2	3	4	9
AASHTO-LRFD	3	1	7	11
B3	6	6	1	13
CEB MC-90	4	5	5	14
ACI 209	5	4	6	15
GL2000	7	7	3	17

Applicability of Prediction Models

Creep and shrinkage behavior depends heavily on the compressive strength of a concrete mixture. HSC has a more dense cement matrix and less free water than normal-strength concrete, which are factors that limit the amount of time-dependent water movement within the cement matrix. For a prediction model to predict creep and shrinkage strains accurately for HSC, it should include compressive strength as an important input parameter. Table 13 presents the applicability of each prediction model to HSC.

Table 13 Prediction Model Compressive Strength Parameters, HSC

Model	f'_c Limit MPa (psi)	Strength Adjustment Factor?	
		Creep	Shrinkage
ACI 209	none	no	no
ACI 209 Modified	none	yes	yes
CEB 90	89.7 (13000)	yes	yes
AASHTO-LRFD	none	yes	no
GL2000	69.0 (10000)	no	yes
Tadros	none	yes	yes
B3	69.0 (10000)	yes	yes

In this study, the models that did not include compressive strength as an input parameter greatly overpredicted the experimental strains. In some cases, the models considered compressive strength for creep but not shrinkage and vice versa (AASHTO-LRFD and GL2000).

The Bazant B3 and Gardner GL2000 prediction models were not expected to be accurate for the laboratory mixtures because the laboratory compressive strengths exceeded the limits of applicability for each model. B3 considers compressive strength, but this parameter must be modified if the model is to be applied to concretes with compressive strengths over 69.0 MPa (10000 psi). The GL2000 creep model does not consider compressive strength.

LTHSC

Compressive Strength

The accelerated cure LTHSC compressive strengths immediately after curing are approximately the same or greater than the Bayshore results. The Bayshore specimens had a larger strength increase with time. The Bayshore specimens were stored outside with the beams. The environmental conditions in this area are relatively humid considering the plant is surrounded by water on three sides. These conditions appear to have allowed hydration to continue. After curing, the LTHSC specimens were exposed to a drying environment of 50% relative humidity, as were the loaded and unloaded specimens.

Accelerated cure batch 4 was approximately 35% stronger than batch 5 after curing. The accelerated curing process increased the variability of the batches. Maturity is calculated as the area under the temperature-time curve from 14^{o}F or -10^{o}C (Mehta and Monteiro, 1993). The maturity difference between the Bayshore Beams was 20%, 1000 and 830^{o}C-hr. The maturity of batch 4 (1040 ^{o}C-hr) is 10% higher than for batch 5 (940 ^{o}C-hr) since it had 2 hours less of a preset before the temperature increase began. This was due to an experimental error with the match cure system. The target maturity was to be the average of the two beams, 915 C-hr. The maturity of batch 4 and 5 was 990 C-hr.

An additional difference between batches 4 and 5 was the unit weight of 1930 kg/m^3 and 1875 kg/m^3 (120.3 pcf and 117.1 pcf), respectively. The Bayshore beams had unit weights of 1955 kg/m^3 and 1905 kg/m^3 (122.0 pcf and 118.8 pcf) for BB1 and BB2, respectively. There was a variability between batches or beams, but this was similar in the laboratory and in the field. The variability in unit weight corresponds with the variation in compressive strengths. A higher unit weight results in a higher compressive strength between the accelerated cure batches and between the bridge beams.

The strength differences in accelerated cure batch strengths were directly related to the creep strains not meeting the ASTM precision requirements. If the maturity and/or unit weight is significantly different, then creep behavior is likely to be significantly different between batches.

Neither the accelerated nor the standard cure lightweight concrete batches reached the 8000 psi design strength. This can be attributed to the specimens being placed in a drying environment, which slowed hydration and strength gain. The Bayshore specimens reached the required strength and were stored outside with the beams in a relatively humid environment. The standard cure, accelerated cure, and bridge beam specimens reached the required release strength of 31 MPa (4500 psi) at loading or release.

Tensile Strength

The LTHSC 28-day tensile strength measurements were within the range of the Bayshore measurements. There is a strong correlation between the tensile strength being equivalent to one tenth of the compressive strength for the LTHSC specimens. The Bayshore specimens had

higher compressive strengths, but the tensile strengths were not significantly different from those of the LTHSC specimens. Both the laboratory and beam tensile tests were greater than the AASHTO 28-day design cracking stress for lightweight aggregate concretes.

Modulus of Elasticity

The Bayshore 28-day modulus measurements were slightly higher than the respective LTHSC measurements, which supports the observation that the specimens appear to have continued hydration in a moist environment after the accelerated cure. The variability of the LTHSC measurements was a function of the testing procedure and the specimen size.

The modulus of elasticity was measured on 150 mm x 300 mm (6 in. x 12 in.) and 100 mm x 200 mm (4 in. x 8 in.) cylinders for the standard cure and the accelerated cure methods, respectively. The variability between measurements appeared to be less for the larger specimens. The smaller volume to surface area ratio for the 100 mm x 200 mm (4 in. x 8 in.) specimen could contribute to the increased variability.

Thermal Coefficient

The linear coefficient of thermal expansion for the LTHSC mixture was found to be 5.3 microstrain per ^{o}F (9.5 microstrain per ^{o}C) with a confidence interval of ± 0.13 microstrain microstrain per ^{o}F (±0.24 microstrain per ^{o}C). This agrees with the ACI 213 Guide for Structural Light weight Aggregate Concrete, which states the thermal coefficient for lightweight concrete is 4 to 6 microstrain per ^{o}F (7 to 11 microstrain per ^{o}C) depending on the amount of natural sand used.

Experimental and Predicted Strains

The model limitations must be considered when applying the models to lightweight concrete. Only one of the four models, ACI 209, included lightweight aggregate concretes in the development of the model, although, the GL 2000 model does consider aggregate stiffness. The LTHSC proportions meet the cement type requirements for the four examined models, but the models were not developed on test data that included additional mineral admixtures. GL2000 considers this by allowing the model to be calibrated for additional binders with a K factor.

Accelerated Cure vs. Standard Cure

Figures 74 through 76 present the relationship between the average strains of the accelerated cure versus the standard cure. The standard cure and accelerated cure specimens had 38 mm (1.5 in.) and 25 mm (1.0 in.) volume to surface area ratios, respectively. The specimens had different curing regimens, but the size factor seemed most significant. The equivalency line represents paired data of equal magnitude.

Figure 74 presents the average total strain of the two curing conditions. The accelerated cure total strain was slightly higher. The smaller specimen had higher total strain because the moisture loss across its cross section was greater.

Figure 75 presents the creep strain. The creep strain for the smaller, accelerated cure specimen was higher at early ages as these smaller specimen underwent greater drying creep. Over time, the standard and accelerated cure specimen creeps become equal.

Figure 76 presents the shrinkage strain. The accelerated cure specimens had a higher magnitude of shrinkage strain due to higher drying shrinkage rate over a smaller cross section and different hydration fabric.

Shrinkage Prisms vs. Cylinders

Figure 77 presents the standard cure volume to surface relationship between the prisms and the shrinkage cylinders. The prisms have a volume to surface area ratio of 7 mm (0.67 in.) compared to 38 mm (1.5 in.) for the shrinkage cylinders. The smaller specimens initially had a greater magnitude of shrinkage but will become equal at later ages.

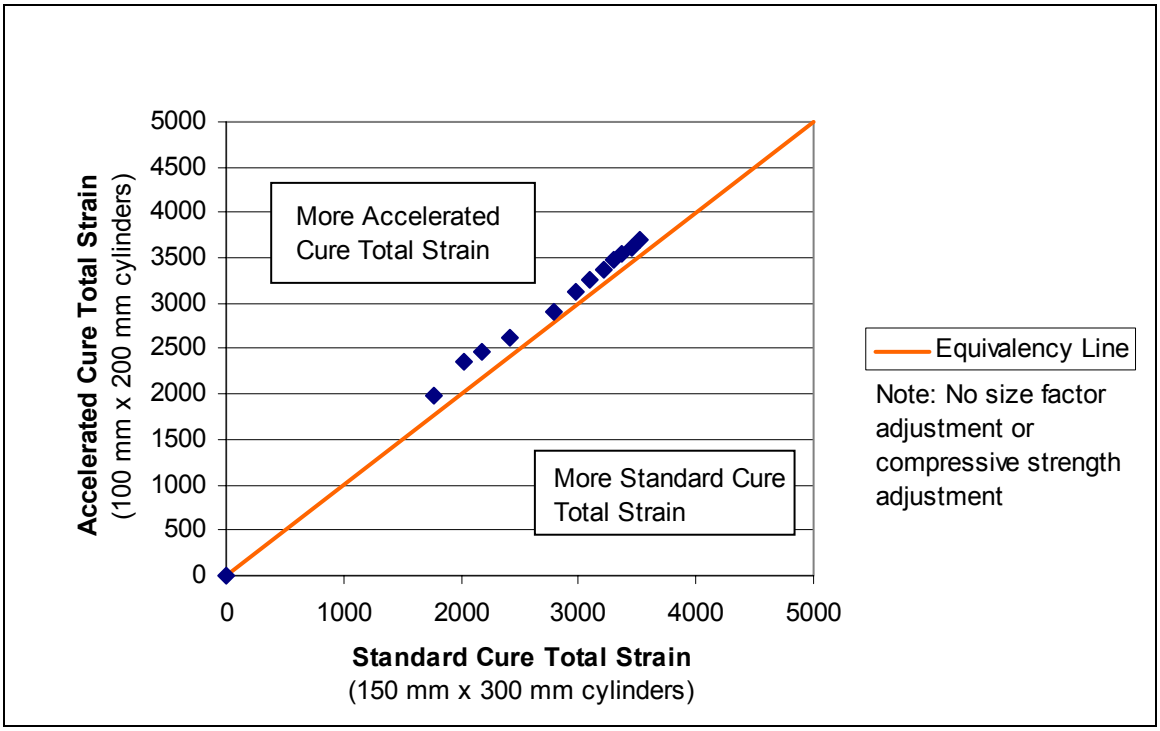

Figure 74 Average Total Strain: Size and Curing Relationship (microstrain), LTHSC

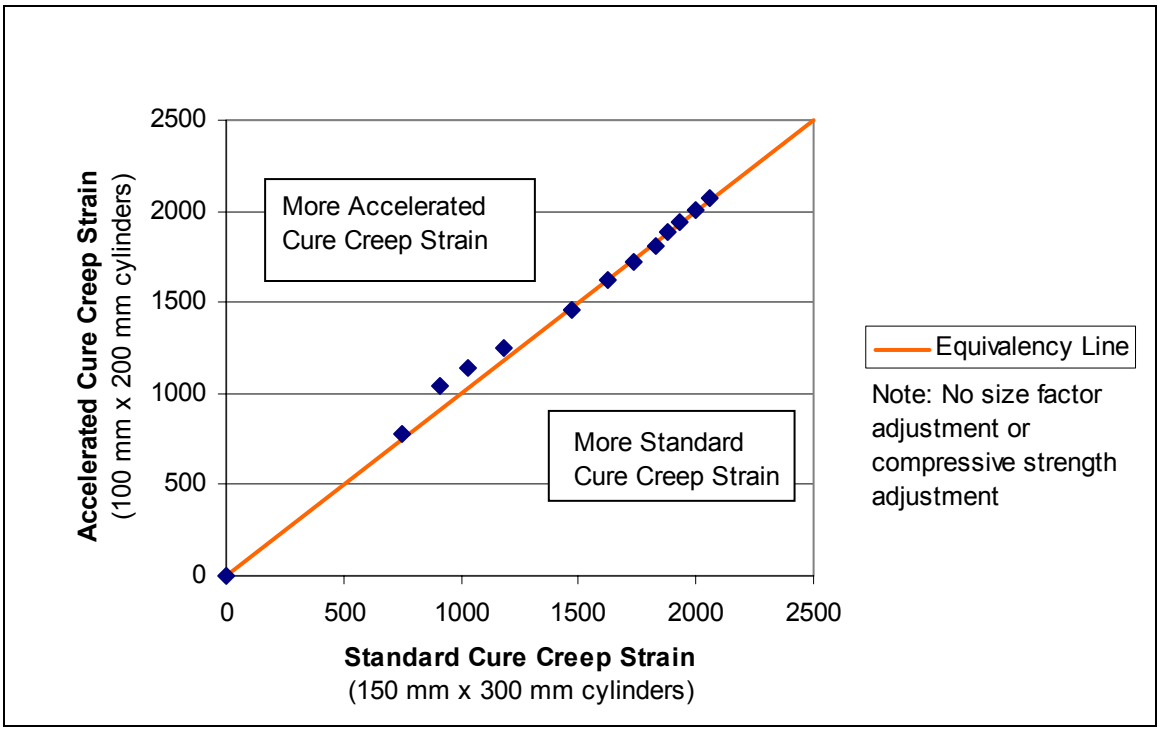

Figure 75 Average Creep Strain: Size and Curing Relationship (microstrain), LTHSC

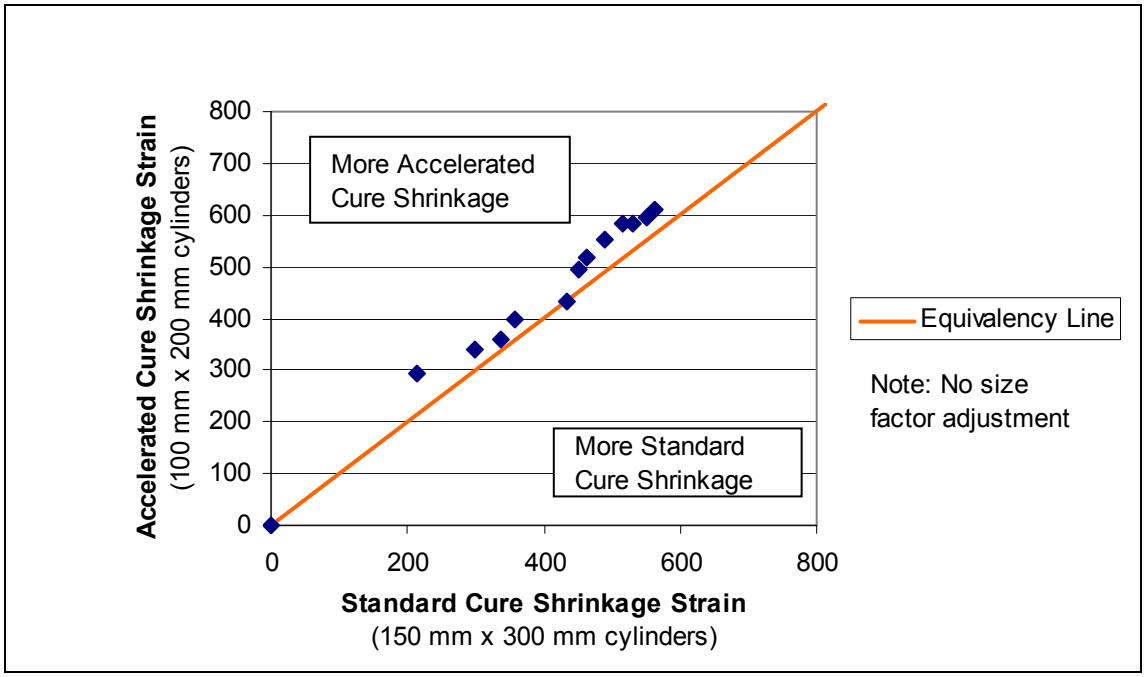

Figure 76 Average Shrinkage Strain: Size and Curing Relationship (microstrain), LTHSC

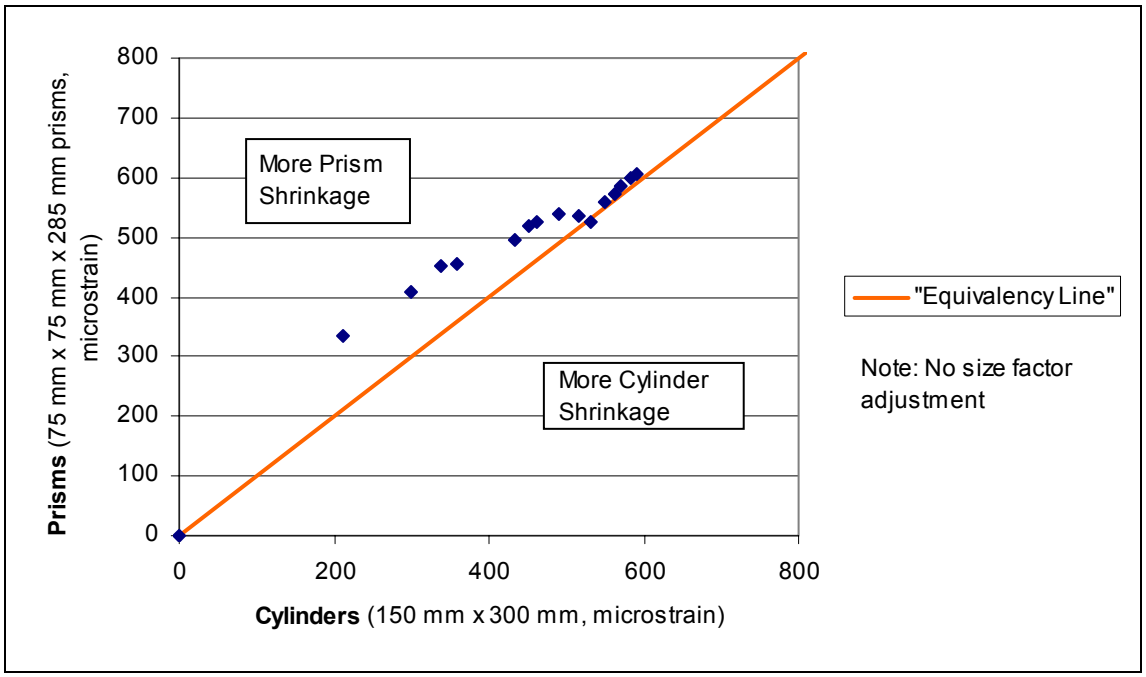

Figure 77 Standard Cure Shrinkage Specimens: Volume to Surface Area Relationship, LTHSC

Field Data

The Chickahominy River Bridge has three 85-ft spans with integral backwall abutments. With a composite deck and diaphragms, the bridge acts as a continuous span for live load and simply supported for dead load. The prestressed beams are ASSHTO Type IV with harped strands. The 43-ft-wide deck provides composite action with the five beams per span. Both the deck and beams are cast with the same lightweight high-strength concrete mixture. The prestressed beams are steam cured, and the deck is cast in place.

As shown in Figure 78, the laboratory total strain significantly overpredicted the field total strain, as was the case for the HSC. Thus, based on laboratory test results, field prestress losses will be significantly overpredicted and service load capacity will be underpredicted.

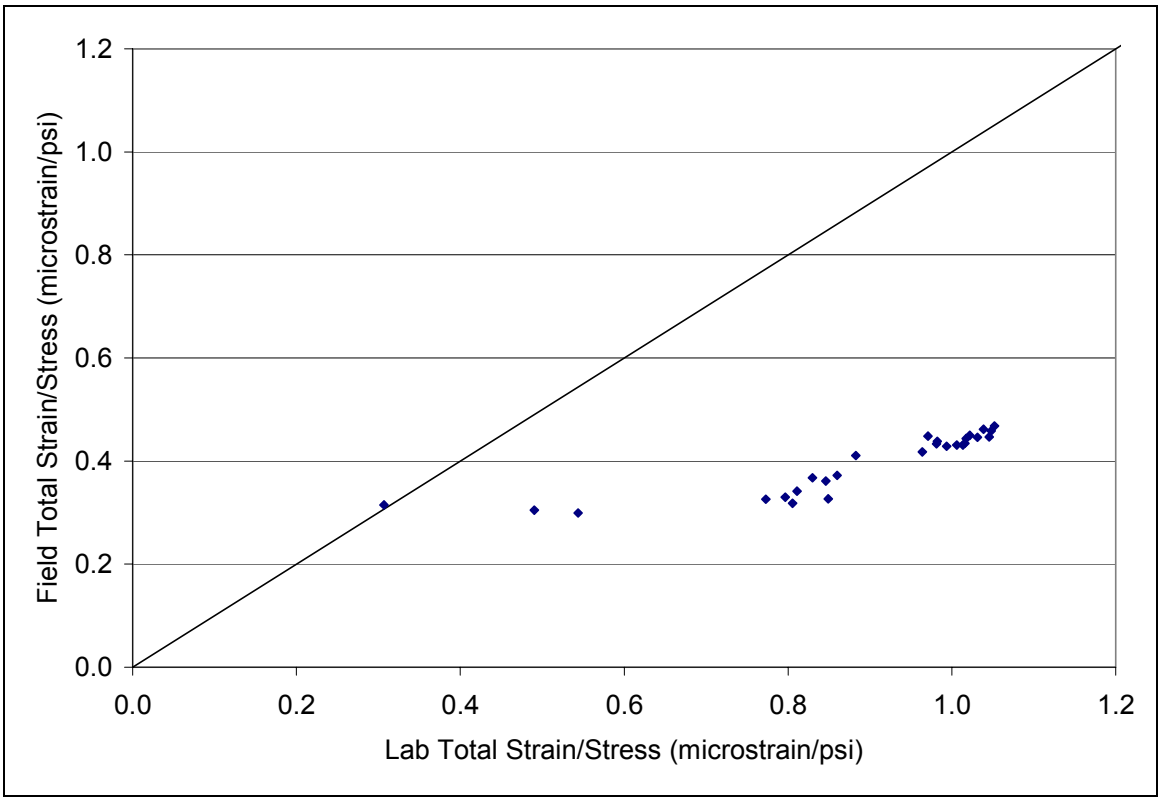

Figure 78 Field vs. Laboratory Accelerated Cure Total Strains, HSC

Prediction Model Residuals

The residuals are calculated as the mean and the 95% confidence limits at the given test time. The standard cure residuals are for batches 2 and 3 combined for a total of six test values, whereas the accelerated cure residuals are for batches 4 and 5, separately. Models that have a residual of zero or fall within the 95% confidence limits are not significantly different from the experimental data and are identified with parentheses (). If a residual could not be distinguished as positive or negative, then the model is described as good in the chart. The models may overpredict (positive residual value) or underpredict (negative residual value). The accelerated cure values can be positive and negative since those two batches could not be combined because the strains are significantly different. For the accelerated cure batches, parentheses () indicate that at least one accelerated cure batch was not significantly different from a model.

Standard Cure Residuals

As shown in Table 14, the ACI 209, CEB 90, and GL2000 models predict total strain within the experimental 95% confidence limits for the standard cure data set. The CEB 90 model appears to be the best total strain predictor for the standard cure method.

The ACI 209 predicts all three measurements within the experimental confidence limits. Total strain and creep are underpredicted whereas shrinkage is overpredicted.

CEB 90 is a good predictor of total strain as a result of overpredicting creep and underpredicting shrinkage. The shrinkage strain is the only parameter that did not fall within the experimental confidence limits.

The B3 model underpredicts total strain as a result of underpredicting creep and shrinkage. B3 does predict creep within the experimental confidence limits.

GL2000 predicts total strain and creep within the experimental confidence limits, whereas all three are underpredicted.

Table 14 Standard Cure Mean Residual Summary

	ACI 209	CEB 90	B3	GL2000
Total Strain	(Underpredicting)	(Good)	Underpredicting	(Underpredicting)
Shrinkage Strain	(Overpredicting)	Underpredicting	Underpredicting	Underpredicting
Creep Strain	(Underpredicting)	(Overpredicting)	(Underpredicting)	(Underpredicting)

Accelerated Cure Residuals

The best model cannot be identified with residuals when the experimental total strain and creep data cannot be combined. The residuals do show the trend to overpredict or underpredict strains.

ACI 209 is a good predictor of shrinkage, whereas the CEB 90, B3, and GL2000 models underpredict shrinkage; see Table 15.

Table 15 Accelerated Cure Residual Summary

	ACI 209	CEB 90	B3	GL2000
Total Strain	Both over and under	Both over and under	Both over and under	(Both over and under)
Shrinkage Strain	(Good)	Under	Under	Under
Creep Strain	Both over and under	Over	Over	Over

Prediction Model Rankings

Tables 16 and 17 summarize the standard cure prediction rankings at 56 and 250 days. The GL2000 model was the best predictor of standard cure time-dependent strains. The CEB 90 model was the best predictor of total strain over time.

Table 16 Standard Cure Prediction Model Rankings at 56 Days

At 56 Days	ACI 209	CEB MC 90	B3	GL2000
Total Strain	1/2/3	1/2/3	4	1/2/3
Shrinkage Strain	1	3/4	3/4	2
Creep Strain	3/4	2	3/4	1
Sum of Ranks	5	6	10	4

Table 17 Standard Cure Prediction Model Rankings at 250 Days

At 250 Days	ACI 209	CEB MC 90	B3	GL2000
Total Strain	2/3	1	4	2/3
Shrinkage Strain	1	4	3	2
Creep Strain	4	2	3	1
Sum of Ranks	7	7	10	5

Accelerated Cure Summary

Tables 18 and 19 summarize the accelerated cure predicting model rankings at 56 and 250 days. The ACI 209 model was the best predictor for total strain, creep, and shrinkage. This is a reasonable conclusion since it was the only model developed with lightweight concretes.

Table 18 Accelerated Cure Prediction Model Rankings at 56 Days

At 56 Days	ACI 209	CEB 90	B3	GL2000
Total Strain	1	4	2	3
Shrinkage Strain	1	3	4	2
Creep Strain	1	4	2	3
Sum of Rank	3	10	8	8

Table 19 Accelerated Cure Prediction Model Rankings at 250 Days

At 250 Days	ACI 209	CEB 90	B3	GL2000
Total Strain	1	4	2	3
Shrinkage Strain	1	3	4	2
Creep Strain	1	4	2	3
Sum of Rank	3	10	8	8

Shrinkage Prisms Model Rankings

Table 20 summarizes the model rankings for the standard cure prism shrinkage specimens at 56 and 250 days. However, these rankings are inconclusive. Although the CEB 90 model was the best early age predictor, the B3 model was the best predictor at later ages.

Table 20 Standard Cure Shrinkage Prism Model Ranking

	ACI 209	CEB 90	B3	GL2000
At 56 Days	1/2	1/2	3	4
At 250 Days	4	3	1	2
Sum of Ranks	5	4	4	6

CONCLUSIONS

HSC

For Accelerated Cure Applications

- The total strain of the HSC accelerated cure mixture loaded to 20.7 MPa (3000 psi) was 1342 ± 49 microstrain at 97 days, at a 95% confidence level.

- The ACI 209 model modified by Huo is the most accurate predictor of total, creep, and shrinkage strain for the Bayshore HSC mixture loaded to 20.7 MPa (3000 psi).

- The accelerated curing technique results in higher variability of time-dependent strains than does standard curing.

- Embedded VWG may be used to measure laboratory time-dependent strains. VWG elastic and creep strain measurements are comparable to Whittemore gage measurements. VWG drying creep and shrinkage strains are significantly lower than Whittemore shrinkage strains because more drying occurs at the outside surface of a specimen than at center of the specimens.

For Standard Cure Applications

- The total strain of the HSC standard cure mixture loaded to 20.7 MPa (3000 psi) was 1276 ± 38 microstrain at 98 days, at a 95% confidence level.

- The ACI 209 model modified by Huo is the best overall predictor and the best predictor of total strain for the Bayshore HSC mixture loaded to 20.7 MPa (3000 psi).

- The AASHTO-LRFD model is the best predictor of creep strain for the Bayshore HSC mixture loaded to 20.7 MPa (3000 psi).

- The B3 model is the best predictor of cylinder shrinkage strain for the Bayshore HSC mixture, and the GL2000 model is the best predictor of prism shrinkage strain.

LTHSC

For Accelerated Cure Applications

- The total strains of the accelerated cure LTHSC batches were 2510 ± 20 and 3800 ± 160 microstrain at 90 days and 2930 ± 40 and 4470 ± 180 microstrain at 250 days, respectively, at a 95% significance level.

- The ACI 209 model is the best predictor of total strain for the Bayshore LTHSC mixture when loaded to 40% of the ultimate compressive strength and an accelerated curing method is used.

- The ACI 209 model is the best predictor of time-dependent deformations.

- The use of the accelerated cure method significantly increased the variability of the strength and creep strains. Maturities and unit weights should be kept as similar as possible.

For Standard Cure Applications

- The total strain of the standard cure LTHSC batches was 2970 ± 330 microstrain at 90 days and 3510 ± 370 microstrain at 250 days at a 5% significance level.

- The CEB Mode Code 90 model is the best predictor of total strain for the Bayshore LTHSC mixture when loaded to 40% of the ultimate compressive strength and a standard cure is used.

- The GL2000 model is the best predictor of time-dependent deformations.

RECOMMENDATIONS

HSC

1. Creep and shrinkage models should contain modification factors for compressive strength. In this study, the models that contained such modification factors predicted much more accurately than those that did not consider compressive strength.

2. The AASHTO Standard Specification is used in Virginia, but it significantly overpredicts prestress losses due to creep and shrinkage for high-strength concrete. It should be updated by using a model that is applicable to high-strength concrete.

3. Whenever possible, laboratory specimens should be cast in the field from the concrete batches being used in the test girders, so that the specimens are of the same material as the girders. This would eliminate significant discrepancies in material properties between the laboratory concrete and girder concrete.

4. Creep testing of sealed specimens could be useful in order to compare with creep strains inside a large bridge girder, where basic creep dominates.

LTHSC

1. The relationship between laboratory specimens under a constant applied stress and prestressed beams that have a decreasing applied stress due to prestress losses needs to be developed or the laboratory testing procedure needs to be modified with a time step approach.

2. The relationship between the laboratory specimen and bridge beam volume to surface area ratios should be developed. The study of basic creep and drying creep separately could be of significance. Laboratory specimens undergo a great deal more drying creep and drying shrinkage than does a bridge beam placed over a river.

3. Further examination of the GL2000 model should be conducted with specimens of various volume to surface area ratios. The equation for shrinkage with time may need adjustment.

HSC and LTHSC

1. For normal and lightweight high-strength concretes, the LRFD creep and strength functions should be determined for VDOT concretes in order to estimate prestress losses better.

REFERENCES

ACI Committee 209. Prediction of creep, shrinkage and temperature effects in concrete structures. *Manual of Concrete Practice*, Part 1, 209R 1-92, 1990.

Alexander, M.G. Aggregates and the deformation properties of concrete. ACI *Materials Journal*, v. 93, n. 6, 1996, pp. 569-577.

Chern, J.C., and Chan, Y.W. Deformations of concretes made with blast furnace slag cement and ordinary portland cement. *ACI Materials Journal*, v. 86, n. 4, 1989, pp. 372-382.

Collins, T.M. Proportioning high strength concrete to control creep and shrinkage. *ACI Materials Journal*, v. 86, n. 6, 1989, pp. 567-580.

Mehta, P.K., and Monteiro, P.J.M. *Concrete Structure, Properties, and Materials,* 2nd Ed., Prentice Hall, Englewood Cliffs, NJ, 1993.

Meyerson, R. Compressive creep of prestressed concrete mixtures with and without mineral admixtures. Masters thesis, Virginia Polytechnic Institute & State University, Blacksburg, February 2001.

Mokhtarzadeh, A., and French, C. Time-dependent properties of high-strength concrete with consideration for precast applications. *ACI Materials Journal*, v. 97, n. 3, 2000, pp. 263-271.

Nawy, E.G. Fundamentals of High Strength High Performance Concrete, 2nd Ed. John Wiley, New York, 2001.

Neville, A.M. Creep of Concrete: Plain, Reinforced, and Prestressed. North-Holland Pub. Co., Amsterdam, 1970.

Paulson, K.A., Nilson, A.H., and Hover, K.C. Long term deflection of high strength concrete beams. *ACI Materials Journal*, v. 88, n. 2, 1991, pp. 197-206.

Shah, S.P., and Ahmad, S.H. High Performance Concrete: Properties and Applications. McGraw-Hill, Inc., New York, 1994.

Smadi, M.M., Slate, F.O., and Nilson, A.H. Shrinkage and creep of high, medium, and low strength concretes, including overloads. *ACI Materials Journal*, v. 84, n. 3, 1987, pp. 224-234.